

NOAA Technical Report EDIS 31



Calibration and Intercomparison of the Gate C-Band Radars

November 1979

**U.S. DEPARTMENT OF COMMERCE
National Oceanic and Atmospheric Administration
Environmental Data and Information Service**

NOAA TECHNICAL REPORTS

Environmental Data and Information Service Series

The Environmental Data and Information Service (EDIS) archives and disseminates a broad spectrum of environmental data gathered by the various components of NOAA and by the various cooperating agencies and activities throughout the world. EDIS is a "bank" of worldwide environmental data upon which the researcher may draw to study and analyze environmental phenomena and their impact upon commerce, agriculture, industry, aviation, and other activities. EDIS also performs studies to put environmental phenomena and relations into proper historical and statistical perspective and to provide a basis for assessing changes in the natural environment brought about by human activities.

The EDS and EDIS series of NOAA Technical Reports are a continuation of the former series, the Environmental Science Services Administration (ESSA) Technical Report, EDS.

Reports in the series are available from the National Technical Information Service, U.S. Department of Commerce, Sills Bldg., 5285 Port Royal Road, Springfield, VA 22161. Prices on request for paper copies; \$3.00 microfiche. Order by accession number shown in parentheses.

ESSA Technical Reports

- EDS 1 Upper Wind Statistics of the Northern Western Hemisphere. Harold L. Crutcher and Don K. Halligan, April 1967, 20 pp. (PB-174-921)
- EDS 2 Direct and Inverse Tables of the Gamma Distribution. H. C. S. Thom, April 1968, 30 pp. (PB-178-320)
- EDS 3 Standard Deviation of Monthly Average Temperature. H. C. S. Thom, April 1968. (PB-178-309) Richard M. Whiting, Revised April 1978, 31 pp. (PB282152)
- EDS 4 Prediction of Movement and Intensity of Tropical Storms Over the Indian Seas During the October to December Season. P. Jagannathan and H. L. Crutcher, May 1968, 49 pp. (PB-178-497)
- EDS 5 An Application of the Gamma Distribution Function to Indian Rainfall. D. A. Mooley and H. L. Crutcher, August 1968, 47 pp. (PB-180-056)
- EDS 6 Quantiles of Monthly Precipitation for Selected Stations in the Contiguous United States. H. C. S. Thom and Ida B. Vestal, August 1968, 5 pp. (PB-180-057)
- EDS 7 A Comparison of Radiosonde Temperatures at the 100-, 80-, 50-, and 30-mb Levels. Harold L. Crutcher and Frank T. Quinlan, August 1968, 10 pp. (PB-180-058)
- EDS 8 Characteristics and Probabilities of Precipitation in China. Augustine Y. M. Yao, September 1969. 35 pp. (PB-188-420)
- EDS 9 Markov Chain Models for Probabilities of Hot and Cool Days Sequences and Hot Spells in Nevada. Clarence M. Sakamoto, March 1970, 26 pp. (PB-193-221)

NOAA Technical Reports

- EDS 10 BOMEX Temporary Archive Description of Available Data. Terry de la Moriniere, January 1972. 304 pp. (COM-72-50289)
- EDS 11 A Note on a Gamma Distribution Computer Program and Graph Paper. Harold L. Crutcher, Gerald L. Barger, and Grady F. McKay, April 1973, 92 pp. (COM-73-11401)
- EDS 12 BOMEX Permanent Archive: Description of Data. Center for Experiment Design and Data Analysis, May 1975, 327 pp. (COM-75-11116)
- EDS 13 Precipitation Analysis for BOMEX Period III. M.D. Hudlow and W. D. Scherer, September 1975, 40 pp. (PB-246-870)
- EDS 14 IFYGL Rawinsonde System: Description of Archived Data. Sandra M. Hoexter, May 1976, 53 pp. (PB-258-057)
- EDS 15 IFYGL Physical Data Collection System: Description of Archived Data. Jack Foreman, September 1976, 175 pp. (PB-261-829)

(Continued on inside back cover)

NOAA Technical Report EDIS 31



Calibration and Intercomparison of the Gate C-Band Radars

M. Hudlow, R. Arkell, V. Patterson,
P. Pytlowany, and F. Richards

Center for Environmental Assessment Services
National Oceanic and Atmospheric Administration

S. Gentis
Department of Meteorology
Massachusetts Institute of Technology

November 1979

U.S. DEPARTMENT OF COMMERCE

National Oceanic and Atmospheric Administration

Richard A. Frank, Administrator

Environmental Data and Information Service

Thomas D. Potter, Acting Director

CONTENTS

	<u>Page</u>
Abstract	1
1. Introduction	2
2. GATE radar systems and sampling	7
2.1 C-Band radar systems	7
2.2 Radar data collection and treatment	9
3. Basic equations	10
3.1 Radar equations	10
3.2 Analysis of variance of transmitter outputs and digitizer input-output transfer functions	11
3.3 Reflectivity-rainfall relationships	13
4. Pre-GATE radar comparison with dense Florida rain-gage networks	15
4.1 Description of equipment and networks	15
4.2 Equations for Florida analysis	17
4.3 Analysis and results	20
4.4 Conclusions from Florida experiment	22
5. System gain measurements	24
5.1 Standard horn method	25
5.2 Standard target technique	27
5.3 Conclusions from system gain measurements	31
6. Comparisons made prior to September 1975 between overlapping reflectivity measurements	32
6.1 Cross-correlation of reflectivity fields	34
6.2 Comparison of areal mean parameters in the central overlap region	40
6.3 Comparison of volumetric-water versus echo-area relationships	41
6.4 Synopsis of calibrations when reflectivity archival processing began	43
7. Range effects	44
7.1 Attenuation effects	44
7.2 Mean range performance curves	55

	<u>Page</u>
8. Comparisons during periods that radars were collocated . . .	59
8.1 Comparison of areal rainfall estimates at various ranges	59
8.2 Conclusions from collocated intercomparisons	59
9. Volumetric water distribution comparisons within fixed geometric areas	61
9.1 Reflectivity frequency-distribution software	62
9.2 Radar-to-radar comparisons before bias adjustments . .	62
9.3 Radar-to-gage comparisons before bias adjustments . . .	66
9.4 Tentative bias corrections and radar-to-radar comparisons after bias corrections	67
9.5 Conclusions from volumetric water comparisons and mean GATE distributions	73
10. Mean bias corrections used in derivation of final rainfall estimates	73
10.1 Verification of <u>Quadra-Oceanographer</u> relative bias through comparison of instantaneous reflectivity fields	73
10.2 Synopsis of bias corrections for all four radars	77
11. Verification of bias corrections	78
11.1 Comparison of Phase III mean rainfall rates from individual radars with gage catches	80
11.2 Comparison of Phase mean rainfall rates from merged radar data with gage catches	80
11.3 Comparison of daily rainfall rates from merged radar data with gage catches	82
11.4 Comparison of hourly rainfall rates from NOAA radars with "collocated" gage catches	84
11.5 Overall validity of bias corrections	84
12. Concluding remarks	87
12.1 Calibration and intercomparison procedures	87
12.2 Probable accuracies of the GATE radar rainfall estimates	89
Acknowledgments	93
References	94

CALIBRATION AND INTERCOMPARISON
OF THE GATE C-BAND RADARS

M. Hudlow¹, R. Arkell, V. Patterson, P. Pytlowany, and F. Richards

Center for Environmental Assessment Services
National Oceanic and Atmospheric Administration
Washington, DC 20235

and

S. Geotis
Department of Meteorology
Massachusetts Institute of Technology
Cambridge, MA 02139

ABSTRACT. The field portions of a major experiment within the Global Atmospheric Research Program (GARP), the GARP Atlantic Tropical Experiment (GATE), were conducted from June through September 1974. A central objective of GATE was to establish a high quality data base for studying the interactions between the large scale circulations and the smaller scale weather systems over the tropical Atlantic Ocean. Better understanding of these interactions is needed to improve the parameterization of convection in the numerical weather prediction models.

A significant ingredient of the data base is accurate quantitative rainfall estimates covering the primary ship array; for example, such estimates are required to assess the precipitation component of the atmospheric water and energy budgets. Digital data from four C-band shipboard radars, supplemented with shipboard rain-gage data, formed the primary sources of information for deriving the rainfall estimates.

Since the success of water and energy budget studies depends on accurate precipitation estimates, which, in turn, directly depend on the accuracy of the overall calibrations of the C-band radars, a multifaceted approach for calibrating and intercomparing the data from the four C-band systems was taken. Comprehensive calibration and intercomparison of the GATE radars were particularly important since many of the subassemblies were built specifically for GATE, which precluded a lengthy record of calibration characteristics prior to GATE. Steps were taken to provide for (1) accurate calibration of the radar hardware; (2) adequate pre-GATE testing of the radar systems; (3) consistency, in the mean, between the reflectivity fields from the

¹ Now with the Office of Hydrology, National Weather Service, NOAA.

individual radars, based on various intercomparison techniques; (4) assessment and removal of systematic biases; (5) verification of estimated systematic biases based on "ground-truth" comparisons with the shipboard rain gages; and (6) assessment of probable accuracies of the final rainfall estimates.

To identify and assess the magnitudes of any systematic biases between sensors the hardware aspects of the overall calibration problem were first considered; included were system characteristics, system tests, hardware calibration procedures (for the receiver/digital-processor and the total system gain), and analysis of the hardware calibration data. Next, reflectivity data from the radar systems were inter-compared to evaluate the consistency in relative calibrations between radars. Although comparisons were made between "collocated" radars while they were briefly together during official intercomparison periods, most of the comparisons were made while the ships were on station and separated by approximately 165 km. The on-station comparisons were made using reflectivity data from overlap regions, usually located between the radar sites. Because the data being compared were sometimes located at different ranges, and because the range effects could vary from radar to radar, the range performance characteristics of the four C-band radars were examined. Also, the effects of atmospheric and rainfall attenuation on range performance were evaluated.

The radar-to-gage "ground-truth" comparisons were first done on an individual radar basis using selected gages within the field of view of a radar. Based on the results from these comparisons, those from the radar-to-radar intercomparisons, and on the excellent stability of the hardware calibrations, systematic biases were estimated for the radars. The validation of these bias estimates was accomplished by comparing the final merged radar-rainfall estimates with the rain-gage data from all ship stations. Finally, still using the shipboard gages as "ground truth," expected accuracies of the radar estimates for several space and time scales were assessed.

1. INTRODUCTION

The field portions of a major experiment within the Global Atmospheric Research Program (GARP), the GARP Atlantic Tropical Experiment (GATE), were conducted from June through September 1974. The fundamental objectives of GATE have been discussed elsewhere; for example, see Kuettner et al. (1974) and Austin (1975). Briefly stated, the central objective was to provide a

basis for developing methods to determine the interactions between the large scale circulations and the smaller scale weather systems over the tropical Atlantic Ocean. Parameterization models of tropical convection, which realistically account for control by, and feedback to the synoptic scale, must be developed by carefully considering such scale interactions. If these interactions can be clearly defined based on GATE data, the accuracy of global numerical prediction can be improved.

Analysis and validation of the GATE data sets fell under the auspices of five major subprograms that divide GATE according to major disciplines (Kuettner et al., 1974). The radar analyses were an integral part of the Convection Subprogram (Betts, 1974; Betts and Rodenhuis, 1975; Hudlow, 1975).

Shipboard meteorological radar measurements during GATE were taken with a total of four C-band and four X-band systems. Figure 1 shows the deployment and approximate coverage of the radars for Phase I of GATE. Table 1 gives the countries, ships, and the principal organizations involved in taking GATE radar measurements.

Refined quantitative precipitation estimates covering an area somewhat larger than the B-scale hexagonal array shown in figure 1 have been derived at the Center for Experiment Design and Data Analysis (CEDDA)² as a major task within the Convection Subprogram. C-band radar data, supplemented with shipboard rain-gage data, formed the primary data base for deriving the rainfall estimates. Because of the large attenuations that occur with high rainfall rates in the X-band and because the B-scale array was adequately covered by C-band radars, X-band data were not used at CEDDA in the derivation of the comprehensive series of precipitation maps covering the three GATE field Phases. However, the X-band data are being used by other Convection Subprogram scientists for detailed case studies of individual echoes or ensembles of echoes and their life histories. Photographs from the X-band radars also were included for the GATE International Meteorological Radar Atlas (Arkell and Hudlow, 1977), which contains 3-hourly mosaics of the radar photographs from the C- and X-band radars for 24 days of GATE.

Since the success of the B-scale water and energy budget studies depends on accurate B-scale precipitation estimates, which in turn directly depend upon the accuracy of the calibration of the C-band radars, a multifaceted approach for calibrating and intercomparing the data from the four C-band systems was taken. The calibrations also affect the quality of the three-dimensional distributions of hydrometeor content derived from the GATE radar data. Comprehensive calibration and intercomparison of the GATE radars were particularly important since many of the subassemblies were built specifically for GATE, which precluded acquiring a lengthy record of calibration characteristics prior to GATE.

² Now the Center for Environmental Assessment Services (CEAS).

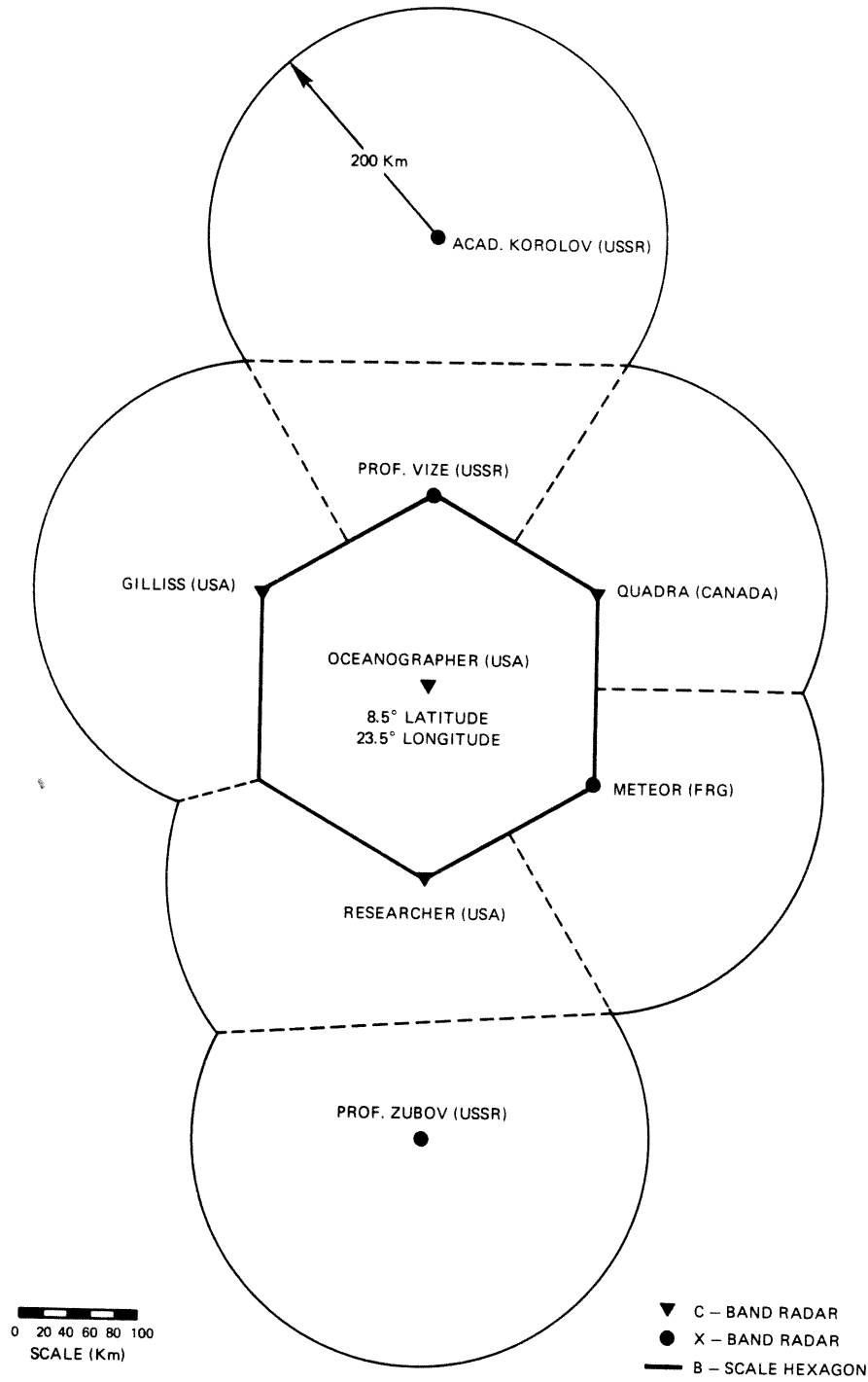


Figure 1.--The GATE B-scale array and radar network showing the deployment of C-band and X-band radars during Phase I, and the maximum coverage included in the pictorial atlas (Arkell and Hudlow, 1977). The quantitative coverage is considerably less.

Table 1.--Countries, ships, and organizations involved
in taking GATE radar measurements

Country	Ship(s)	Organization(s)
Canada	<u>Quadra</u>	McGill Weather Radar Observatory and the Physics Department, McGill University, Montreal.
Federal Republic of Germany (FRG)	<u>Meteor</u> <u>Planet</u>	Institute for the Physics of the Atmosphere, DFVLR, Oberpfaffen- hofen. Meteorological Institute at the University of Bonn.
Union of Soviet Socialist Repub- lics (USSR)	<u>Acad. Korolov</u> <u>Prof. Vize</u> <u>Prof. Zubov</u>	Hydrometeorological Service (Moscow and Leningrad). Central Aerological Observatory, Moscow. Arctic and Antarctic Research Institute, Leningrad.
United States of America (USA)	<u>Gilliss</u> <u>Oceanographer</u> <u>Researcher</u>	Center for Experiment Design and Data Analysis, NOAA, Washington, D.C. Department of Atmospheric Sciences, University of Washington, Seattle, Wash. Department of Meteorology, Massachu- setts Institute of Technology, Cambridge, Mass. Department of Physics, University of Puerto Rico, San Juan.

Two basic plateaus were reached in the calibration and intercomparison efforts at CEDDA. The first was late in the summer of 1975 when the transfer coefficients in the edit-preprocess computer program were "frozen," and production processing was begun in September 1975 on the data sets from the Oceanographer and Researcher radars. The evaluation and validation of all hardware calibration data were complete by then, and selected intercomparisons of reflectivity fields in regions of overlap between the two radars verified that the equivalent reflectivity factors³ generally agreed to within 2 to 3 dB. One subroutine in the preprocess

³ The terms reflectivity factor and reflectivity are used interchangeably in this report.

program transformed the digital machine numbers to reflectivities (dBZ's), which were output to tape for archiving.

In addition to the calibration and intercomparison studies performed at CEDDA prior to September 1975, for the two National Oceanic and Atmospheric Administration (NOAA) radars (Oceanographer and Researcher), similar studies that included the Quadra and Gilliss radars were carried out in parallel at McGill University and the Massachusetts Institute of Technology (MIT). Data from the Gilliss radar also were archived as reflectivities, while the Quadra data were archived as coded values that can be transformed to reflectivities.

The second plateau in the calibration and intercomparison analyses at CEDDA was reached in April 1977. At that time the following additional studies had been completed:

1. Analysis of the GATE drop-size data by scientists at MIT, the University of Toronto, and NOAA's National Hurricane and Experimental Meteorology Laboratory (NHEML), culminating in a proposed reflectivity versus rainfall-rate relationship for GATE. Subsequent analyses by Cuning and Sax (1977) and Austin and Geotis (1979) resulted in somewhat conflicting relationships that will be discussed in section 3.3.
2. Evaluation of signal degradation with range for the four C-band radars.
3. Comparison of rainfall estimates from measurements taken with the radars when they were collocated during special intercomparison periods.
4. Comparison of Phase III reflectivity and volumetric water distributions from the four radars, and comparison of preliminary Phase III mean rainfall rates from the radars with those from selected shipboard gages.
5. Comparison of the final radar rainfall estimates from the individual radars with the shipboard rain gages.

Some of the initial intercomparison studies at CEDDA included data from the two NOAA radars only, since data from the Gilliss and Quadra were not available until after the archival processing had been completed at MIT and McGill University. However, the MIT and McGill groups became involved in their parallel efforts as early as May 1975 when they visually compared their data with hardcopy printouts of selected intercomparison data from the NOAA radars made available to them at that time. The variety of CEDDA intercomparison analyses, many of which included all four C-band radars, complemented by the MIT and McGill studies, form a definitive evaluation of the calibrations for all four C-band radars.

From the results presented in subsequent sections of this report, it was concluded that any significant systematic biases⁴ in the radar estimates had been identified, and the final processing for the B-scale precipitation maps was begun in May 1977. These final estimates were based on data merged from two or more radars. As a final verification of the precipitation estimates, comparisons between the merged radar estimates and rain-gage catches on the various ships in the B-scale for daily and Phase totals were made.

2. GATE RADAR SYSTEMS AND SAMPLING

2.1 C-Band Radar Systems

Table 2 summarizes the technical characteristics and specifications of the four GATE C-band radars. All four systems were equipped with a digital video integrator and processor (DVIP). Basically, the DVIP's averaged the output video from the radar receivers over polar data bins of pre-defined sizes and recorded the numerical values on magnetic tape. The DVIP units for the Quadra and the NOAA radars were identical in design, while the Gilliss unit included a programmable integrator that provided, for example, greater flexibility in the selection of data resolutions or bin sizes (Silver and Geotis, 1976). The size of the polar bins used for recording the GATE data were 2° x 2 km for the NOAA radars, 1° x 1 km for the Quadra radar, and they varied from 1° x 0.25 km at close ranges to 1° x 1 km at far ranges for the Gilliss radar.

The block diagram shown in figure 2 illustrates the total Oceanographer radar system and the interfacing of the various components and subassemblies. The configurations of the Researcher and Quadra radar systems were very similar to the Oceanographer's, but the Gilliss system included a dedicated minicomputer that facilitated antenna control, data collection commands, and data handling (Silver and Geotis, 1976).

As mentioned above, the DVIP units for the two NOAA radars and the Quadra were identical in design. The theory for this design was based on research carried out at NOAA's Severe Storms Laboratory (Sirmans and Doviak, 1973). The DVIP's were very similar to the operational units undergoing implementation by the National Weather Service (Shreeve, 1974). The data bin averages are derived from equally weighted range samples and exponentially weighted

⁴ A principal objective of this report is to identify systematic biases, sometimes simply referred to as biases, which we define as the mean difference between the overall calibration of two sensors [between radars and/or between radar(s) and rain gage(s)], as determined from comparative analyses using a large data sample [e.g. one Phase of data (≈ 20 days)]. The biases might result from systematic hardware calibration errors and/or from errors in the transfer equations, including differences caused by the use of erroneous mean coefficients in the reflectivity-rainfall relationship. Although range effects are considered in chapter 7, the systematic biases, as defined for this report, are not range-dependent.

Table 2.--Radar characteristics and specifications

Characteristics	<u>Oceanographer</u>	<u>Researcher</u>	<u>Gilliss</u>	<u>Quadra</u>
Wavelength	5.3 cm	5.3 cm	5.3 cm	5.3 cm
Peak power transmitted	215 kW	225 kW	250 kW	1000 kW
Pulse length	0.57 km	0.60 km	0.60 km	0.30 km
Minimum detectable signal	-100 dBm	-100 dBm	-100 dBm	-90 dBm
Antenna gain (referenced to directional coupler)	39.9 dB	35.0 dB	39.0 dB	43.5 dB
Pulse repetition frequency	259 Hz	250 Hz	250 Hz	320 Hz
Polarization	Horizontal	Horizontal	Horizontal	Vertical
Beam width	1.5°	2.0°	1.5°	1.0°
Base elevation tilt-angle	0.6°	0.5°	0.5°	0.6°
Radome	Yes	No	Yes	Yes

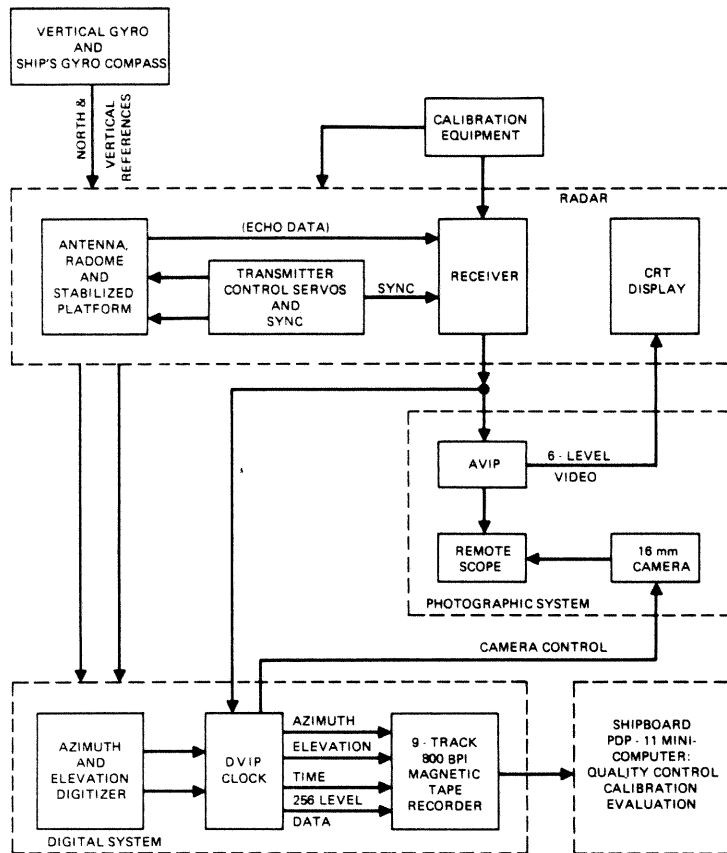


Figure 2.--Radar system on the Oceanographer.

pulse-to-pulse (azimuthal) information. The weight given to successive pulses follows an exponential decay in the direction of the older pulses (Shreeve, 1974). With the time constant scaling factor and antenna rotation speeds used with these three GATE radars, decay to e^{-1} occurred in approximately 0.33° of antenna rotation.

Instead of continuous integration with exponential time weighting, as for the NOAA DVIP, a rectangular window was applied with the Gilliss programmable processor, and an integration cycle corresponding to 1° of antenna rotation was used. Both integrators reduced the standard deviation of pulse-to-pulse fluctuations from a precipitation echo to less than 1 dB. Differences in integrator accuracies affecting the intensity estimates, and their spatial resolution, are not explicitly considered in the calibration and intercomparison analyses that follow. However, the NOAA integrator and the one designed at MIT apparently give comparable precision when hydrologic estimates are derived for the scales considered in this study as is demonstrated by the overall agreement from the various intercomparisons.

2.2 Radar Data Collection and Treatment

Except for scheduled and unscheduled maintenance and calibration periods, the GATE radar installations were normally operated 24 hr a day during all

three Phases of GATE. Antenna-tilt sequences consisting of 360° scans at a series of antenna elevation angles were collected nominally every 15 min with the Gilliss, Oceanographer, and Researcher radars and every 5 min with the Quadra radar. Also, higher frequency observations were collected with all radars during special intercomparison periods.

The intercomparison analyses presented in the following sections are based on low-altitude digital data from the various radars. For several of the analyses, sea clutter was eliminated by using data from the 2° or 4° tilt scan at close ranges, instead of from the base-tilt scan, which was nominally collected at 0.5°. Elimination of sea clutter was essential for the collocated radar/rain-gage comparisons presented in section 11.4.

Most of the data analyses have been done using Cartesian data arrays obtained by rectifying the polar reflectivity fields. One exception was the use of polar coordinate data for range-dependent comparisons of special measurements from the C-band radars when they were collocated (ch. 8). The range-dependent evaluations presented in chapter 7 for the two NOAA radars, which were derived from the Cartesian data, were compared with those derived directly from the polar coordinate data. These comparisons showed no significant differences.

The size of the Cartesian data bins (4 km x 4 km) was standardized for all radars; albeit, the polar to Cartesian rectification algorithms used at CEDDA, MIT, and McGill to transform the NOAA, Gilliss, and Quadra data, respectively, differed in some of the details. Identification of biases originating from these differences has not been explicitly considered as part of the intercomparison studies. The overall consistency in the results from the various intercomparison analyses seems to show that any biases originating from differences between the polar to Cartesian rectification algorithms are generally small. Pragmatically, if general agreement is achieved among all radars in the overlap regions and between individual radars and the shipboard rain gages, then the possibility that compensating biases still exist is of secondary importance.

3. BASIC EQUATIONS

3.1 Radar Equations

The average power, \bar{P}_r , received at the radar antenna from a volume of hydrometeor particles uniformly filling a nonattenuated circular radar beam is given by (Probert-Jones, 1962):

$$\bar{P}_r = \left[\left(\frac{\pi^3}{710} \right) \left(\frac{P_t G^2 h \theta^2}{\lambda^2} \right) \right] \left[|K|^2 \frac{Z_e}{r^2} \right] , \quad (1)$$

where P_t is the peak transmitted power, G is the antenna gain, h is the pulse width (distance units), θ is the beam width, λ is the wavelength, Z_e is the equivalent reflectivity factor, r is the slant range to the target, and

$$K = (m^2 - 1)/(m^2 + 2) ,$$

where m is the complex index of refraction of the hydrometeors.

For example, substituting the values for the Oceanographer's radar characteristics given in table 2 into eq. (1), solving for Z_e , and expressing the resultant relationship in decibels gives

$$Z_e^* = \bar{P}_r^* + 20 \log (r) + 70.0 \quad , \quad (2)$$

where

$$Z_e^* \equiv 10 \log (Z_e) \quad ,$$

and

$$\bar{P}_r^* \equiv 10 \log (\bar{P}_r) \quad ,$$

where the units of Z_e and \bar{P}_r are mm^6/m^3 and mW , respectively. The units for r in eq. (2) are km.

With a logarithmic receiver, the DVIP gives $\overline{\log P_r}$ and not $\log \bar{P}_r$. The bias given by $\log \bar{P}_r - \overline{\log P_r}$ is approximately +2.5 dB (Marshall and Hitschfeld, 1953). Another bias results from the analog-to-digital (A/D) conversion. In the A/D converters of the NOAA DVIP's, the digital values for the instantaneous analog voltages are truncated at 6 bits. A 64-dB dynamic range gives 1-dB class intervals, and the truncation, therefore, causes a 0.5-dB bias (half of the class interval). To account for these biases when using eq. (2), 2.5 dB + 0.5 dB = 3.0 dB should be added to the right-hand side of the expression. Thus, the Oceanographer's radar equation becomes

$$Z_e^* = \bar{P}_r^* + 20 \log (r) + 73.0 \quad . \quad (3)$$

Equations analogous to (3) for the other three C-band radars will not be presented here, but they were derived in an analogous manner using the radar characteristics given in table 2 by Hudlow (1976), Austin (1976), and Catalfamo (1978) for the Researcher, Gilliss, and Quadra, respectively.

3.2 Analysis of Variance of Transmitter Outputs and Digitizer Input-Output Transfer Functions

"Bench" calibrations of the NOAA radar were made every few days. They consisted of injecting a range of test signals from a C-band signal generator into the directional coupler and recording the outputs from the digital processor. The output power from the radar transmitter and the noise (threshold) level of the receiver/processor were also continually monitored. Similar calibrations of the Gilliss and Quadra radars were made at approximately the same intervals.

The output powers from the NOAA radar transmitters were never observed to fluctuate by more than 5 percent from the values given in table 2. All calibration runs from the individual radars exhibited excellent internal consistency and system stability. As an example of the precision that can be achieved with modern solid-state radar components, figure 3 summarizes the results from the 12 Oceanographer bench calibrations made during GATE

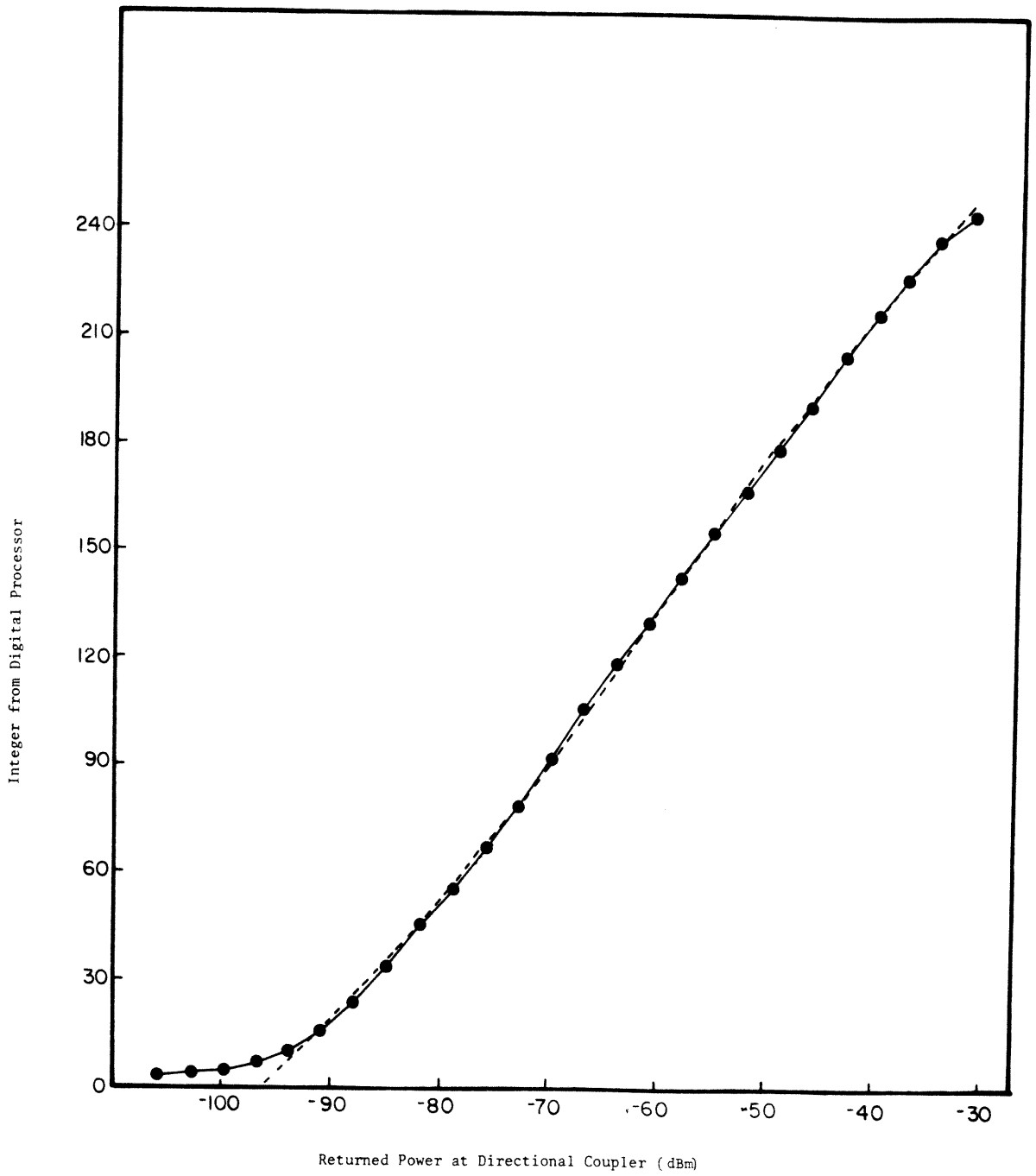


Figure 3.--The mean (solid) and least-squares (dashed) fits to the data from all Oceanographer "bench" calibrations.

and illustrates the good stability of the digital processor, which also reflects the stable characteristics of the radar receiver. The dashed curve is the least-squares fit of a third-degree polynomial to all individual data points from the 12 bench calibrations (258 points). Each calibration run consisted of points that spanned the dynamic range of the receiver/processor in 3-dB increments. However, the lower 4 points were deleted from the 12 sets of calibration data before the least-squares fit was made. The solid curve depicts the mean of the 12 sets of calibration data.

Before the 12 Oceanographer calibration runs were lumped into one group, they were kept separate for the three GATE Phases, and a least-squares fit for each Phase was obtained. The additional variance explained by the Phase subgroupings was insignificant when compared with the ± 1 -dB possible error in the input calibration signals from the generator. Therefore, the Oceanographer data for all periods were processed using the third-degree polynomial curve shown in figure 3. The accompanying mathematical expression is

$$\bar{P}_r^* = -96.28 + 0.35 D - 8.66 \times 10^{-4} D^2 + 2.10 \times 10^{-6} D^3, \quad (4)$$

where D is an integer (0-255) from the digital processor, and \bar{P}_r^* is the corresponding return power. The correlation coefficient for the least-squares fit, eq. (4), is 0.999, and the standard error of estimate is 0.74 dB.

Analysis of the variance of the input-output response curves for the Researcher's radar receiver/processor was performed in an identical manner to that described above for the Oceanographer. Again, the stability of the Researcher's system was found to be good, although the standard error of estimate (≈ 1.0 dB) was somewhat larger than for the Oceanographer curve. Also, because of a change in the alinement of the Researcher DVIP between Phases I and II, it was necessary to apply two calibration curves: one for Phase I and another for Phases II and III (Hudlow, 1976). Calibration curves analogous to the one for the Oceanographer (fig. 3) also were determined for the Quadra and Gilliss at McGill University and MIT, respectively, where the reflectivity measurements from these two radars were processed (Catalfamo, 1978; Austin, 1976).

3.3 Reflectivity-Rainfall Relationships

The first step in converting radar reflectivity measurements into rainfall rate estimates usually consists of using an empirical relationship that relates the reflectivity factor to rainfall rate. The equation normally takes the form of the following logarithmic function:

$$Z = A R^B, \quad (5)$$

or

$$\log (Z) = \log (A) + B \log (R), \quad (6)$$

where Z is the reflectivity factor in mm^6/m^3 , R is the rainfall rate in mm/hr, and A and B are regression coefficients. A and B are usually determined from

a least-squares fit of eq. (6) to a set of Z's and R's, which are calculated from raindrop size data collected at the Earth's surface. An estimate of R from eq. (5) can be obtained by taking Z_e (sec. 3.1) as the estimate for Z. Multiplying eq. (6) by 10, the reflectivity in decibels can be expressed as

$$Z_e^* = 10 \log (A) + B R^* , \quad (7)$$

where

$$R^* \equiv 10 \log (R).$$

Surface raindrop-size measurements were made by three groups aboard various ships during GATE: (1) MIT aboard the Gilliss, (2) NOAA's National Hurricane and Experimental Meteorology Laboratory (NHEML) aboard the Researcher, and (3) the Physics Department, University of Toronto, aboard the Dallas during Phase I and the HJW Fay during Phase III. A preliminary Z-R relationship was derived from the data collected aboard the Dallas soon after Phase I. This preliminary relationship,

$$Z = 300 R^{1.3} , \quad (8)$$

was used for all intercomparison studies prior to June 1976, at which time a revised Z-R relationship based on a comprehensive analysis of available GATE drop-size data was reported by Austin et al. (1976). The revised relationship became

$$Z = 230 R^{1.25} , \quad (9)$$

which in the mean gives about 25 percent higher rainfall amounts for the observed distributions of GATE reflectivities than does eq. (8).

Since that time Cunning and Sax (1977) arrived at a Z-R relationship with a considerably higher exponent (1.52). Their analysis was based on the drop-size data collected from one of the GATE aircraft (DC-6). More recent work by Austin and Geotis (1979) compared the DC-6 data with those collected by another aircraft (US C-130) and with the shipboard measurements. They concluded that the best estimate for the exponent is 1.35. Hudlow and Arkell (1978) experimentally show, using observed GATE reflectivity distributions, that variations in the exponent of the Z-R relationship, over a range from 1.25 to 1.6, would not seriously affect the accuracy of the rainfall estimates for the space and time scales being considered for atmospheric budget studies (≥ 3 hr, ≥ 4000 km²), if the systematic bias introduced by changes in the Z-R relationship is first removed.

The fact that eq. (8) was used for some of the earlier GATE intercomparison analyses is not considered critical since all such analyses have been confined to relative intercomparisons between radars. The radar estimates used in all radar/rain-gage intercomparisons are based on eq. (9). For the pre-GATE

Florida test a Z-R relationship for Miami was used, which will be discussed in the next chapter.

4. PRE-GATE RADAR COMPARISON WITH DENSE FLORIDA RAIN-GAGE NETWORKS

Shipboard installation of the basic Researcher radar system was complete by mid-July 1973. The installation was accomplished while the ship was berthed at Dodge Island in the port of Miami, Fla. This location provided the opportunity to "piggyback" a pre-GATE test on the 1973 Florida Area Cumulus Experiment (FACE, see Simpson and Woodley, 1975; Woodley et al., 1975). This opportunity to test a GATE radar was taken because of good available ground truth from the ongoing FACE measurements, including rainfall observations from a densely instrumented rain-gage network and the Miami WSR-57 10-cm radar. Observations were also obtained from a smaller, modestly instrumented rain-gage network. The physical arrangement of the National Weather Service and GATE radars and the two rain-gage networks is shown in figure 4.

Although the primary motivation for the test was to determine the absolute accuracy of rainfall estimates derived from the Researcher radar measurements, other secondary objectives included evaluation of: (1) the overall performance of a GATE C-band digital radar under shipboard conditions, (2) the then specified GATE radar operational plan for data collection and quality control, and (3) calibration procedures. The Florida test completely fulfilled these three secondary objectives. Unfortunately, the primary objective was not completely fulfilled, because only two storms passed over the rain-gage networks when the Researcher radar was operational. However, as will be shown in this and subsequent sections, the small set of Florida observations, supported by the excellent ground truth, was crucial in providing collaborating evidence that the initial gain measurements for the Researcher radar antenna were in error. The fact that the results from this pre-GATE test were consistent, when interpreted in light of the subsequent calibration and intercomparison analyses, adds a great deal of confidence to the GATE C-band radar measurements.

4.1 Description of Equipment and Networks

As was stated in section 2.1, the DVIP on the Researcher was similar to the operational DVIP units undergoing implementation by the National Weather Service. This statement also applies to the WSR-57 installation in Miami, which in support of FACE was one of the first National Weather Service radars equipped with a DVIP. Therefore, the data collection, processing, and recording characteristics, as well as the beam widths and sensitivities, were quite similar for the Researcher (see ch. 2) and the WSR-57 radars. The major difference was the WSR-57's 10-cm wavelength versus 5.3 cm for the Researcher. Wiggert and Ostlund (1975), who also provided the WSR-57 radar rainfall estimates and the FACE rain-gage measurements used in this section, give details on the calibration, data collection, and processing of the digital data from the Miami WSR-57.

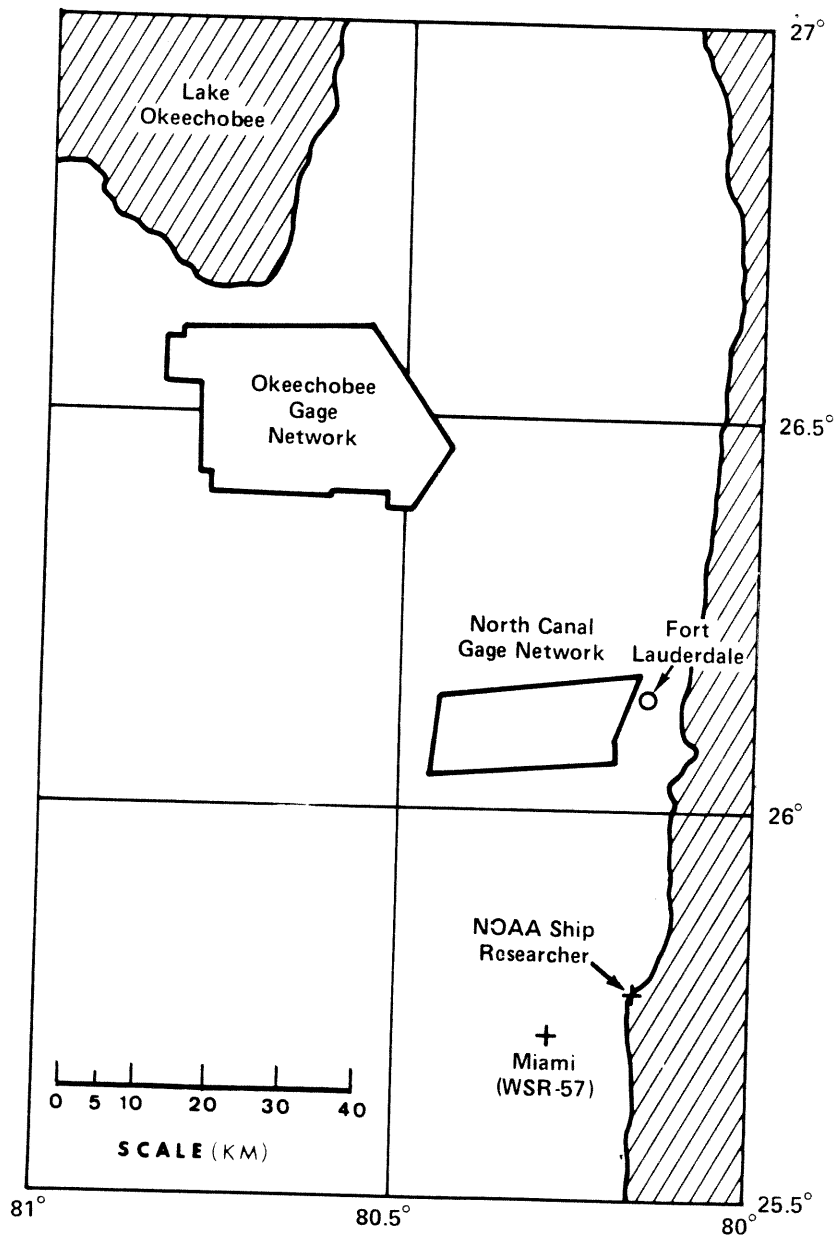


Figure 4.--Location of the Researcher and WSR-57 radars and the rain-gage networks for the pre-GATE test in southern Florida during July 1973.

The Okeechobee rain-gage network outlined in figure 4 provided an average gage density of about one gage per 3 km² (Woodley et al., 1975), with the 230 gages almost uniformly distributed over the 650-km² area. Ten percent of the sites had tipping-bucket recording rain gages while the other 90 percent only had nonrecording gages. The North Canal gage network illustrated in figure 4 was far less densely instrumented than the Okeechobee network, with only seven gages in the 325-km² area or one gage per 45 km². Four of the seven gages were recording and three were nonrecording.

4.2 Equations for Florida Analysis

The Researcher radar equation at the time of the Florida analysis, expressed in a form analogous to eq. (3), was

$$Z_e^* = \bar{P}_r^* + 20 \log (r) + 77.5 . \quad (10)$$

In addition, an attenuation correction term was added to eq. (10), giving

$$Z_e^* = \bar{P}_r^* + 20 \log (r) + 77.5 + A_2 , \quad (11)$$

where A_2 is two-way attenuation in decibels. The A_2 values used for deriving the radar estimates over the Okeechobee and North Canal gage networks are given in table 3.

The C-band atmospheric attenuation values given in table 3 are approximately equal to those given by the equations derived in section 7.1 for a mean GATE atmosphere. The 0.75-dB correction for intervening rainfall is a somewhat arbitrary amount based on examination of the instantaneous radar rain-rate maps. An example of a typical map is the one shown in figure 5 from the WSR-57 for 1840 EDT, July 27, 1973, which illustrates that the intervening rainfall between the Researcher radar site and the rain-gage network (in this case the North Canal network) was light to moderate. Although the rainfall rates over the North Canal network were much heavier in the first and last hours of the 3-hr storm than they were at 1840 EDT, heavy rainfall cores were typically not observed between the radar site and the closest boundary of the gaged area. The same was true for the 3-hr observation period over the Okeechobee network on July 26.

Table 3.--Total two-way signal attenuation (dB), by atmospheric constituents and intervening rainfall, used for deriving the C-band radar rainfall estimates over the Okeechobee and North Canal Networks.

Network	Range to network centroid	Atmospheric (O ₂ + H ₂ O)	Rainfall	A ₂
North Canal	40 km	0.9	0.75	1.65
Okeechobee	95 km	1.9	0.75	2.65

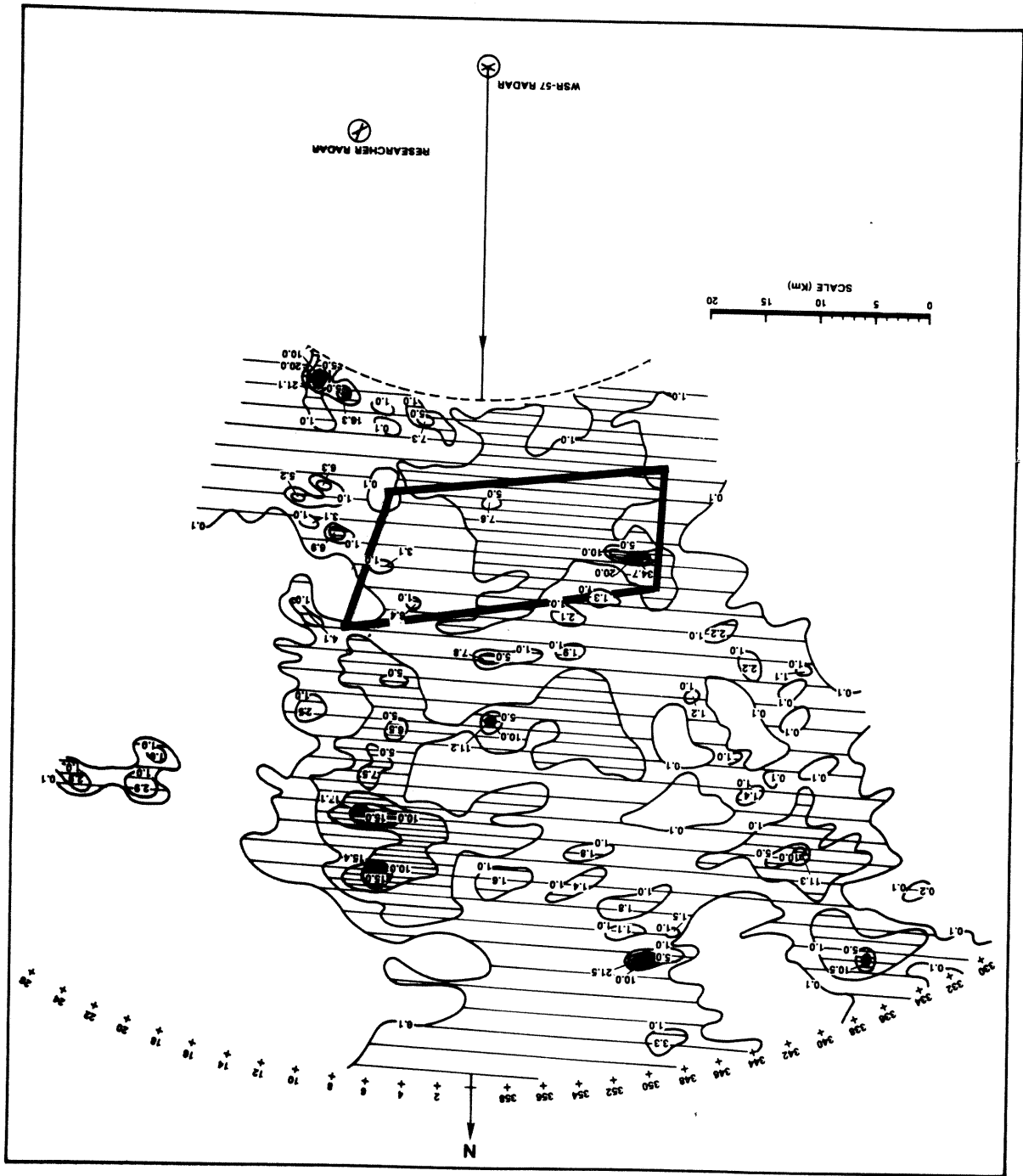


Figure 5.--Map of instantaneous rain-rate (mm hr^{-1}) from WSR-57 radar data at 1840 EDT, July 27, 1973.

The 0.75-dB rainfall attenuation correction is founded partly on the observation that heavy attenuation from very intense intervening rainfall cores or lines lying between the radar site and the boundary of the gage networks was generally not encountered during the two test periods. Also, based on intercomparison of fields from the Researcher's 5-cm radar and the unattenuated 10-cm WSR-57, the constant 0.75 dB applied to all Researcher estimates appeared to compensate, in the mean, for rainfall attenuation between the radar origin and the gage networks. This amount of attenuation roughly corresponds to that expected from, for example, a uniform rainfall rate equal to 10 mm/hr along a 20-km one-way path (round trip path equal to 40 km).

Because of the great spatial and temporal variability of convective precipitation, a significant part of the uncertainty accompanying the Researcher radar estimates presented in this chapter still can be attributed to rainfall attenuation. Space- and time-dependent corrections for rainfall attenuation were included in the derivation of the refined precipitation estimates for GATE.

Except for the transmitter power and the antenna gain, the "radar constant" term (77.5 dB) in eq. (11) is based on the radar characteristics given in table 2, and incorporates the 3.0-dB processing bias described in section 3.1. The best estimate for the gain of the Researcher's antenna at the time of the Florida test was 36.7 dB. This estimate was based on measurements made on an antenna range just prior to the shipboard implementation. The transmitter power measured at the time of the Florida test was 205 kW at the directional coupler. The resultant difference in the radar constant term given in eq. (11) and that ultimately used for processing the GATE reflectivities is

$$[2(\text{Gain}_F - \text{Gain}_G) + 10 \log \left(\frac{P_{t,F}}{P_{t,G}} \right)] , \quad (12)$$

where the Florida and GATE antenna gains and transmitter powers are given by Gain_F and Gain_G , and $P_{t,F}$ and $P_{t,G}$, respectively. The gains expressed in decibels are multiplied by 2 because the gain (G) appears as a squared quantity in the basic radar equation, (1). Therefore, the difference is

$$[2(36.7 - 35) + 10 \log \left(\frac{205}{225} \right)] \approx 3.0 \text{ dB}$$

The Researcher radar receiver and DVIP were aligned on July 25, 1973, and a "bench" calibration identical to those carried out during GATE was made (see sec. 3.2). A least-squares fit to these calibration data using a third-degree polynomial model, as was done for deriving eq. (4), gave

$$\bar{P}_r^* = -101.35 + 0.48 D - 2.07 \times 10^{-3} D^2 + 4.94 \times 10^{-6} D^3 , \quad (13)$$

with a standard error of estimate equal to 1.25 dB. A check of the calibra-

tion curve at the end of the Florida test period on July 27 showed no departures greater than 1 dB from eq. (13). The Researcher DVIP was realigned before GATE, and new calibration curves were determined (sec. 3.2).

For the Florida analysis, a Z-R relationship based on raindrop-size data collected in the Miami vicinity was used (Wiggert and Ostland, 1975). The Miami relationship is

$$Z = 300 R^{1.4} , \quad (14)$$

where the units are as given in section 3.3.

4.3 Analysis and Results

A 3-hr period of rainfall was observed over the eastern two-thirds of the Okeechobee network between 1640 and 1940 EDT on July 26, 1973. Figure 6 shows an isohyetal map for the 3-hr period based on an analysis of the rain-gage catches in the Okeechobee network. The largest 3-hr totals exceeded 45 mm (1.75 in.) in the north-central portion of the network. The dashed lines are isochrones of rain start times, which were derived from the recording rain-gage records.

The 3-hr amounts from the nonrecording rain gages were distributed into hourly amounts using the records from the recording rain gages, and arithmetic mean rainfall depths over the eastern two-thirds of the Okeechobee network were calculated for each hour. The left portion of figure 7 compares the hourly, and 3-hr, totals from the rain-gage analysis for the July 26 storm with the estimates from the Researcher and WSR-57 radars. The agreement between the WSR-57 estimates and those from the gages is remarkably good for all hours. However, the Researcher estimates are significantly low for all hours.

On July 27, the day after the Okeechobee measurements, radar observations were made of rainfall occurring over the North Canal network from 1700 to 2000 EDT. Figure 8 is an isopercental analysis of the rainfall distribution over the North Canal network based on data from the four recording rain gages located at the corners of the network. The isolines provide an estimate of the percent of the daily catch by the nonrecording rain gages during the 3-hr period. The upper and lower numbers shown in figure 8 for the recording gage sites are the 3-hr and daily rainfall totals (inches), respectively, and the values given at the nonrecording gage sites are the daily totals.

Using the isopercental analysis and only the data from the central nonrecording gage, together with the data from the four recording gages, an arithmetic mean was calculated for the 3-hr depth of rainfall over the North Canal area. No attempt was made to distribute the rainfall into hourly amounts, as was done over the Okeechobee network for July 26. The relatively sparse rain-gage network in the North Canal area was considered inadequate for resolving the hourly distribution because of the large spatial and temporal variabilities that exist in convective precipitation (figs. 5 and 6).

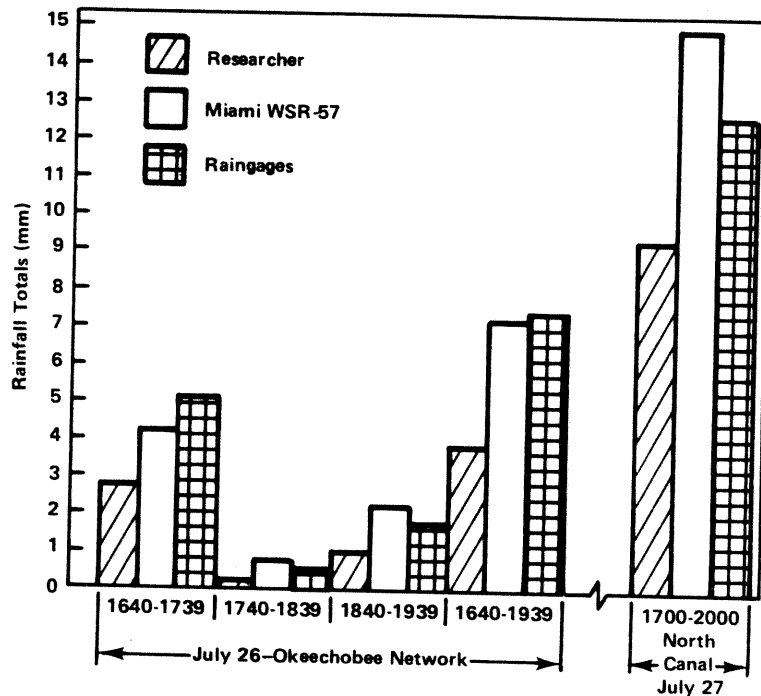


Figure 7.--Comparison of radar and rain-gage network estimates for the July 26 and July 27 storms.

The extreme right part of figure 7 compares the estimates for the 3-hr rainfall total over the North Canal network determined from the gages, the WSR-57 radar, and the Researcher radar. As in the case of the comparisons over the Okeechobee network for July 26, the Researcher estimate is low relative to both the rain gages and the WSR-57. The fact that the Researcher radar is in closer agreement with the North Canal gages than with the Okeechobee network is not considered significant, since the error in the estimate from the gages is potentially large because of the low gage density in the North Canal network. In this case, the WSR-57 radar estimate may be the best estimate of the "true" rainfall.

4.4 Conclusions From Florida Experiment

The pre-GATE Florida test was invaluable for assessing the overall performance of one of the C-band digital radars under shipboard conditions. Experience gained during the test and the post-analysis periods resulted in feedback that was used further to streamline the system and the observational procedures.

Although the small number of radar/gage and radar/radar comparisons, when considered alone, was insufficient to draw final conclusions about the absolute accuracy of the calibration of the Researcher radar system, several results are worth noting.

The Researcher rainfall estimates were consistently low relative to both the WSR-57 and the rain gages. Table 4 summarizes the rainfall and reflectivity differences between the estimates from the Researcher and those from either gage measurements or the WSR-57. The estimate from the Okeechobee

- = NON-RECORDING RAINGAGE
- ⊙ = RECORDING RAINGAGE

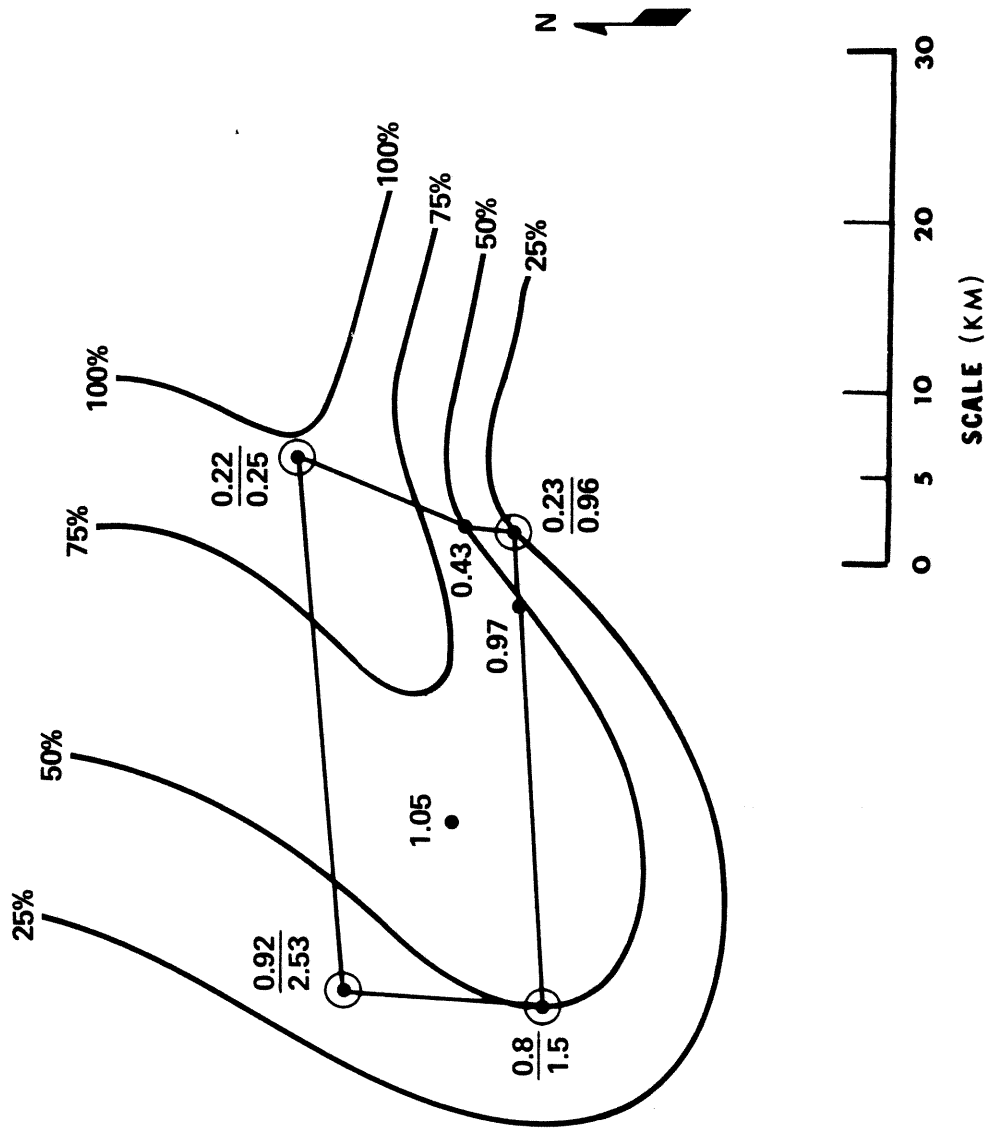


Figure 8.--Isopercental analysis for the North Canal network giving the percent of the daily rainfall on July 27, 1973, that fell from 1700 to 2000 EDT.

Table 4.--Differences in decibels between the 3-hr rainfall totals measured with the Researcher radar, the Okeechobee rain gage network, and the WSR-57 radar, and the equivalent differences in decibels in the mean reflectivities using the Miami Z-R relationship.

	1640-1940 EDT, July 26 (<u>Researcher</u> minus gages)	1700-2000 EDT, July 27 (<u>Researcher</u> minus WSR-57)
Rainfall	-2.8	-2.1
Reflectivity	-3.9	-3.0

rain-gage network was used as the standard for the July 26 period; while, for reasons discussed in section 4.3, the WSR-57 was used as the standard for the July 27 period.

Low radar rainfall estimates do not necessarily signal bad hardware calibrations if the magnitudes of the discrepancies are less than, say, a factor of two (3 decibels). Even with apparently accurate hardware calibrations, many other investigators have observed the tendency for radar to underestimate the magnitudes of rainfall unless the theoretical radar equation is adjusted by a factor derived from an experimental comparison with independent data (e.g., with a rain-gage network; Jones and Bigler, 1966, pp. 11-13). Woodley et al. (1975) reported that the Miami WSR-57 rainfall estimates from data collected in 1972 for FACE, unadjusted by gages, underestimated the gage catches by approximately 35 percent in the mean. Considering this finding, it may be fortuitous that the WSR-57 estimates presented here are so remarkably close to the gage catches. It is likely that a larger sample of storms would have revealed some cases with low WSR-57 estimates and even lower Researcher estimates. In any case, the fact that the Researcher estimates are consistently low relative to both the gage catches and the WSR-57 remains a significant finding.

Based on the results from the Florida analysis, it seemed probable, but not conclusive, that a bias existed in the hardware calibrations of the Researcher radar. The magnitude of the bias was estimated to be 3 to 4 decibels for reflectivity factor estimates (table 4). The biggest uncertainty in the derivation of the rainfall estimates from the Researcher data was the method used to correct for intervening rainfall attenuation. However, considering the arguments presented in section 4.2, it is unlikely that this source of error could explain more than 1 or 2 decibels of the bias. Corroborating evidence that the initial gain measurements for the Researcher's radar antenna were in error is given in the next chapter.

5. SYSTEM GAIN MEASUREMENTS

As shown in eq. (1), an accurate determination of the antenna gain (G) is a prerequisite for obtaining good quantitative estimates of the equivalent reflectivity factor (Z_e) with a radar. Of all the radar parameters in eq. (1), G is the most difficult to evaluate accurately and has been known with

the least certainty in many previous radar experiments. Because G appears as a squared quantity in the radar equation, even a relatively small error in G can lead to a significant error when solving for Z_e .

One of the common, and probably one of the most accurate, methods used for determining the gain of an antenna is the gain-comparison method described by Smith (1974). It was used to measure the gain of the Researcher radar antenna on an antenna range before shipboard implementation and the subsequent Florida pre-GATE test in July 1973 (ch. 4). This technique is frequently used by engineers to evaluate the efficiency (gain) of an antenna before it is integrated into a radar system, but it is difficult to use once the antenna becomes a part of the fully assembled radar system. Further, the gain comparison approach does not take advantage of the fact that a potential source of error in the calibration procedure can be eliminated by determining an effective system gain that includes the antenna gain minus waveguide, rotary joint, and radome losses.

Two methods of measuring effective system gain, which have acquired general acceptance in the field, are the standard horn and the standard target techniques (Geotis, 1975). Both types of measurements were made for the C-band radars used during GATE.

5.1 Standard Horn Method

The standard-gain horn technique, which might also be called a power-transfer measuring method (Smith, 1974), was first presented by Austin and Geotis (1960) as a viable procedure for measuring the effective system gain of a fully assembled weather-radar system. The following equation is used to relate the transfer of power between the radar antenna and a very accurately calibrated standard antenna (horn):

$$\bar{P}_h = (\bar{P}_t G_t G_h \lambda^2) / (16 \pi^2 r^2), \quad (15)$$

where r is the distance (range) between the two antennas, \bar{P}_t and G_t are the average transmitted power and the gain of the transmitting (radar) antenna, respectively, and \bar{P}_h and G_h are the average received power and the gain of the receiving antenna (standard horn). Equation (15), often called the "Friis transmission formula" (see Smith, 1974), applies when the separation between the two antennas, r , exceeds the minimum far-field distance of both. The two antennas are oriented to give maximum power at the receiving antenna as indicated by a maximum reading on a power meter.

Standard horn gain measurements were made for the Quadra and Oceanographer radars in January 1974, while the two ships were berthed at their home ports in Victoria, B. C., and Seattle, Wash., respectively. Measurements were made again for the Oceanographer radar and for the Researcher and Gilliss radars on June 1, 1974, while the three ships were berthed at Dodge Island, Miami, Fla., just before their departure for the GATE area. Figure 9 shows the physical setup for the Miami gain measurements.

The standard horn technique has several advantages (Smith, 1974; Geotis, 1975). The measured gain is the effective gain. That is, it includes

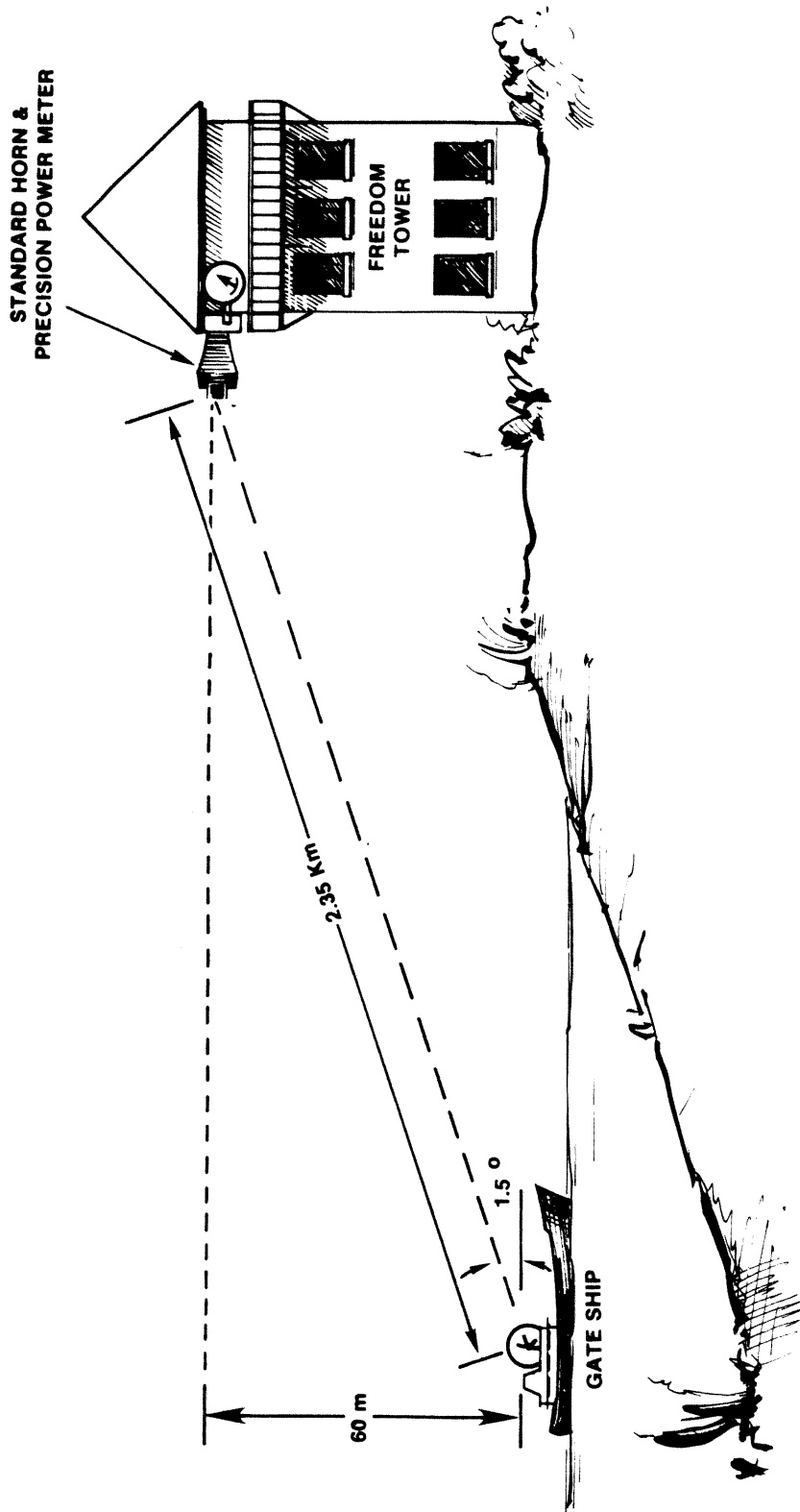


Figure 9.--Physical arrangement of the GATE radar ship(s) and the standard horn located on the Freedom Tower in Miami during the test on June 1, 1974.

Table 5.--Effective antenna system gains for the two NOAA GATE radars as determined by the standard horn technique

Location	Date	Radar	Range to horn (km)	Approximate height of horn (m)	Gain at directional coupler (dB)
Seattle	1/74	<u>Oceanographer</u>	0.75	unknown	39.0
Miami	6/1/74	<u>Oceanographer</u>	2.35	60	39.9
Miami	6/1/74	<u>Researcher</u>	2.35	60	33.9

transmission losses through the waveguide and radome. Second, any errors in the directional coupler insertion loss, which is used both in measuring \bar{P}_t and in routine calibrations of the receiver with a signal generator, will cancel out in the final measurements of reflectivity. Also, if the same power meter (or one calibrated against it) is used to measure the power transmitted and the power received and to set the signal generator, errors in the absolute calibration of the power meter will cancel out. Figure 10 illustrates an arrangement of the test equipment with respect to the radar system components whereby these advantages can be realized.

Solving for G_t from eq. (15) gives

$$G_s = \left(\frac{16\pi^2 r^2}{\lambda^2 \bar{P}_t G_h} \right) \bar{P}_h, \quad (16)$$

where G_t has now been replaced by G_s to indicate system gain. The manufacturer of the standard horn, a Microlab/FXR C638A, specified the gain, G_h , at 5600 MHz to be 21.5 ± 0.2 dB. The range, r , was determined with an X-band tele-meter for the Seattle test and from a navigation chart for the Miami test. The error in r should be no more than 5 m and 100 m for the Seattle and Miami measurements, respectively. After both \bar{P}_t and \bar{P}_h had been measured with the same power meter, as discussed above, G_s was calculated from eq. (16). Table 5 gives the results from the Miami and Seattle tests for the NOAA radars. The values of G_s determined from eq. (16) for the Gilliss and Quadra radars are those given in table 2.

5.2 Standard Target Technique

The standard target technique consists basically of measuring the power returned from a suspended target of a known geometric cross section, which is large compared with the wavelength of radiation and small compared with the pulse volume. For these conditions, the effective antenna system gain can be calculated from the basic radar equation (Smith, 1974) as

$$G_s = 8(\pi)^{3/2} (r^2/\lambda) [P_r/(P_t \sigma)]^{1/2} \quad (17)$$

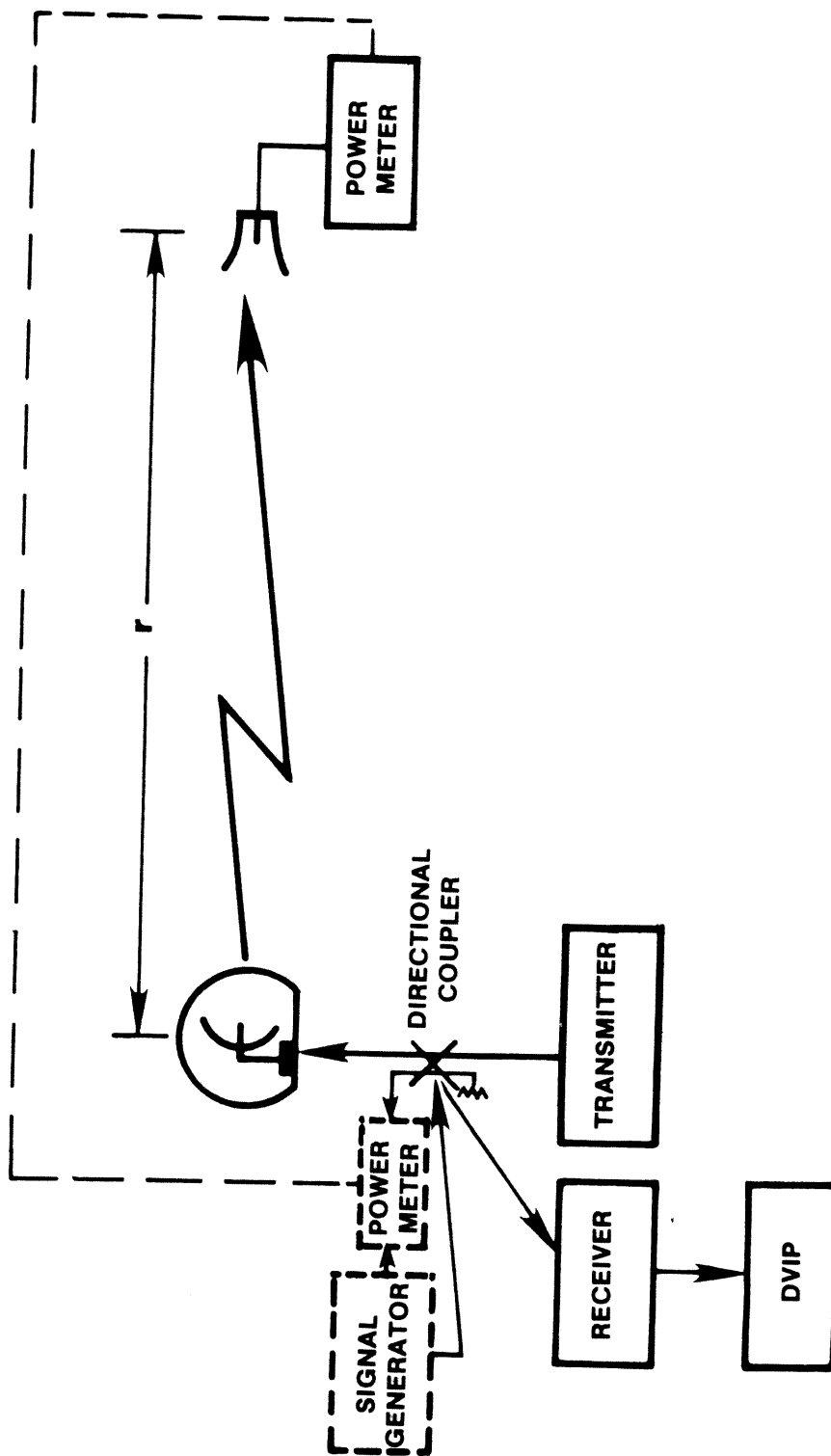


Figure 10.--Arrangement of the test equipment and the radar system components for the standard-gain horn measurements.

where r is the slant range to the target, λ is the wavelength of radiation, σ is the cross-sectional area of the target, and P_t and P_r are the peak transmitted and received powers, respectively.

To minimize problems associated with the attitude of the target, a metallic sphere is often used. For a sphere, σ becomes πR_s^2 , where R_s is the radius of the sphere, and eq. (17) can be rewritten as

$$G_s = \frac{8\pi r^2}{\lambda R_s} \sqrt{(P_r/P_t)} . \quad (18)$$

For GATE, an inflatable mylar sphere with a silver metallic coating was used as the standard target. The nominal diameter of the sphere calculated from the circumference, which was measured before and after each flight, was 122 cm. Slight leakage of the gas charge during the flights, volume changes induced by radiational heating and atmospheric temperature fluctuations, and wind loading caused some deviations from this nominal diameter. It is also likely that wind gusts distorted the sphere into slightly prolate or oblate configurations. Such distortions were assumed negligible, and a sphere with radius equal to 61 cm was assumed for all computations.

A large blimp type balloon, which was routinely deployed during GATE for carrying boundary layer instrument packages, was used for supporting the standard sphere target on June 17, 1974. Figure 11 illustrates the physical setup for collecting the standard target data. The procedures used for taking measurements from the standard target were essentially those described by Smith (1974). First, the average transmitted power (\bar{P}_t) was measured at the directional coupler with a precision power meter (fig. 10); the frequency, shape, and duration of the radar pulses were verified from an oscilloscope display. From this information the peak power transmitted (P_t) was calculated as

$$P_t = \bar{P}_t / (\tau F), \quad (19)$$

where τ is the pulse duration, and F is the pulse repetition frequency.

Next, the radar antenna was oriented toward the captive sphere, the antenna was adjusted to maximize the echo from the target, and the signal strength was noted on an oscilloscope connected to the receiver output. The received power was determined by injecting an RF comparative signal from a signal generator connected to the directional coupler. The slant range to the target was taken from the amplitude-range oscilloscope display, which was calibrated to resolve range to 0.05 km.

The echoes from the calibration target were observed to fluctuate rapidly, making it necessary to continually peak the return by adjusting the antenna elevation and azimuth handwheels. The highest peak that could be obtained by several repetitions of antenna adjustments was taken as one observation. The rapid signal fluctuations often observed from standard targets, which are seldom clearly understood and which make it difficult to obtain a stable

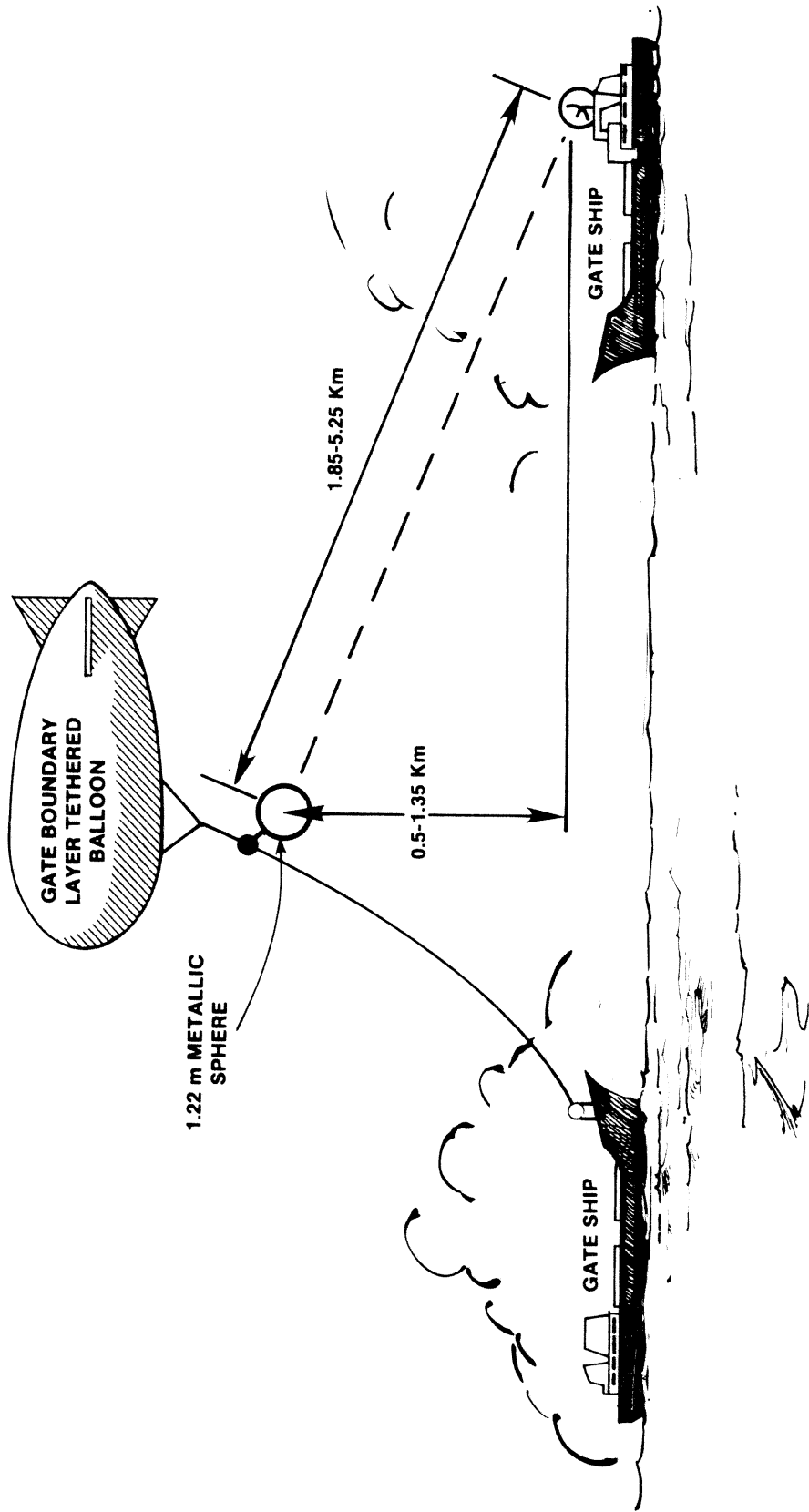


Figure 11.--Physical arrangements of the GATE ships and balloons for the standard target test on June 17, 1974.

measurement, are a serious disadvantage of this technique (Austin and Geotis, 1960; Smith, 1974; Geotis, 1975). Geotis (1975) states: "Measurements of the cross sections of standard targets may be used as checks on overall system performance but are not reliable as absolute calibrations because of the fluctuating nature of the signal." It was in this spirit that the standard target tests were made for GATE; i.e., the measurements were taken to provide a rough check on the gains determined from the standard horn technique. Table 6 gives the values of G_s calculated from eq. (18) for several observations made with the NOAA radars.

Table 6.--Effective antenna system gains for the NOAA radars determined by the standard target technique during a GATE intercomparison period on June 17, 1974

Observation Number	Radar	Slant range to sphere (km)	Flight altitude of sphere (m)	Gain at directional coupler (dB)
1	<u>Oceanographer</u>	3.55	500	42.3
2	"	3.75	500	40.3
3	"	3.75	500	40.3
4	"	5.25	1350	41.2
5	"	4.95	1350	41.2
6	"	4.50	1350	40.4
1	<u>Researcher</u>	3.75	500	34.0
2	"	1.85	500	35.6
3	"	1.85	500	34.4

5.3 Conclusions From System Gain Measurements

Comparison of tables 5 and 6 shows that the standard horn and standard target techniques gave gains that generally agreed to within 1 to 2 dB. However, the standard target method consistently gave higher gain values, possibly because of oscillations in the size and shape of the target and the maximizing procedure used to obtain an observation (sec. 5.2). Generally, the greatest weight should be attached to the standard horn measurements for the reasons previously discussed.

Based on the gain data presented in tables 5 and 6, a value of 39.9 dB was selected as representative for the Oceanographer radar. This corresponds to the value determined from the standard horn gain measurement on June 1, 1974, in Miami, which also falls halfway between the Seattle measurement made in January 1974 and the average of the gain values determined from the standard target observations. It is unlikely that an error exceeding 0.5 dB will be made by selecting 39.9 dB as the best estimate for the Oceanographer radar gain.

The decision to select 35.0 dB (table 2) as the representative value for the gain of the Researcher radar combined consideration of the gain data presented in tables 5 and 6 with the results from the 1973 Florida analyses (ch. 4). As was anticipated based on the findings from the 1973 Florida analyses, all the system gain measurements given in tables 5 and 6 are significantly lower than 36.7 dB, which was the value determined by subtracting the measured "microwave plumbing" losses from the antenna gain, G_t , obtained on an antenna range using the gain-comparison method. Considering eq. (12) and the results presented in section 4.4, it seems likely that the "true" system gain for the Researcher radar is no higher than 35 dB = 36.7 dB - 1.7 dB. Similarly, it is unlikely that the gain is as low as the 33.9 dB given in table 5, since the reflectivity factor estimates using 33.9 dB would be more than 5 dB greater than those based on the 36.7 dB gain used for the 1973 Florida analysis. Although the standard horn technique generally is superior to the standard target technique, this is apparently not the case here. This may be because the Researcher radar antenna and the standard horn were slightly misoriented for the maximum power transfer. Also, the gain estimates from the standard target technique for the Researcher may be proportionally low, since the Researcher's antenna could not be controlled with the precision needed to maximize rapidly the echo from the target.

A somewhat subjective decision was made to select 35 dB as the best estimate for the Researcher radar gain, which still gives a 2.5 dB greater difference between the Oceanographer and Researcher gains than can be explained due to differences in beam widths alone. However, the next chapter, which includes intercomparisons of reflectivity fields in areas of overlapping coverage between the two NOAA radars, confirms this was a good decision.

6. COMPARISONS MADE PRIOR TO SEPTEMBER 1975 BETWEEN OVERLAPPING REFLECTIVITY MEASUREMENTS

One method of identifying relative biases between the reflectivity measurements from two or more radars is to compare reflectivity factor estimates from the various radars for the same areas and times. This technique is simplified for collocated sensors (ch. 8), but it can also be used for separated sensors by selecting suitable overlap regions. Wilson and Pollock (1974) have used this approach to compare hourly estimates, averaged over a 180-km² rain-gage network near Rochester, N.Y., obtained from radars located at Buffalo and Oswego, N.Y.

In general, intercomparisons can be made for instantaneous point estimates or for temporally and/or spatially averaged estimates. Analysis procedures might range from simple visual inspection of Cartesian data displays to objective statistical analyses. Several space and time scales and analysis techniques have been used here.

In May 1975, plan-position indicator (PPI) printer plots were generated for the two NOAA radars, using the radar characteristics given in table 2 for the radar equations, for the times given in table 7. The PPI displays from the NOAA radars for the 23 matching times shown in table 7 were first visually

Table 7.--Times of NOAA radar scans that were used to compare data in overlap areas between the C-band radars

Date (1974)	Julian day	Time (GMT)	<u>Oceanographer</u>	<u>Researcher</u>	Radars compared*
June 30	181	0700	X	X	O & R
		0745	X	X	
July 7	188	1230	X	X	O & R 1230-1500 O & G 1330-1415
		1300	X	X	
		1330	X	X	
		1415	X	X	
		1430	X	X	O & Q 1500-1600
		1500	X	X	
		1530	X		
1600	X				
July 13	194	1900	X	X	O & R
		2000	X	X	O & Q
July 28	209	0015	X	X	O & R
		0100	X	X	
		0430	X	X	
		0530	X	X	O & Q 0530
Aug. 3	215	0200	X	X	O & R
		0300	X	X	
		0400	X	X	
		0430	X	X	
Aug. 8	220	0930	X		O & G
		1015	X		
		1200	X		
Aug. 9	221	2100	X		O & Q
		2200	X		
		2300	X		
		2400	X		
Aug. 10	222	0700	X		O & G
		0800	X		
		0900	X		
		1015	X		
Aug. 12	224	0500	X	X	O & R
		0600	X	X	
Sept. 5	248	1200	X		O & Q 1200-1400
		1300	X		
		1400	X		
		1945	X	X	O & R 1945-2015
		2000	X	X	
		2015	X	X	

* G = Gilliss; O = Oceanographer; Q = Quadra; R = Researcher.

compared at CEDDA. Copies of all NOAA scans (table 7) were then sent to the groups processing the Gilliss and Quadra radar reflectivity data at MIT and McGill University, respectively, for comparison with their data.

Figures 12 and 13 are sample displays of the Oceanographer and Researcher reflectivity data for 0600 GMT August 12, when a line of convection associated with the intertropical convergence zone lay between the two radars. The Oceanographer and Researcher were located at the positions shown in figure 1. Figures 12 and 13 show that the patterns match very well and that the reflectivity factor estimates generally agree to within a few dBZ. This sample comparison of reflectivity patterns from the NOAA radars typifies the good agreement that normally was found for all of the visual intercomparisons done at CEDDA, MIT, and McGill University. The core areas of the reflectivity patterns, in optimum overlap regions between the radars, seldom disagreed by more than 3 dBZ.

The next phase of the analysis consisted of objectively comparing various echo parameters and statistics, derived from the NOAA reflectivity data, in the central overlap region between the Oceanographer and Researcher (fig. 14). The overlap region was defined by the intersection of arcs from 110-km radii circles centered at the radar origins. As will be shown in chapter 7, both radars give good quantitative coverage within the 110-km ranges. The results from the overlap analyses are presented in sections 6.1 and 6.2.

Finally, volumetric water estimates from the NOAA radars were compared for the echo populations observed within 150-km radii of the respective radar origins at the 23 matching times (table 7). The results from this comparison are presented in section 6.3.

6.1 Cross-Correlation of Reflectivity Fields

Cross-correlation of reflectivity fields from the two NOAA radars, inside the 7500-km² overlap region shown in figure 14, was the first objective statistical method used at CEDDA to compare the reflectivity measurements. Initially, the correlations were made for the 23 matching times (table 7) using the instantaneous 4-km x 4-km Cartesian data and only those common data bins for which reflectivity values from one or both of the radars were greater than 24 dBZ (\approx 1 mm/hr). Correlation coefficients were calculated for each time from the following formula:

$$\rho = \frac{\Sigma [(Z_{oi}^* - \bar{Z}_o^*) (Z_{ri}^* - \bar{Z}_r^*)]}{[\Sigma (Z_{oi}^* - \bar{Z}_o^*)^2 \Sigma (Z_{ri}^* - \bar{Z}_r^*)^2]^{1/2}} \quad (20)$$

where ρ is the correlation coefficient; Z_{oi}^* and Z_{ri}^* are the reflectivity values for i th data bin, expressed in decibels, for the Oceanographer and Researcher, respectively; and \bar{Z}_o^* and \bar{Z}_r^* are the corresponding mean reflectivities.

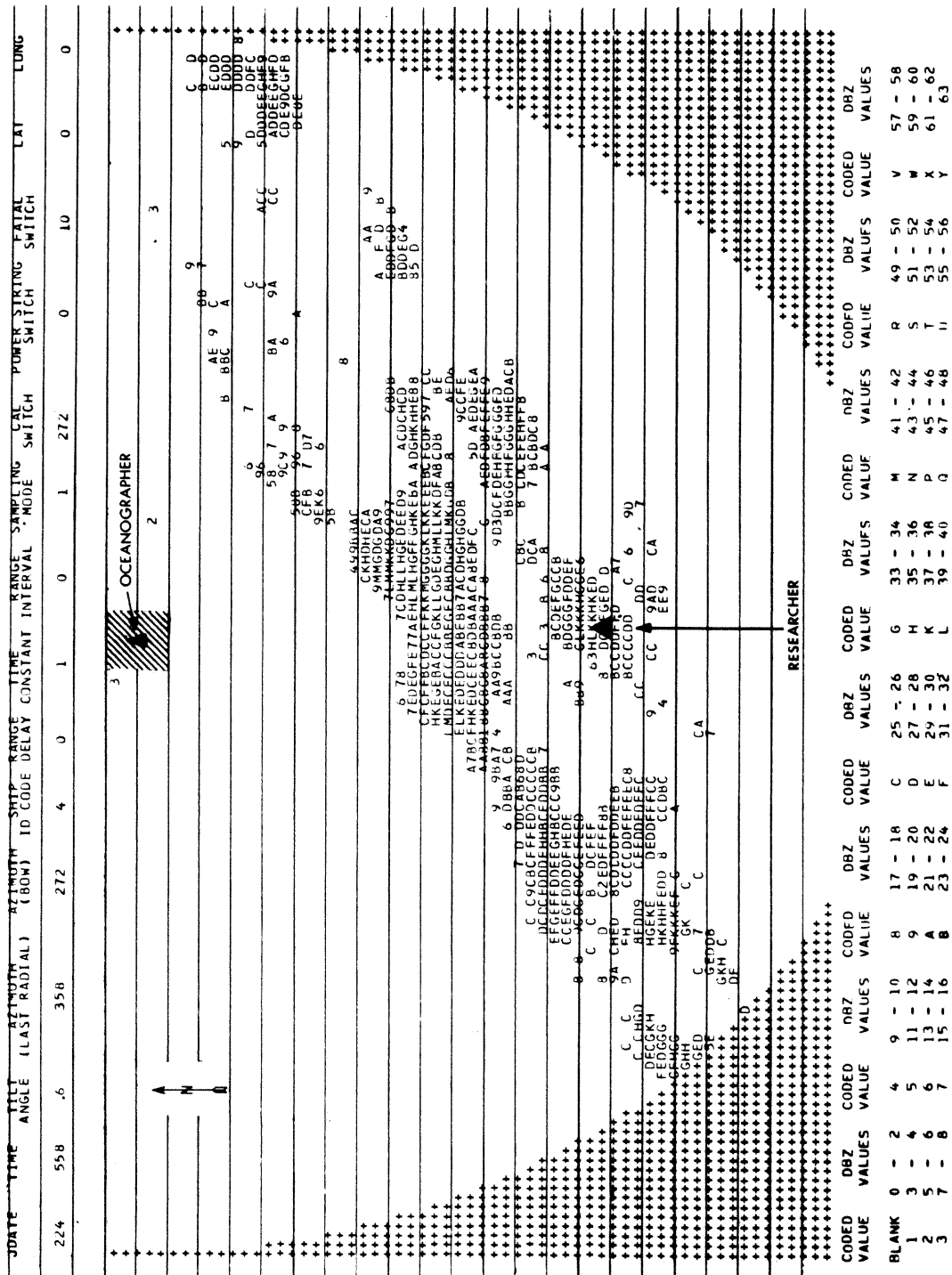


Figure 12.--Display of 4-km x 4-km reflectivity data bins from Oceanographer radar for 0558 GMT August 12.

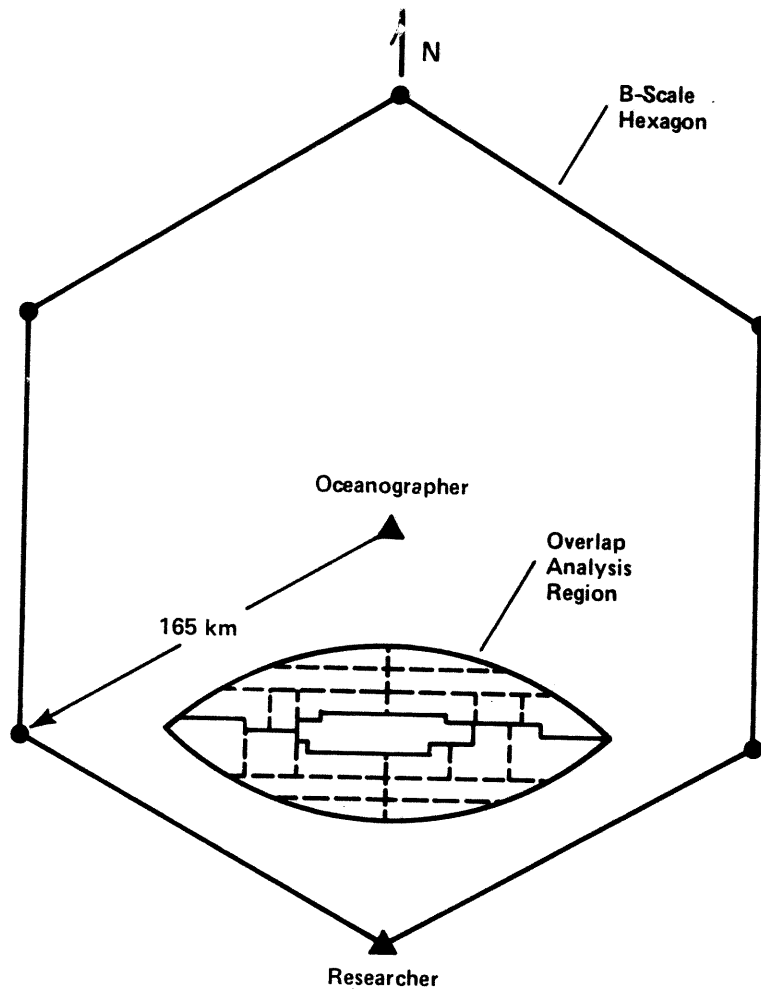


Figure 14.--Schematic for Phases I and II of the central overlap analysis region, and the 21 subareas, between the Oceanographer and Researcher where various echo parameters and statistics were compared.

The variance of the 23 correlation coefficients for the instantaneous 4-km data was found to be very high; ρ ranged from 0.1 to 0.9, and only 25 percent of the values were greater than 0.5. The low coefficients for the bin-to-bin cross-correlations of the instantaneous fields were expected, since the locations of the reflectivity data from the two radars in time and space were not necessarily exactly coincidental. Although every effort was made to synchronize the clocks and the data collection schedules on all GATE ships, differences as large as 1 to 2 min between observation times on the Oceanographer and Researcher sometimes occurred. More important, the relative error in location of the data fields in space may have been as great as 12 km (1 1/2 data-bin error per ship), because both ships were assumed to be located at their Phase mean positions. The high resolution "renavigated" ship positions (Seguin and Crayton, 1975), which were used for the final

B-scale rainfall analysis, were not available when these intercomparison correlations were made.

The reflectivity fields from the two radars showed excellent agreement in the basic structure of the patterns (figs. 12 and 13). However, it seemed clear from the visual comparisons of the 23 sets of displays that the 4-km instantaneous cross-correlations often would have been much improved by lagging the fields relative to each other in the x and/or y directions. This was not done because the effort required to set up the computer software to handle the two-dimensional lag-correlation analysis did not seem warranted for our primary objectives here, which were to determine if the basic features of the patterns were correlated and to identify mean biases between the two radars. Furthermore, bin-to-bin correlations of instantaneous reflectivity data from two noncollocated radars would often be very noisy, even for land-based radars where the data navigation errors should be small. Discrepancies still may originate from differences in, for example, attenuation effects, beam refraction, sampling altitude, and sampling volume.

It seems unlikely, based on the above discussions, that consistently high cross-correlation coefficients can be expected unless the data have been averaged or smoothed in space and/or time. To test this premise, the next part of our analyses consisted of first averaging the reflectivity values, for each radar, within the 21 subareas shown in fig. 14; the average size of the subareas was 360 km^2 . The resultant pairs of average reflectivities, for which the value from one or both radars were nonzero, were then used to calculate ρ for each of the 23 times. Equation (20) was used to calculate the ρ 's where the index, i , now pertains to the 21 subareas. Figure 15 summarizes the results from the cross-correlation calculations in the form of a relative frequency histogram, which shows that the spatial averaging significantly improved the cross-correlations. One hundred percent of the correlation coefficients are greater than 0.5, and 75 percent exceed 0.8. The 25 percent of the cases with ρ less than 0.8 probably corresponds to those times when the data navigation errors were the largest.

Finally, the reflectivity data were also averaged in time, as well as in space, and cross-correlation coefficients were calculated. The averaging periods and resulting correlation coefficients are given in table 8, which shows that the correlations are improved further by averaging in time. The averaging periods are roughly equivalent to 1 1/2- to 2-hr intervals, if we assume that the same number of scans were observed at the routine GATE sampling interval; i.e., one base-tilt scan each 15 min.

In summary, the cross-correlation analyses established that, even with data navigation errors as large as several kilometers, reflectivity fields from the two NOAA radars were very highly correlated when the reflectivities were averaged over spatial and temporal scales ($\approx 360 \text{ km}^2$, $\approx 2 \text{ hr}$) that were smaller than the smallest scales being used for atmospheric energy and water budget studies ($\geq 4000 \text{ km}^2$, $\geq 3 \text{ hr}$).

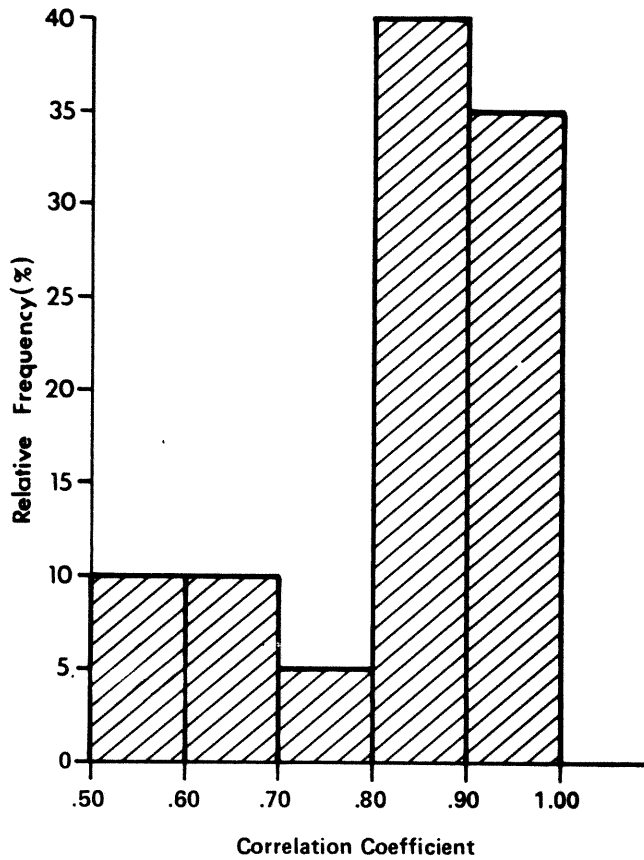


Figure 15.--Relative frequency histogram of the coefficients of cross-correlation between mean subarea reflectivities from the two NOAA radars for 23 intercomparison times.

Table 8.--Coefficients of cross-correlation between the mean subarea, time-averaged reflectivities from the two NOAA radars

Period*	Total No. of scans	Correlation coefficient
Phase I, excluding the scans from Julian day 188	5	0.96
Julian day 188 scans	6	0.96
Phase II scans	10	0.94

* The general periods (scans) identified here comprise the specific times given in table 7.

6.2 Comparison of Areal Mean Parameters in the Central Overlap Region

The previous section established that the basic features of the reflectivity patterns from the two NOAA radars were highly correlated. In this section and in section 6.3, the magnitudes of the reflectivity measurements from the two radars are compared in an attempt to identify any relative biases between the radar systems.

Echo area, which was the first areal parameter compared in the overlap region, was determined by taking the area covered by echo intensities greater than 24 dBZ (≈ 1 mm/hr). Figure 16 is a scatter diagram of the Oceanographer versus Researcher echo areas for the 23 matching intercomparison times. The plot shows good agreement between the two radars, and, for this small sample, there appears to be no significant bias between the radars. The largest echo area observed was approximately 4500 km², or 60 percent coverage of the total overlap analysis region.

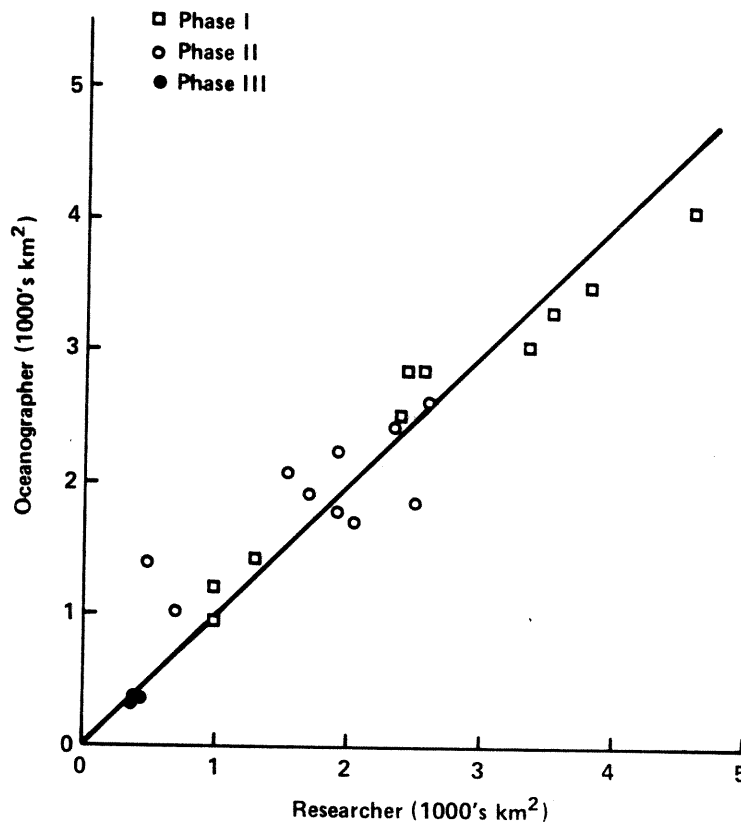


Figure 16.—Scatter diagram of the echo areas observed in the 7500-km² overlap analysis region by the two NOAA radars for 23 intercomparison times.

The next phase of the overlap analysis consisted of comparing mean reflectivities from the two NOAA radars for the total overlap analysis region and for the following three subregions shown in figure 14: (1) the northern area bounded by the 110-km arc from the Researcher and the solid line segments through the center of the overlap analysis region, (2) the small area at the center of the overlap region bounded on all sides by solid line segments, and (3) the southern area bounded by the solid line segments through the center of the overlap region and the 110-km arc from the Oceanographer. The mean reflectivities were calculated from

$$\bar{Z}^*_{jk} = (\sum Z^*_{ijk})/N_j \quad (21)$$

where \bar{Z}^*_{jk} is the areally averaged reflectivity (in decibels) for the j th subregion and the k th time; Z^*_{ijk} is the reflectivity (≥ 24 dBZ) for the i th data bin within the j th subregion at the k th time; and N_j is the total number of 4-km x 4-km data bins within the j th subregion.

Using values calculated from eq. (21), scatter plots were constructed to compare mean reflectivities from the two NOAA radars for the total overlap region and the three subregions. In these scatter plots (fig. 17), no significant mean bias between the reflectivity measurements from the two radars is apparent, except for the northern area. The Researcher estimates over the northern subregion are on the average about 1 dBZ low relative to the Oceanographer estimates. Although, as will be shown in chapter 7, both radars provided good quantitative coverage for all ranges within 110 km, the Researcher radar mean echo-intensity began to degrade slightly at about 80 km and slowly increased to perhaps 1.0 dB at 110 km. The superior beam width and range effect characteristics of the Oceanographer radar, at least partly, explain the small bias between the reflectivity measurements over the northern subregion. Regardless, since the magnitude of this mean bias is small over the northern subregion and since no overall bias is apparent for the comparisons over the total region, central subregion, and southern subregion, it follows that any relative biases between the calibration of the two radar systems must be very small. For the comparisons over the total analysis region, no differences exceeded 2 dBZ, and 70 percent of the points were within 1 dBZ (fig. 17).

6.3 Comparison of Volumetric-Water Versus Echo-Area Relationships

Another technique that was used to quantitatively compare echo parameters derived from the two NOAA radar data sets consisted of comparing volumetric-water flux versus echo-area relationships. Using a computer algorithm described by Marks and Hudlow (1976), all major echo entities observed with the two NOAA radars at the 23 intercomparison times (table 7) were isolated. For each radar, those echoes that had an area exceeding 100 km² (using a 24-dBZ or 1-mm/hr threshold) and that were completely within 150-km range of the radar were used to derive the points for the scatter plots shown in figure 18. None of the ranges to the centroids of the echoes exceeded 110 km.

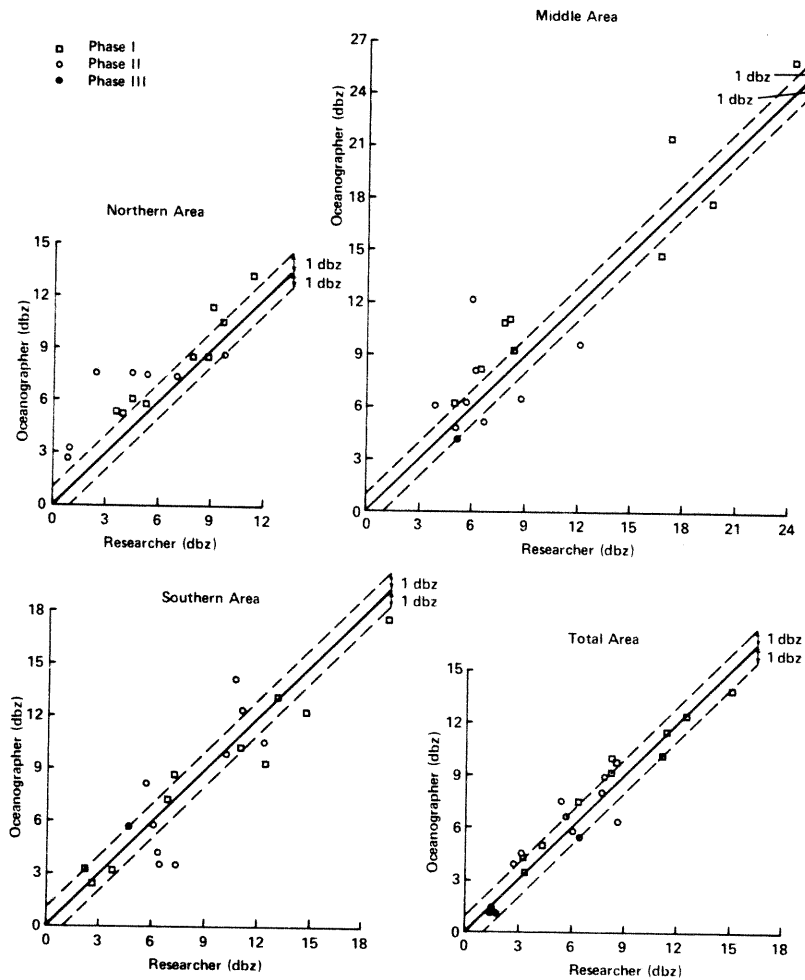


Figure 17.--Comparison of mean reflectivities from the NOAA radar intercomparison data sets over the 7500-km² total overlap analysis region and over the northern, central, and southern subregions.

Since the intercomparison times were selected when major convective activity was concentrated between the Oceanographer and Researcher, most of the echo entities used for the scatter plots were "simultaneously" viewed by both radars, but some of the echoes viewed by one radar were outside the range of the other. Nevertheless, this technique remains a powerful objective procedure for using the statistics of echo populations to evaluate relative calibration differences between two or more radars.

The straight lines shown in figure 18 are least-squares fits based on a logarithmic model analogous to eq. (5). The slope coefficients for the two fits are virtually identical, and the difference in the intercepts is only approximately 0.3 dBR; i.e., this analysis indicates that the Researcher rainfall estimates at middle and closer ranges are overall, in a least-squares sense, 0.3 dBR greater than the Oceanographer estimates. The rainfall estimates

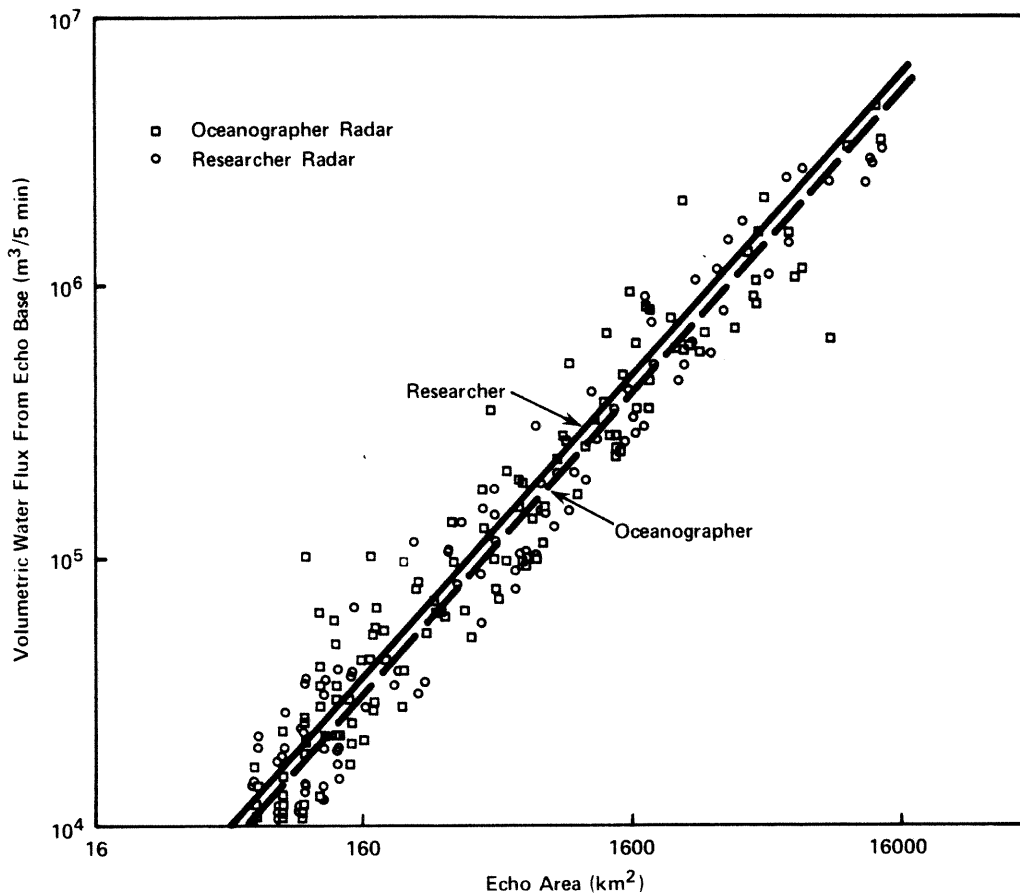


Figure 18.—Volumetric water versus echo area curves derived from the NOAA radar data for 23 intercomparison times.

for both radars were derived using eq. (8), and neither radar set was corrected for atmospheric attenuation nor for the final absolute bias corrections given in section 10.2. To correct approximately for atmospheric attenuation, absolute biases, and for differences resulting from the use of eq. (8) instead of eq. (9), the ordinate values in figure 18 should be multiplied by a factor of 3. This constant adjustment to the volumetric water estimates would not affect the relative intercomparison between the radars.

6.4 Synopsis of Calibrations When Reflectivity Archival Processing Began

Several methods of comparing reflectivity data from the NOAA radars were used to establish that the basic features of the reflectivity patterns from the two radars are highly correlated. Further, the quantitative comparisons presented in sections 6.2 and 6.3 showed that any mean bias between the radar systems was very small.

As noted earlier, the volumetric-water versus echo-area comparison method is a powerful procedure for revealing relative biases between two radars. However, the magnitude of the overall bias detected here was so small, 0.3 dBR, that it could not be judged statistically different from zero. Other evidence will be presented in subsequent sections that supports this finding, namely that the rainfall estimates for Researcher are slightly higher than for the Oceanographer when the radar characteristics given in table 2 are used to derive the radar equations. The small difference was accounted for in the bias corrections used in the derivation of the final rainfall estimates (sec. 10.2), but it was not considered in the processing of the reflectivities for the archives. The characteristics given in table 2 were used, without further adjustment, for processing the reflectivity data for archiving. Also, the reflectivities that were archived from the Gilliss and the two NOAA radars were not corrected for attenuation effects, but attenuation corrections were included in the derivation of the final rainfall estimates.

7. RANGE EFFECTS

As was made clear in section 6.2, it is important to know the performance of a radar as a function of range, if its data are to be used for: (1) quantitative hydrologic work, and/or (2) absolute or relative comparison with another radar. One method that can be used, as a first approximation, to evaluate range effects consists of examining the variation of the mean radar signal, determined from averages over long time periods, as a function of range. The assumption here is that if the time periods are sufficiently long, the true meteorological variations in the rainfall fields will tend to smooth out, and that the remaining range variations will largely represent effects that resulted from deficient beam filling. It will be shown in section 7.2 that while one Phase of GATE data is insufficient to completely satisfy this assumption, it is sufficient to determine first-order range effects.

Another method that sometimes can be used to evaluate radar range effects consists of comparing radar estimates with rain-gage data at various ranges. This method is limited in the case of GATE for determining detailed range performance curves, since gages only existed at a few widely spaced locations aboard the GATE ships (fig. 1). However, comparisons of radar rainfall estimates with shipboard gage catches have been extremely useful as a part of the overall absolute calibration of the radar rainfall estimates (sec. 9.3 and ch. 11).

Deterioration of the mean radar signal with range occurs not only because of deficient beam filling, which results when the spreading and ascending beam is no longer uniformly filled by precipitation particles, but is also due to signal attenuation by intervening rainfall or atmospheric constituents. Attenuation effects are considered in the next section.

7.1 Attenuation Effects

Three sources of attenuation were considered in the derivation of the final radar rainfall estimates (Hudlow, 1977a): (1) atmospheric gases, (2) intervening rainfall, and (3) wet radome. For C-band radiation in the GATE

locality, only attenuation by atmospheric gases has a significant effect on the mean relative range variation curves presented in section 7.2. Of course, the other two sources of attenuation do, at times, significantly affect the absolute magnitudes of the measurements. For example, corrections for wet-radome attenuation were critical to the comparison of the collocated Oceanographer radar and rain-gage estimates (sec. 11.4).

Beginning with normalized attenuation coefficients for diatomic oxygen and water vapor and a GATE mean atmospheric sounding, polynomial expressions giving the total path attenuation from these constituents were derived as a function of range.

Van Vleck (1947a,b) presented the theory of absorption of microwaves by atmospheric gases. More recently, Greene et al. (1963) reviewed the theory of attenuation at wavelengths normally employed for precipitation radars. The atmospheric gases that can cause significant attenuation of microwave radiation are water vapor and oxygen. The gaseous absorption arises principally from the 1.35-cm line of water vapor and the series of lines centered around the 0.5-cm line of water vapor and the series of lines centered around the 0.5-cm line of oxygen. The normalized attenuation coefficients for 5.3-cm wavelength radiation, and a temperature of 15°C, determined from data presented by Bean et al. (1970) are

$$\gamma_{O_2} = 0.007(1.05P^2) , \quad (22)$$

and

$$\gamma_{H_2O} = 0.00028(\rho_w P) , \quad (23)$$

where γ_{O_2} and γ_{H_2O} are the one-way attenuation coefficients (dB km^{-1}) for oxygen and water vapor, respectively, P is atmospheric pressure in atmospheres, and ρ_w is the absolute humidity of the air (water vapor content in grams of water per cubic meter of air). Equations (22) and (23) were derived from the original Van Vleck formulas, except the nonresonant term in the solution for γ_{H_2O} was increased by a factor of four to better satisfy experimental results (Bean et al., 1970). The attenuation coefficients were normalized to 15°C because this corresponds to the temperature of the mean GATE atmosphere at an altitude of about 1.8 km, which corresponds approximately to the height of a radar beam at a slant range of 100 km when emitted from an antenna tilted +0.75° from the horizontal.

The solutions for the total path attenuations from oxygen and water vapor as a function of slant range are

$$A_{O_2} = 2 \int_0^r (\gamma_{O_2}) dr = 2 \int_0^r (0.0074P^2) dr , \quad (24)$$

and

$$A_{H_2O} = 2 \int_0^r (\gamma_{H_2O}) dr = 2 \int_0^r (0.00028\rho_w P) dr, \quad (25)$$

respectively, where A_{O_2} and A_{H_2O} are the total two-way attenuations (dB) for the round-trip between the radar origin and a point located at some slant range, r (km). Before an analytical integration for eq. (24) can be obtained, P must be expressed in terms of r . First, P was expressed in terms of height above sea level, h . This was accomplished by fitting a quadratic to the GATE mean sounding data between the surface and 450 mb ($P \approx 0.45$), which gave

$$P = 0.997 - 1.113 \times 10^{-4} h + 4.238 \times 10^{-9} h^2 , \quad (26)$$

where P is in atmospheres and h is in meters. The standard error of estimate for this least squares fit is 0.001 atmospheres.

To a reasonable approximation, the height of the radar beam above the surface of the earth as a function of range is given by (see Jones and Bigler, 1966),

$$h = 13.07 r + 0.06 r^2 , \quad (27)$$

where, as above, h is height (m) and r is slant range (km). Equation (27) assumes an antenna tilt angle of 0.75° , which is a value near the nominal settings of the NOAA radar antennas during the collection of the low-altitude data that were used for the rainfall analyses.

Next, P was determined as a function of r by substituting the right-hand side of eq. (27) into the right-hand side of eq. (26). The r^3 and r^4 terms of the resultant equations were dropped, since their magnitudes were small relative to the other three terms even for a range of 200 km, and the remaining quadratic expression was substituted into eq. (24). Integration of the squared quadratic yielded a polynomial with five terms. From sensitivity analysis, the magnitude of the r^5 term was found to be insignificant, and the final integral reduced to

$$A_{O_2} = 1.490 \times 10^{-2} r - 2.175 \times 10^{-5} r^2 - 4.755 \times 10^{-8} r^3 + 6.360 \times 10^{-11} r^4 , \quad (28)$$

where A_{O_2} is the two-way attenuation in decibels of the radar signal by oxygen, and r is the slant range in kilometers.

Before an expression analogous to eq. (28) could be derived for A_{H_2O} , one more relationship, which gives ρ_w in terms of h , was required. The desired relationship was obtained by fitting a quadratic to the GATE mean sounding data between the surface and 550 mb ($P \approx 0.55$), which gave

$$\rho_w = 20.65 - 6.60 \times 10^{-3} h + 6.17 \times 10^{-7} h^2, \quad (29)$$

where ρ_w is the absolute humidity (gm m^{-3}) and h is height (m). The standard error for this least-squares fit is 0.275 gm m^{-3} . Using eqs. (26), (27), and (29) to express the integrand in eq. (25) in terms of r and keeping only the significant polynomial terms, the final integral reduces to

$$A_{H_2O} = 1.155 \times 10^{-2} r - 3.250 \times 10^{-5} r^2 - 5.175 \times 10^{-8} r^3 + 2.610 \times 10^{-10} r^4, \quad (30)$$

where A_{H_2O} is the two-way attenuation (dB) of the radar signal by water vapor, and r is the slant range (km).

Corrections based on eqs. (28) and (30) were incorporated in the derivation of the GATE radar rainfall estimates (Patterson et al. 1979) for the Gilliss, Oceanographer, and Researcher. Atmospheric attenuation corrections were applied electronically to the Quadra data before they were recorded. The Quadra corrections were based on a midlatitude mean atmospheric sounding and are somewhat smaller than the corrections applied to the other three radars. Table 9 gives examples of atmospheric attenuation amounts from eqs. (28) and (30) for several ranges.

Table 9.--Two-way attenuation in rainfall rate units (dBR⁺) by water vapor and oxygen for C-band radiation propagating in a mean GATE atmosphere. An antenna elevation of 0.75° is assumed.

Range (km)	H ₂ O	O ₂	H ₂ O + O ₂
10	0.1	0.1	0.2
30	0.25	0.35	0.6
50	0.4	0.55	0.95
70	0.5	0.7	1.2
100	0.65	1.0	1.65
150	0.75	1.3	2.05
200	0.8	1.5	2.3

+ dBR = 0.8 dBZ, using eq. (9)

Attenuation corrections for intervening rainfall also were made to the Oceanographer radar data only during Phases I and II, before the final rainfall estimates were derived. These corrections were included because the quality of the radar data from the Oceanographer, stationed at the center of the B-scale during the first two Phases (fig. 1), was essential to the accuracy of the final estimates obtained by merging the rainfall data from the two NOAA radars (Patterson et al., 1979).

Geotis (1977) derived a relationship between the attenuation coefficient and the reflectivity using electromagnetic theory and drop-size measurements collected on the Gilliss during GATE. The relationship for two-way attenuation expressed in terms of rainfall rate using eq. (9) is

$$\gamma = 1.6 \times 10^{-3} R^{1.1} \quad , \quad (31)$$

where γ is the attenuation coefficient (dBR km⁻¹), and R is the rainfall rate (mm hr⁻¹). A description of the methodology that was developed for applying the intervening rainfall attenuation corrections is given by Patterson et al. (1979).

Large corrections for intervening rainfall attenuation were necessary for only a small percentage of the scans, and significant corrections were confined to only a few data bins within a scan. This is shown by figure 19, which illustrates the magnitude of the corrections for one of the significant attenuation events observed during GATE. The maximum intervening rainfall correction applied to any data bin was less than 5 dBR for all Oceanographer scans. For about 90 percent of the hours during Phases I and II, the maximum correction(s) applied during the hour to any data bin(s) was less than 2 dBR. Table 10 summarizes the number of hours for which various maximum attenuation corrections were applied to at least one data bin sometime within an hour.

Table 10.--Number of hours during Phases I and II when various amounts of maximum intervening rainfall attenuation corrections were applied to one (or more) data bins in one (or more) of the Oceanographer's instantaneous scans used in the integrations to obtain hourly rainfall maps

Number of hours	Maximum intervening rain attenuation corrections applied during hour (dBR)
90 (missing)	- - -
547	0 - 1
165	1 - 2
81	2 - 3
23	3 - 4
6	4 - 5
Total hours	912

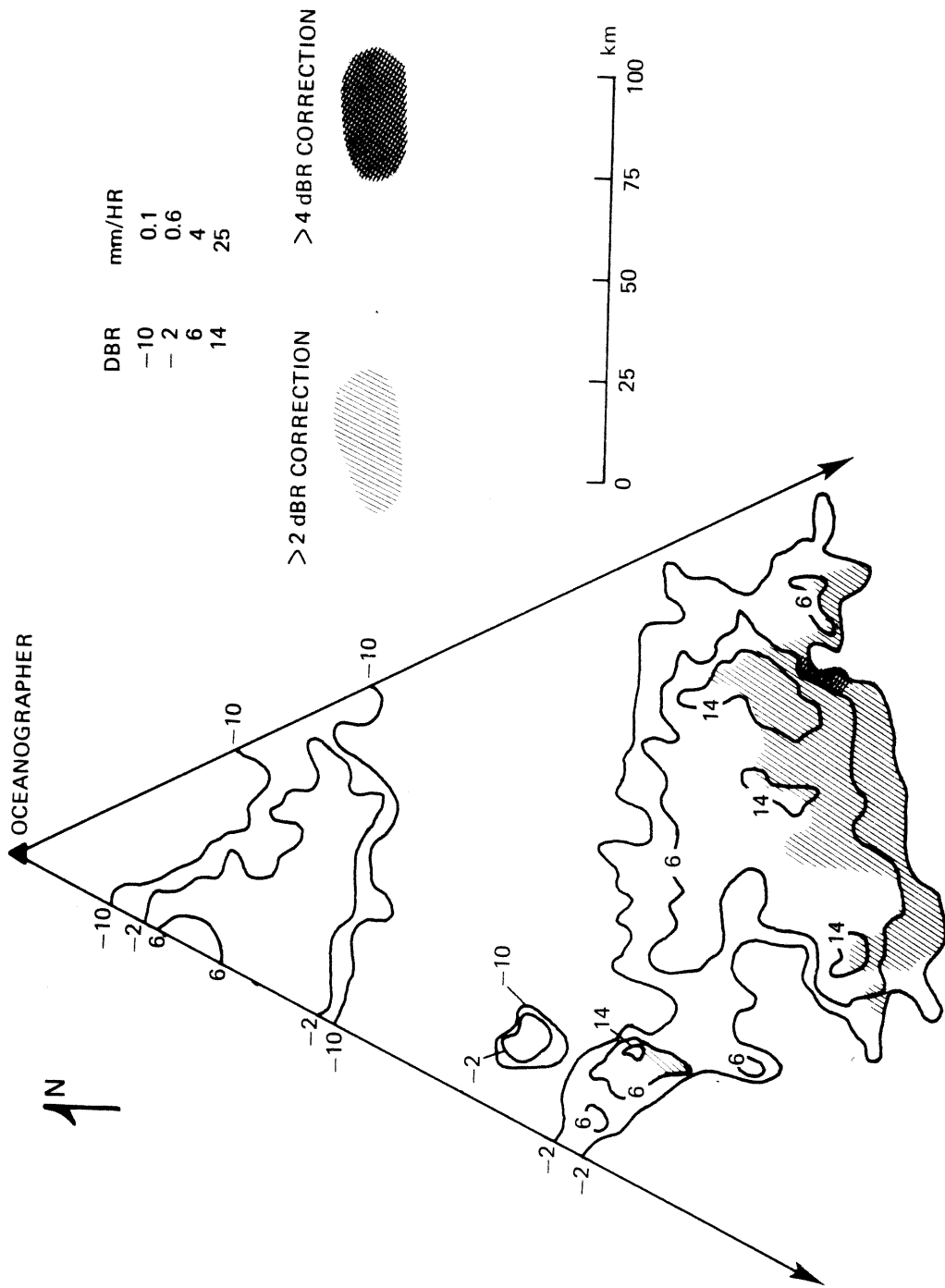


Figure 19.--Illustration of the intervening-rainfall attenuation corrections applied to a sector of instantaneous rainfall data from the Oceanographer radar for one of the significant events during GATE, 2144 GMT June 29, 1974.

Finally, wet-radome attenuation corrections were included in the derivation of the final rainfall estimates from the Oceanographer radar for Phases I and II. Generally, unless a radome skin is a very efficient water repellent (hydrophobic) substance, water film buildup in moderate to heavy rainfall will be sufficient to cause some attenuation in the C-band. Weigand (1973) shows that the construction of a radome, especially the properties of the membrane surface, critically affect the water film buildup. It may be beneficial to treat the radome surface with a special wax or paint. However, the Oceanographer radome, identical in design to those used by the National Weather Service on many of their operational WSR-57 (10 cm) radars, was not treated with an efficient hydrophobic coating.

Thirty-minute rain accumulations from shipboard gages were used to estimate rainfall rates at the time of the scans, and attenuation values were estimated from water film thickness given by an analytical model presented by Gibble (1964). (See Hudlow et al. 1976 and Patterson et al., 1979.) Gibble's model relates the water thickness to the rainfall rate and the radius of the radome (2.75 m for the Oceanographer radome).

Empirical analyses using the GATE Oceanographer radar and rain-gage data indicated that unrealistically high estimates of attenuation for the Oceanographer radome resulted from using water thicknesses given by Gibble's model. Accordingly, the two-way attenuation estimates obtained using Gibble's model were reduced by 1.3 dBR. Figure 20 gives the resultant two-way attenuation values as a function of rainfall rate at a temperature of 30°C, which is approximately 4°C warmer than the mean surface atmospheric temperature observed during GATE.

Figures 21 and 22 illustrate the types of analyses that were made to determine the 1.3-dBR empirical factor, used to adjust the attenuation values obtained with Gibble's model. The upper panels in both figures are time series of volumetric rainfall in dBR units, accumulated for the total B-scale array, and the lower panels are rainfall rates at the Oceanographer based on stern rain-gage catches. Normally, the volumetric water accumulated over a large geometric area, such as the B-scale, should remain rather conservative over short time periods. Sharp dips, as can result from wet-radome attenuation, or sharp rises, as can occur from overcorrecting for attenuation, generally should not appear in the "true" time series. Therefore, the objective was to devise a correction procedure for radome attenuation that minimized these sharp irregularities in the time series of volumetric water. Of course, rapid real changes in the integrated volumetric water can occasionally occur because of boundary effects or when the storm undergoes explosive development or diminution.

The volumetric water curves shown in figures 21 and 22 are all corrected for atmospheric attenuation (including the lower curves that are labeled uncorrected); as indicated, the upper curves also include attenuation corrections for intervening rainfall and/or water on the radome. When the full radome corrections were applied, it was observed that the larger magnitudes frequently resulted in very high intervening rainfall attenuation corrections and physically unrealistic rainfall rates. This would certainly have been true if the intervening rainfall attenuation correction had been included for the upper

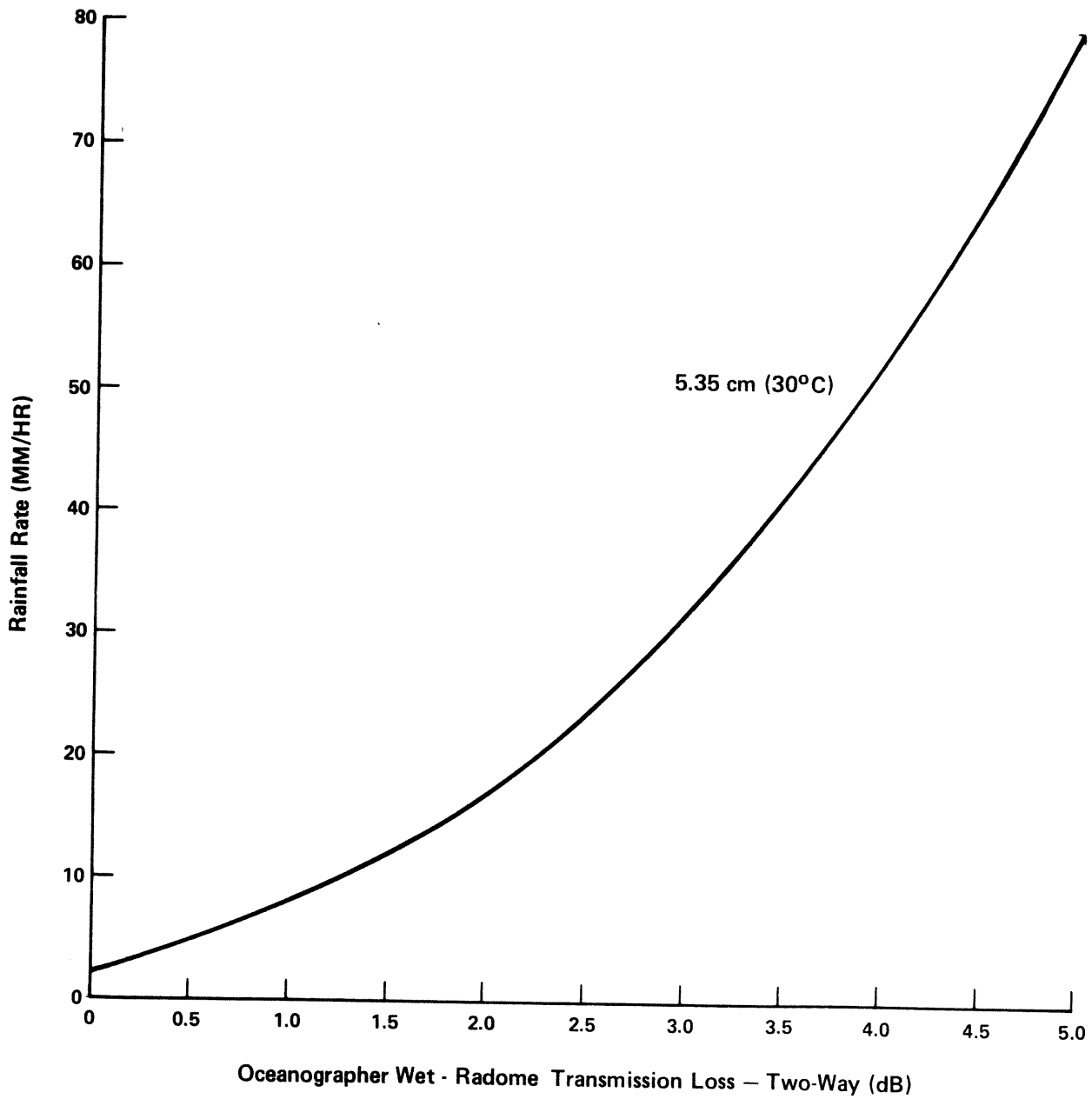


Figure 20.--Estimated wet-radome attenuation (dB = 1.25 dBR) as a function of rainfall rate (mm hr^{-1}) for the Oceanographer radome based on Gibble's model modified by a 1.3 dBR empirical factor.

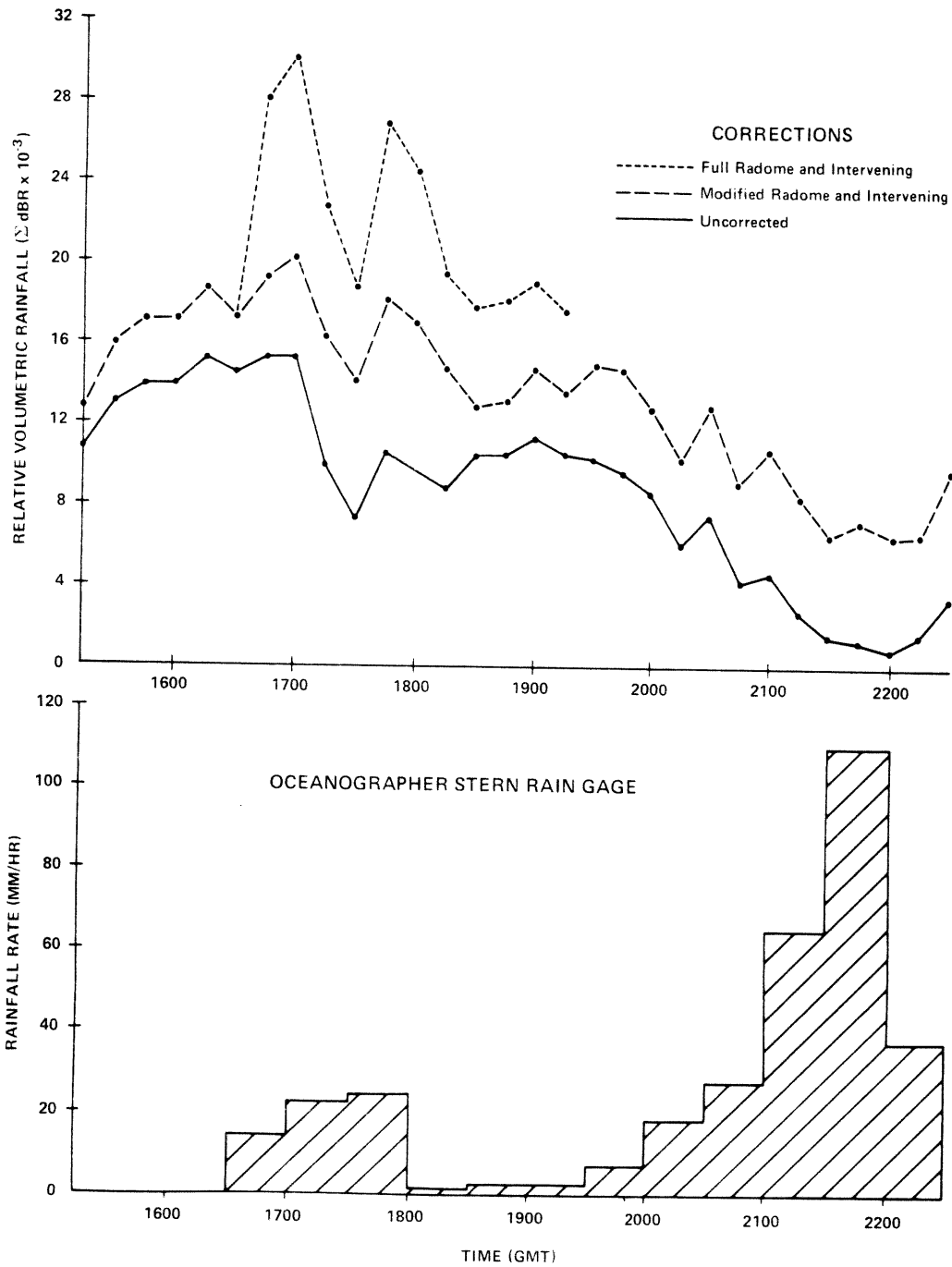


Figure 21.--Time series of volumetric water over the B-scale array (upper panel), estimated from the Oceanographer radar with various modes of attenuation correction, and time series of 30-min mean rainfall rates at the Oceanographer (lower panel), based on measurements with the stern rain gage, for a major precipitation event on July 7, 1974.

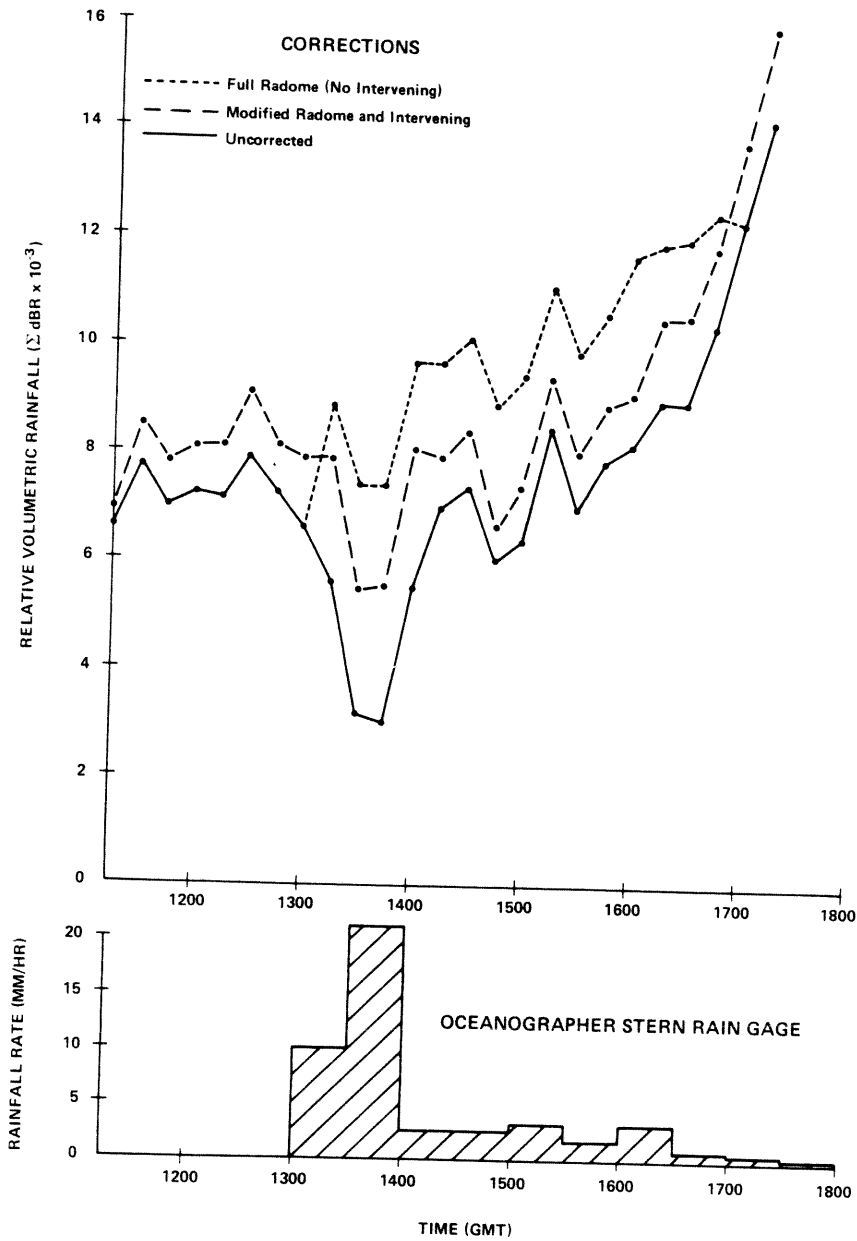


Figure 22.--Time series of volumetric water over the B-scale array (upper panel), estimated from the Oceanographer radar with various modes of attenuation correction, and time series of 30-min mean rainfall rates at the Oceanographer (lower panel), based on measurements with the stern rain gage, for a squall line event on September 4, 1974. This period from Phase III was used to test the attenuation correction routines used during Phases I and II; however, as explained in the text, no explicit rainfall attenuation corrections were made in the derivation of the final rainfall estimates for Phase III.

Table 11.--Number of hours in Phases I and II when various amounts of maximum wet-radome attenuation correction were applied to one (or more) of the Oceanographer's instantaneous scans used in the integrations to obtain hourly rainfall maps.

Number of hours	Maximum radome attenuation correction applied during hour (dBR)
90 (missing)	- - -
770	0.0
18	0.01 - 0.5
16	0.5 - 1.0
8	1.0 - 1.5
4	1.5 - 2.0
3	2.0 - 2.5
0	2.5 - 3.0
1	3.0 - 3.5
1	3.5 - 4.0
0	4.0 - 4.5
1	4.5 - 5.0
Total hours = 912	

curve of figure 22. The modified radome curves include the 1.3-dBR empirical modification (i.e., full correction minus 1.3 dBR). Other modifications to the wet-radome model were tried, but the 1.3-dBR adjustment seemed to best restore the time continuity of the volumetric series without resulting in unrealistic overcorrections leading to instabilities in the overall solution.

Wet-radome attenuation was seldom a significant factor, since heavy precipitation occurred infrequently at the Oceanographer radar. For example, the estimates of wet-radome attenuation were less than 1.0 dBR for more than 98 percent of the hours during Phases I and II. The maximum correction of 4.7 dBR was applied at 2145 GMT July 7 (see fig. 21). Table 11 summarizes, in 0.5-dBR classes, the number of hours during Phases I and II when various amounts of maximum wet radome attenuation were applied sometime within an hour.

Attenuation corrections were not applied to the reflectivity data from the Oceanographer and Researcher radars for the comparative analyses that were presented in chapter 6; even atmospheric attenuation corrections were not considered critical for these analyses, since the comparisons were being made for echoes located at approximately equal ranges from both radars. The radar estimates, used in the analyses for all subsequent sections, were corrected for atmospheric attenuation. In addition, the hourly rainfall estimates from the Oceanographer presented in section 11.4 were corrected for wet-radome

attenuation, and the estimates for Phases I and II presented in sections 11.2 and 11.3 were further corrected for rainfall attenuation. Rainfall attenuation corrections were not considered as significant in the derivation of the final rainfall estimates for Phase III because data were merged from several radars, each of which viewed the precipitation within the interior of the array from different directions (Patterson et al., 1979).

As shown by figure 23, the combined effect of the wet-radome and intervening rainfall attenuation corrections on the Phase I and II mean rainfall rates is small. Consequently, the lack of these corrections for some of the analyses presented in subsequent sections should have little effect on the validity of the results, since the objective is to identify systematic biases and not to determine the errors that might be introduced into the rainfall estimates over very small localized areas by rainfall attenuation.

The reason that significant intervening rainfall attenuation occurred infrequently and was restricted to localized areas (see fig. 19) probably resulted from the fact that the reflectivities in GATE, for the 4-km x 4-km data bins, rarely exceeded 50 dBZ (Hudlow and Arkell, 1978), which is the magnitude above which Hildebrand (1978) finds C-band signals are seriously attenuated. During GATE, intense rain cores exceeding 50 dBZ had very small horizontal dimensions (Geotis, 1977).

7.2 Mean Range Performance Curves

Figure 24 gives what we will refer to in this report as the "mean range performance curves" for the four C-band radars. These curves were determined by averaging the precipitation values, which had been corrected for atmospheric attenuation, for all azimuths and for 20-km range increments. The relative mean-rainfall intensity, as defined by the ordinate labels, was then plotted as a function of range; R_{40} and R_r are the rainfall rates at 40 km and the other ranges on the abscissa, respectively. A range of 40 km was selected for normalization, since it was assumed that beam-filling problems would not seriously degrade the quantitative estimates out to at least this range. By averaging over long time periods, this method gives, to a first approximation, the degradation of the radar measurements as a function of range. Of course, real rainfall variations with range, which remain in the Phase averages, will have some influence on the shape of the range performance curves; for example, the Oceanographer and Researcher were apparently stationed in local rainfall minima during both Phase I and Phase III, resulting in the negative ordinate values in figure 24 at close ranges for these radars. However, the fact that the Phase I curves, as illustrated in figure 24 for the Oceanographer and Researcher, are very similar to the Phase III curves, support the usefulness of this procedure for determining the first-order range performance of a radar. Comparison of the four curves for the Oceanographer and Researcher also verifies that no significant systematic biases were introduced when the data were rectified from polar to Cartesian coordinates.

The superior range performance characteristics exhibited by the Oceanographer radar data probably resulted from the use of "optimum" nominal settings of the antennae elevation angle, for the collection of the two lowest scans, and from the preprocessing procedure that selected the maximum reflectivities from the

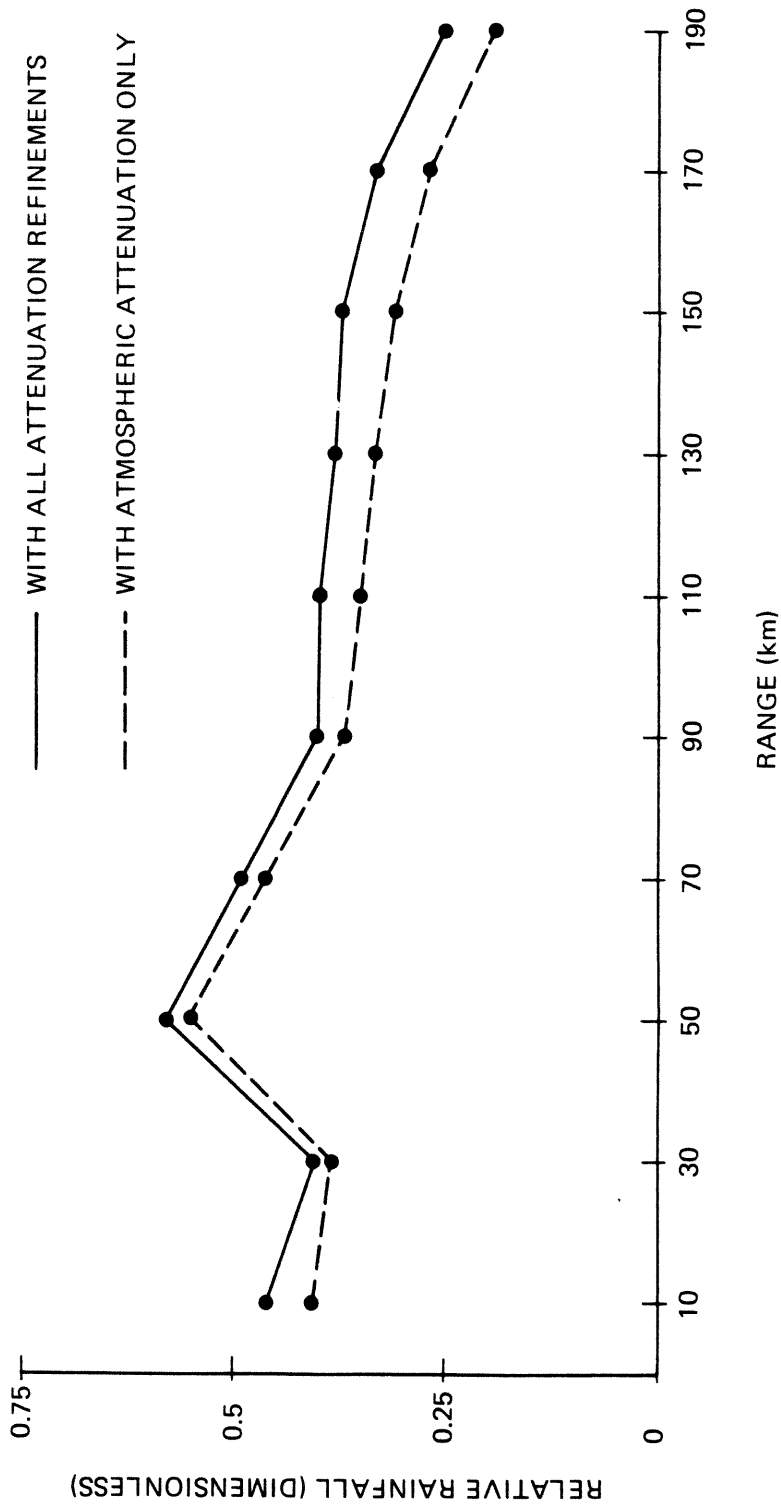


Figure 23.--Plots of mean relative rainfall versus range, for Phases I and II combined, as derived from the Oceanographer radar data, including all attenuation corrections (solid) and with atmospheric attenuation corrections only (dashed).

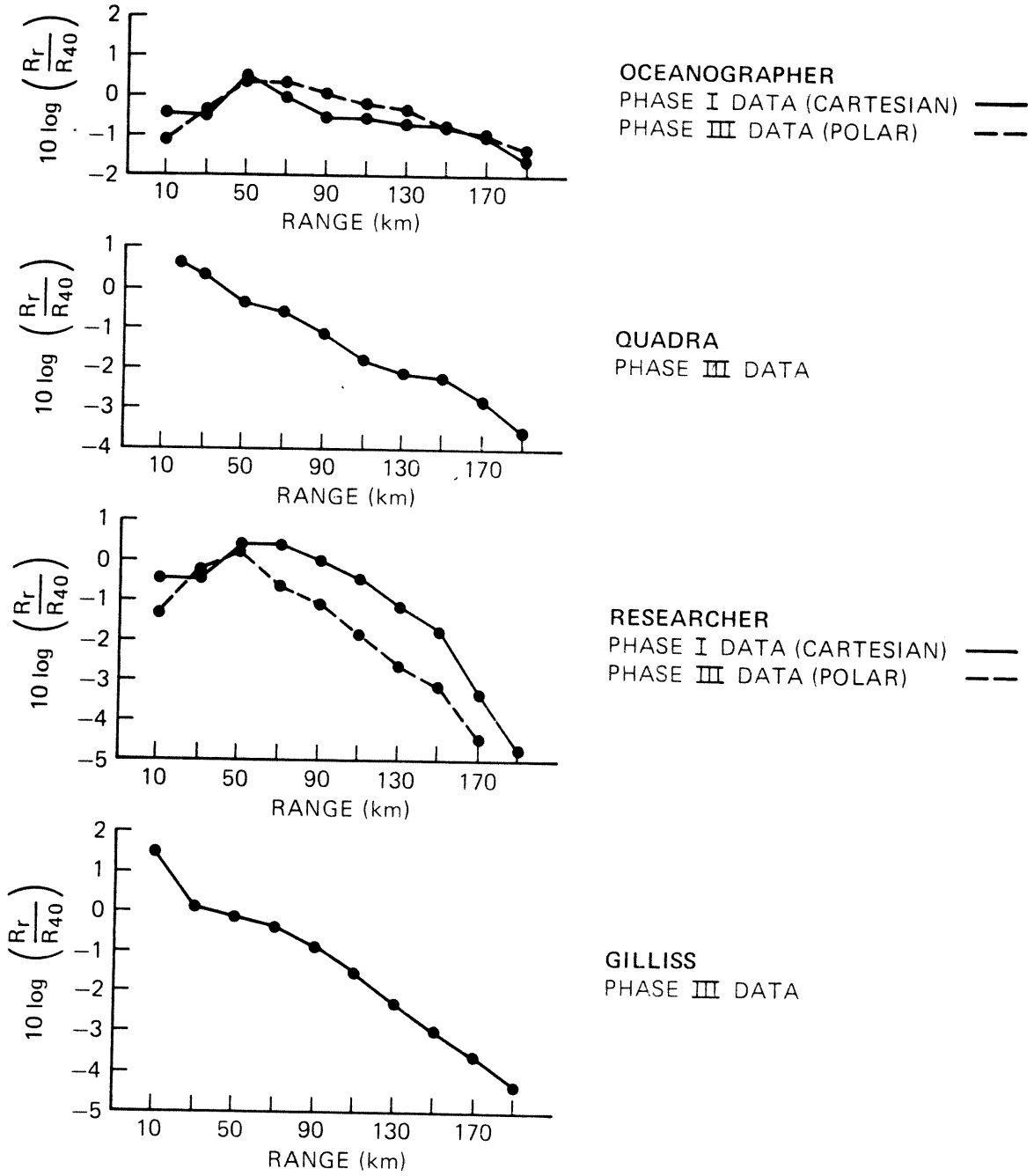


Figure 24.--The variation with range of the Phase-mean relative rainfall as derived from data collected with the four C-band radar systems, which gives, to a first approximation, an assessment of the range performance of the various radars.

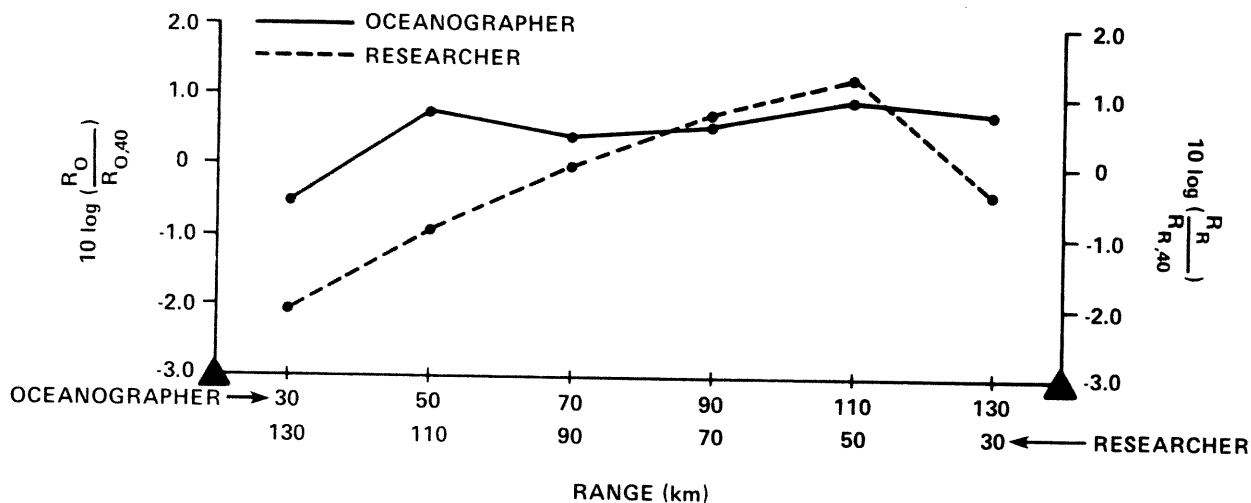


Figure 25.--The variation with range of the mean relative rainfall, for Phases I and II, as derived from data collected with the Oceanographer radar "looking" south toward the Researcher (solid) and from the Researcher radar "looking" north toward the Oceanographer (dashed).

two lowest tilt scans. This bi-scan maximization approach is discussed by Richards and Hudlow (1977). The preprocessing steps described in chapter 9 were performed on the Gilliss and the Quadra data, as appropriate, subsequent to the derivation of the range performance curves.

The curves shown in figure 25 were determined in a similar manner to those for figure 24; except, all data from Phases I and II were used, and the data were only integrated for 60° of azimuth. The 60°-sectors for the Oceanographer and Researcher radars were centered on due south and north, respectively, i.e. each radar was "looking" toward the other (fig. 1).

Consistent with figure 24, figure 25 illustrates that the Researcher data begin to degrade sooner and more rapidly than the Oceanographer data. Comparisons between the radar estimates and the remote shipboard gage catches are also in general agreement with the range performance curves shown in figure 24 (see sec. 11.1). All analyses indicate that the Oceanographer radar data remain, in the mean, within about 1 dB for ranges out to 175 km. On the other hand, the radar-gage analysis indicates that the range degradation for the other three radars is somewhat less than suggested by figure 24, leading to the conclusion that the mean deterioration for them probably remains within 2 dB out to 150 km. Therefore, the Oceanographer radar normally provided good quantitative coverage of the total B-scale array during Phases I and II, when the Oceanographer was stationed at the center of the array (fig. 1). Accurate rainfall mapping over the B-scale array during Phase III, when the Oceanographer switched positions with the Meteor, was obtained by merging data from all four C-band radars (Patterson et al., 1979).

8. COMPARISONS DURING PERIODS THAT RADARS WERE COLLOCATED

Three official intercomparison periods were set aside to conduct special tests and comparisons of various sensors while the sensor platforms (ships) were approximately collocated; one was before Phase I, one was between Phases II and III, and one followed Phase III. It was during the first such intercomparison period that the system gain measurements, described in section 5.2, were made using the standard target technique. During the last two intercomparison periods, precipitation data were collected for short periods while designated radars were nearly collocated (ships within 2 km of each other).

8.1 Comparison of Areal Rainfall Estimates at Various Ranges

Collocated reflectivity data were collected for the pairs of radars and periods as shown in figure 26. The instantaneous reflectivity data were corrected for atmospheric attenuation and converted to rainfall rates using eq. (9), then were integrated for the total period and averaged over 20-km annuli. Decibels, defined as 10 times the logarithm of the ratios of these resultant rainfall values, were then plotted as a function of range for the various radar pairs (fig. 26); where R_O , R_R , and R_G are radar rainfall values from the Oceanographer, Researcher, and Gilliss radars, respectively. To minimize range effects, comparisons were limited to ranges within 110 km.

8.2 Conclusions From Collocated Intercomparisons

Generally, the comparisons shown in figure 26 do not reveal any strong range dependencies, except that the Gilliss radar appears to consistently give higher rainfall estimates, compared to the Oceanographer or Researcher, at close ranges. This finding is consistent with the mean range performance curves presented in section 7.2 and with results presented in chapter 9, which ultimately led to the decision to apply a different bias correction to the Gilliss data for close ranges. However, the overall difference in magnitudes between the rainfall rates measured by the Researcher and the other two radars are not entirely consistent with the results presented in chapter 6 or chapter 9.

The comparisons presented in chapter 6, and those presented below in chapter 9, establish that any systematic calibration difference between the Oceanographer and Researcher radar estimates, excluding range effects, must be small; in fact, the best estimate of the difference is that the Researcher radar gives about 0.5 dB higher estimates, in the mean, than the Oceanographer radar. While the mean difference between the two radars for the collocated comparison is in the right direction, it is substantially larger (2.5 dBR, see fig. 26). The zero mean difference between the Gilliss and Researcher radars for the collocated comparison is also somewhat inconsistent with the conclusions presented in chapter 9, which establish that the Researcher radar estimates are, in the mean, about 1.25 dB lower than for the Gilliss. The difference between the Oceanographer and Gilliss radar rainfall estimates, verified by the other analyses in this report, is about 1.5 dBR in the mean, which is in reasonable agreement with the collocated comparison.

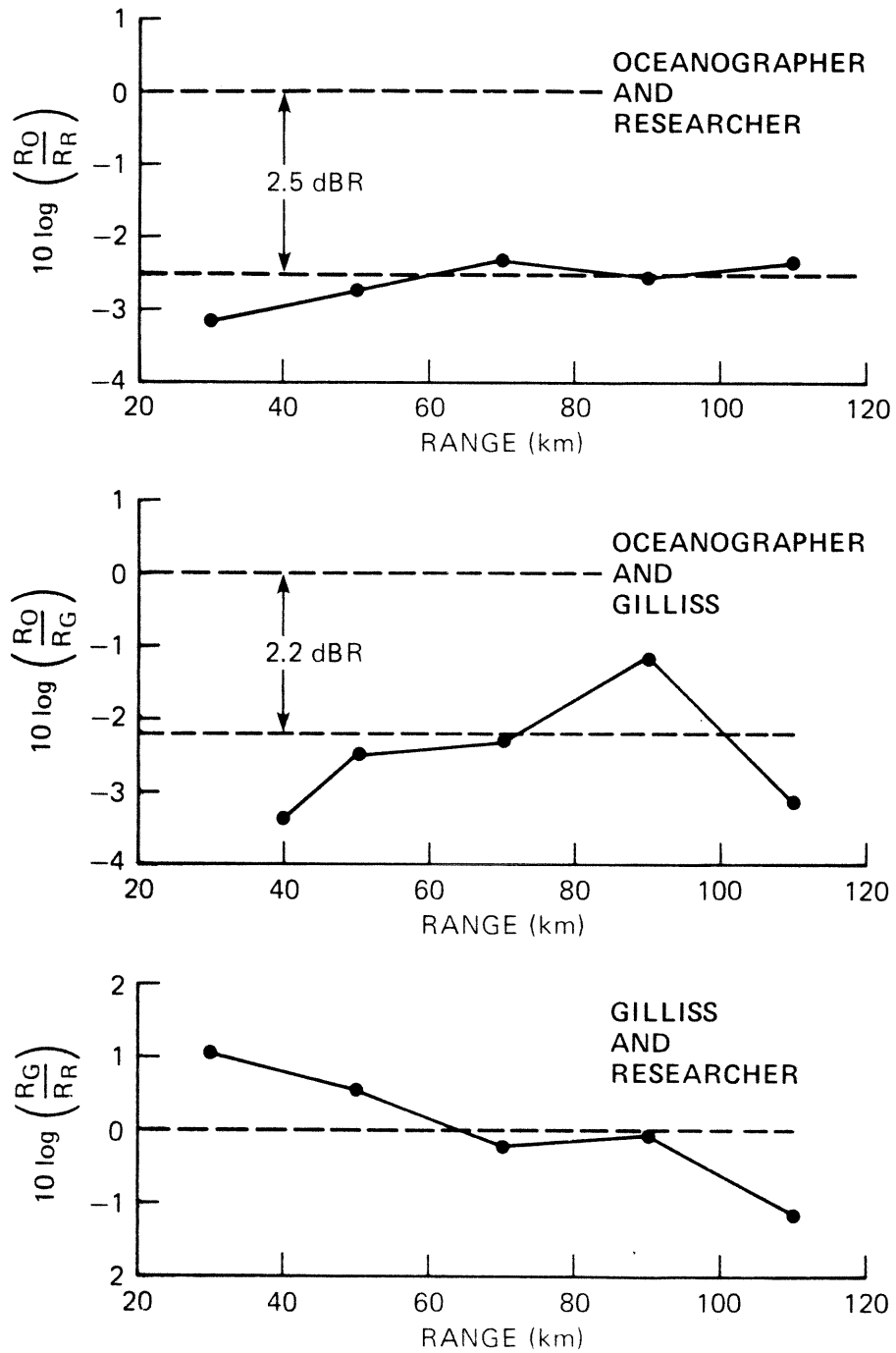


Figure 26.--Mean relative rainfall comparisons, within ranges of 110 km, for GATE radars during periods of collocated intercomparison--upper panel, 0845-1045 GMT August 18, 1974; middle panel, 1000-1200 GMT September 20, 1974; lower panel, 1015-1300 GMT September 21, 1974.

In summary, and to put things in perspective, it is a remarkable achievement to find that the calibrations, performed by different individuals, of two radars (even collocated ones) agree to within 2-3 dB. Nevertheless, while the sign of the average differences between the rainfall estimates from the various radars is consistent for the collocated analyses versus the other analyses presented in this report, the magnitude of the differences do not entirely agree. It should be emphasized that the collocated analyses are limited by the small number of samples. As previously illustrated in figure 17, although the NOAA radars estimates normally agreed to within 1 dBZ for the "total" overlap region, they occasionally disagreed by 2-3 dBZ. Temporal integration of the data will help reduce the error resulting from random departures from the mean, but it is not likely that we will be able to reduce the average error in the radar estimates much below 1 dB without using independent "ground-truth" information. The largest excursions observed probably correspond to periods when one radar estimate deviated low and the other high. This coincidentally may have been the case for the two periods of collocated measurements used to compare the Researcher with the other two radars. Also, the dispersion of the errors about the mean for the Researcher estimates might be expected to be somewhat larger than for the Oceanographer estimates, since the variance of the transfer function is slightly higher for the Researcher radar (sec. 3.2). Because of the small sample, great weight cannot be attached to the collocated analyses, but they do serve as another important consistency check on the overall calibration of the radar systems.

9. VOLUMETRIC WATER DISTRIBUTION COMPARISONS WITHIN FIXED GEOMETRIC AREAS

As described previously, it was necessary to merge data from all four C-band radars during Phase III in order to map accurately the rainfall over the total B-scale array. Once the edited Cartesian coordinate data became available for all four radars (the last data set was received at CEDDA in early January 1977), plans were initiated to verify the quality and consistency of the multiple data sets before the merging process. Preliminary assessments of the Cartesian reflectivity data from the Gilliss and Quadra radars, based on visual inspection of microfilms and volumetric-water time series, indicated that an additional independent editing and preprocessing routine was needed to resolve isolated problems for these radars. Specifically, software was designed to take certain corrective action when flags relating to particular arrays were set (Patterson et al. 1979). These corrective actions, which could be applied to an individual radar as appropriate, consisted of: (1) elimination of "noisy" or otherwise bad scans, (2) maximization of reflectivities over two consecutive instantaneous scans when significant data degradation resulted from inaccurate antenna stabilization, (3) zeroing of sea clutter for no rain or very light rain cases, and (4) elimination of background radio-frequency noise by specifying a threshold reflectivity value below which an assignment of zero reflectivity was made. The specific actions that pertain to each radar, and the number of individual scans for which specific corrective actions were taken, are given by Patterson et al. (1979).

After the isolated problems described above were resolved, an approach was sought to ensure that the calibrations of the four radars were internally consistent and that the overall calibrations generally agreed with the ship-board rain gages. Comparisons presented in chapter 6 support the conclusion

that any systematic difference in the calibration of the two NOAA radars must be small, probably within 0.5 dBZ. However, the collocated analyses presented in chapter 8, based on a very small sample, suggested that the magnitude of the difference between the Researcher and Oceanographer might be larger. The collocated analyses further indicated that the difference between the Researcher and Gilliss was not entirely consistent with the collocated comparison of the Oceanographer and Gilliss, when the results from chapter 6 are considered.

Because of the small sample, great weight cannot be attached to the results from the collocated analyses; therefore, an approach was sought that would enable a large data sample to be used for intercomparing the four radars and for comparing rainfall estimates from the individual radars to measurements from selected shipboard rain gages within radar range. The approach adopted basically consisted of comparing the volumetric water distributions within geometric areas that were optimally located relative to the radars being compared. For the radar rain-gage comparisons, the geometric areas were centered on the rain gages (ship positions) selected for "ground truth" verification. These comparisons included data from all matching periods during Phase III. Because the Oceanographer radar developed a serious antenna stabilization problem on September 8, 1974, only data from the first 9 days of Phase III were used for comparisons with the Oceanographer. Figure 27 illustrates the geometric areas that were used for the various comparisons. The large boxes, Nos. 5, 12, and 13, were used for intercomparing the volumetric water distributions obtained from the four radar data sets. All other boxes were used for the radar rain-gage comparisons. A brief description of the computer software, used to extract the radar reflectivity distributions for the various geometric areas, and the results of the volumetric water comparisons are given in sections 9.1 through 9.5.

9.1 Reflectivity Frequency-Distribution Software

A computer program was designed to extract and classify the instantaneous Cartesian reflectivity values from any specified rectangle lying totally within the field of view of a particular radar. The software included an algorithm to correct the reflectivity data from the three U.S. radars for atmospheric attenuation, since this had not previously been done. As discussed in section 7.1, atmospheric attenuation corrections were applied electronically to the Quadra data before they were recorded.

The computer program was set up to accumulate the frequencies within 2 dBZ classes over an inclusive period specified by start and stop times. Such accumulated frequency distributions for Phase III and for the 14 boxes illustrated in figure 27 form the basis for the volumetric water comparisons presented in the rest of this chapter.

9.2 Radar-to-Radar Comparisons Before Bias Adjustments

From the instantaneous-reflectivity frequency distributions, accumulated for Phase III over the specified boxes (fig. 27), volumetric water distributions were computed using the following relation:

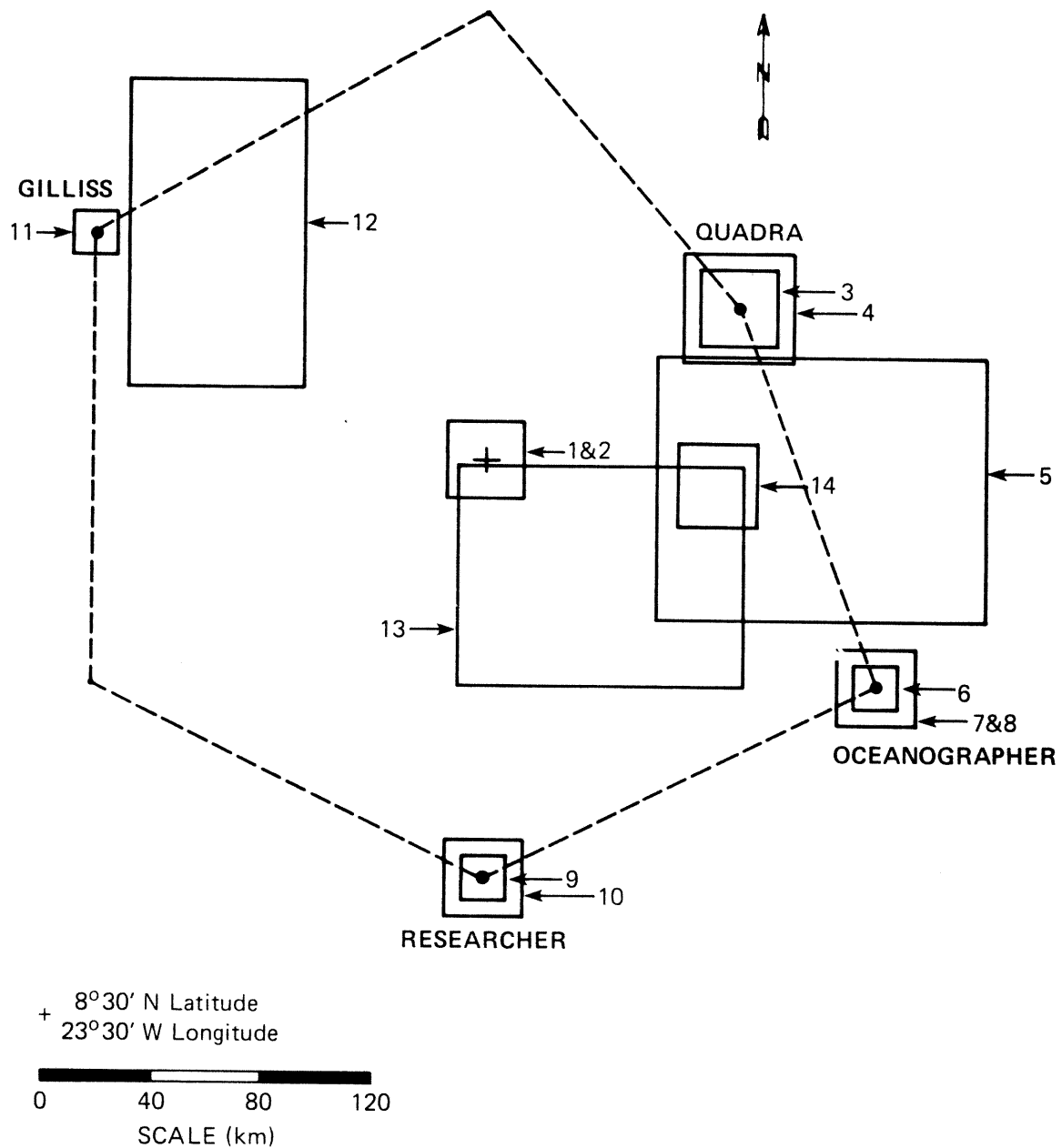


Figure 27.--Schematic of the B-scale array during Phase III illustrating the 14 boxes used for intercomparing the volumetric water (distribution) measurements from the radars and for comparing radar derived water totals with selected shipboard rain gages.

$$R_{vi} = f_i R_i \quad , \quad (32)$$

where R_{vi} is the volumetric water for the i th reflectivity class, f_i is the number of 4-km x 4-km elements within the reflectivity class, and R_i is the rainfall rate (mm hr^{-1}) corresponding to the i th reflectivity class. Substituting eq. (9) into eq. (32) gives

$$R_{vi} = 0.013 (f_i Z_i^{0.8}) \quad , \quad (33)$$

where Z_i is the reflectivity ($\text{mm}^6 \text{ m}^{-3}$) corresponding to the i th reflectivity class.

Figure 28 gives plots of volumetric water (R_i) versus rainfall rate [and reflectivity (dBZ)] derived from the applicable radar data for boxes 5, 12, and 13 (fig. 27). The center panel of figure 28 provides a direct comparison of Quadra and Oceanographer data within a common box (No. 5) located between the two radars. Similarly, the lower panel gives a direct comparison between the Researcher and Oceanographer radars. Because of the large distance between the Gilliss and the other three radars, accurate comparison of the Gilliss radar data with those from one of the other radars, within a box common to both, was not feasible. However, the volumetric water distribution for box No. 12, which was optimally located relative to the Gilliss, was derived (upper panel, fig. 28) for the purpose of making general comparisons with the curves from the other radars. To facilitate comparison with the other curves, the ordinate values for the Gilliss curve were scaled by a multiplicative factor equal to the ratio of the lengths of the analysis periods; i.e., 9 days/20 days = 0.45.

Table 12 gives the total volumetric water for all reflectivity classes, obtained by summing the values for the 2-dBZ classes plotted in figure 28, i.e.

$$R_{vt} = \sum R_{vi} = \sum f_i R_i \quad , \quad (34)$$

where R_{vt} is the total volumetric water.

From examination of the volumetric water distributions given in figure 28 and the total volumes of water given in table 12, without bias adjustment, several conclusions can be drawn. First, the Quadra value for box 5 is almost three times larger than the Oceanographer value. The distributions shown for box 5 suggest that this discrepancy is not uniform for all reflectivity magnitudes and tends to be greatest in the midrange of reflectivities. Second, the volumetric water totals and distributions from the Oceanographer and Researcher radars can be considered in very close agreement, bearing in mind the differences in range performance characteristics of the two radars. This supports the results from chapter 6 and further confirms that the apparent discrepancy between the Researcher and Oceanographer measurements during their brief collocation (sec. 8.2) was an anomalous result. Finally, although definite conclusions cannot be reached concerning the calibrations of the Gilliss

BEFORE BIAS ADJUSTMENTS

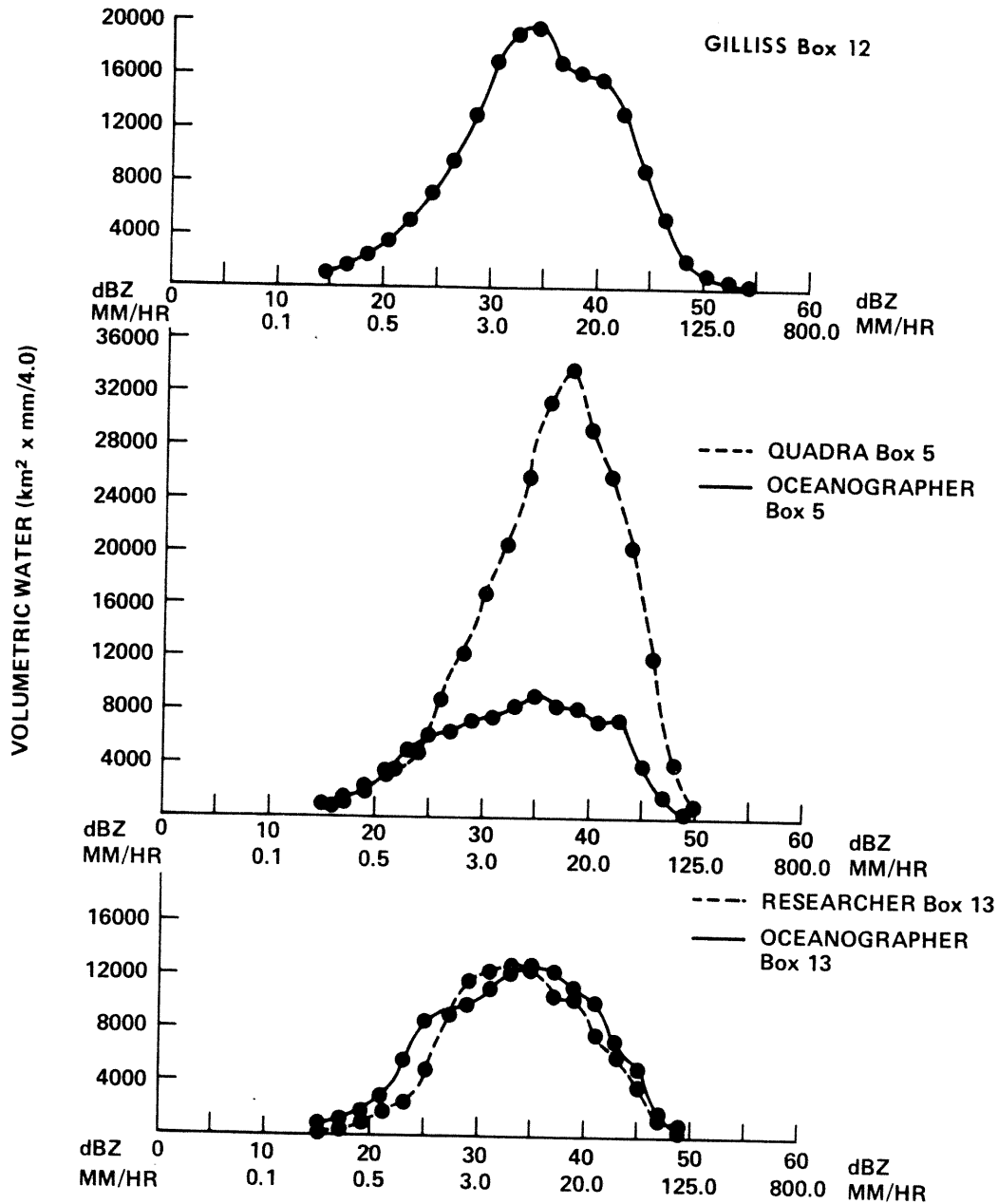


Figure 28.--Plot of volumetric water in 2-dBZ classes, before bias adjustments; derived from the instantaneous Cartesian reflectivity data by accumulating those values within selected boxes used to intercompare the data from Phase III.

Table 12.--Comparison of total volumetric water estimates within boxes 5, 12, 13 (fig. 27), as derived from the C-band radar measurements before and after bias corrections.

Box	Radar	Analysis period	Volumetric water (km ² x mm/4.0)	
			Without bias adjustment	With bias adjustment
5	<u>Oceanographer</u>	} First 9 days of Phase III	92,200	154,000
5	<u>Quadra</u>		254,000	181,000
12	<u>Gilliss</u>	All of Phase III (≈20 days)	379,000	455,000
13	<u>Oceanographer</u>	} First 9 days of Phase III	123,000	205,000
13	<u>Researcher</u>		108,000	164,000

radar relative to the other radars, since the analysis domain is not common with another radar, the following observations can be made: (1) the shape of the Gilliss volumetric-water distribution curve corresponds more closely to those from the Researcher and Oceanographer than to the Quadra curve, and (2) if we assume that the "true" rate of water production was roughly equal in boxes 5, 12, and 13, then the total accumulated volume of water should be directly proportional to the number of days in the analysis period (this assumption was made in scaling the Gilliss curve by the 0.45 multiplicative factor); however, from table 12 we see that (9 days/20 days) x 379,000 = 170,550, which gives a magnitude approximately 1.7 dBR larger than the average of the Oceanographer and Researcher values in box 13. This result is consistent in sign, and approximately equal in magnitude, to the difference derived from the Oceanographer/Gilliss collocated analysis (see fig. 26).

9.3 Radar-to-Gage Comparisons Before Bias Adjustments

Accumulated rainfall depositions for Phase III were also calculated, using eqs. (33) and (34), for the 11 smaller boxes shown in figure 27. These accumulations were then divided in each case by the appropriate Σf_i to obtain mean rainfall rates in mm hr⁻¹, which could then be compared to those based on measurements from the shipboard rain gages. The various size boxes were selected for the comparisons as follows: 16-km x 16-km boxes were used for comparing a radar estimate with a rain gage aboard the same ship, except a larger 40-km x 40-km box was used for the "collocated" Quadra/rain-gage comparison, because Quadra data were not available for ranges inside 16 km. (See Patterson et al., 1979, sec. 3.3.) The 28-km x 28-km boxes were used for comparing the radar estimates with the rain-gage measurements on remote ships. These relatively large areal averages were compared with the shipboard gage catches to smooth out the potential errors that may result

from the combination of gradients in the rainfall fields and data navigation inaccuracies. Although the radar data are being smeared considerably in space, the "box" estimates, when averaged for all Phase III data, should be useful for deducing the approximate mean differences between the radar and gage measurements. More accurate location of the gage/radar data has enabled the two types of measurements to be compared with less smoothing in chapter 11.

Table 13 compares the mean rainfall-rate estimates from the radars and the gages for the various boxes. The Gilliss radar was compared only to the Gilliss gage, since the closest remote gage was approximately 175 km away (fig. 27). From comparison of the Radar₁ estimates with the gage rates, we see that the Quadra radar rates were consistently larger than the gage rates, while the Researcher and Oceanographer radar rates were consistently lower. Although the Gilliss radar estimate is 1.1 dBR higher than the Gilliss gage measurement at the radar origin, the range performance curves presented in figure 24 suggests that the Gilliss radar would overestimate only at very close ranges. Therefore, it appears that the Oceanographer and Researcher radar estimates, and probably the Gilliss estimates except at close ranges, are low relative to the selected "ground truth;" however, the Quadra estimates are high.

9.4 Tentative Bias Corrections and Radar-to-Radar Comparisons After Bias Corrections

We tentatively conclude that the Oceanographer and Researcher radar rainfall estimates were biased low by approximately 2.2 dBR (2.75 dBZ) and 1.8 dBR (2.25 dBZ), respectively, based principally on (1) the radar-gage comparisons shown in table 13, with most weight being given to the gage measurements at the radar origins; (2) the unadjusted volumetric water comparisons in box 13 (see table 12 and fig. 28); and (3) the results presented in chapter 6, especially figure 18. Although not initially obvious, the results from (2) are consistent with those from (1) and (3). Because the Researcher intensities underwent range degradation of roughly 1 dBR (see fig. 24 using a range of 115 km--the distance from the Researcher to the centroid of box 13), the unadjusted Oceanographer estimate from (2) is about 0.5 dBR larger than the corresponding Researcher estimate.

We further concluded, primarily based on the Gilliss radar rain-gage comparison (table 13) and the Gilliss range performance curve (fig. 24), that the Gilliss rainfall estimates were biased high by approximately 0.8 dBR (1.0 dBZ) within ranges of, say, 25 km. This positive bias at close ranges was traced to a shift register problem in the digital integrator by Spiros Geotis at MIT. Conversely, based on the volumetric water comparison (sec. 9.2) and the collocated comparison between the Oceanographer and Gilliss, we tentatively concluded that the Gilliss radar rainfall estimates would be biased low by approximately 0.8 dBR (1.0 dBZ) at ranges greater than 25 km.

From examination of table 13, it can be seen that agreement between the radar rates, from the Researcher, Oceanographer, and Gilliss, and the rain-gage rates was significantly improved in all cases by the bias adjustments. In fact, all differences are reduced to well within 1.0 dBR.

Table 13.--Comparison of Phase III mean radar-rainfall measurements, for boxes in fig. 27, with those based on shipboard rain-gage measurements for matching periods.

Without bias adjustment-- Radar ₁ estimate (mm/hr)	Gage catch (mm/hr)	With bias adjustment-- Radar ₂ estimate (mm/hr)	Difference (dBR) $10 \log \left(\frac{\text{Radar}_2}{\text{Gage}} \right)$	Box
<u>Quadra</u> 0.74	<u>Meteor</u> 0.45	<u>Quadra</u> 0.51	0.54	1
<u>Quadra</u> 1.29	<u>Quadra</u> 0.50	<u>Quadra</u> 0.70	1.46	4
<u>Quadra</u> 0.57	<u>Oceanographer</u> 0.34	<u>Quadra</u> 0.40	0.71	7
<u>Quadra</u> 1.05	<u>Dallas</u> 0.55	<u>Quadra</u> 0.79	1.57	14
<u>Researcher</u> 0.22	<u>Meteor</u> 0.40	<u>Researcher</u> 0.33	-0.84	2
<u>Researcher</u> 0.22	<u>Oceanographer</u> 0.34	<u>Researcher</u> 0.33	-0.13	8
<u>Researcher</u> 0.32	<u>Researcher</u> 0.48	<u>Researcher</u> 0.48	0	9
<u>Oceanographer</u> 0.13	<u>Quadra</u> 0.18	<u>Oceanographer</u> 0.21	0.67	3
<u>Oceanographer</u> 0.20	<u>Oceanographer</u> 0.34	<u>Oceanographer</u> 0.33	-0.13	6
<u>Oceanographer</u> 0.43	<u>Researcher</u> 0.60	<u>Oceanographer</u> 0.72	0.79	10
<u>Gilliss</u> 0.78	<u>Gilliss</u> 0.60	<u>Gilliss</u> 0.65	0.35	11

After adjusting the reflectivity data by +2.75 dBZ, the volumetric water distribution curve for the Oceanographer was rederived as described in section 9.2. Then, the new Oceanographer distribution was plotted on the same diagram with the old Quadra distribution (fig. 29). Comparison of the two distributions

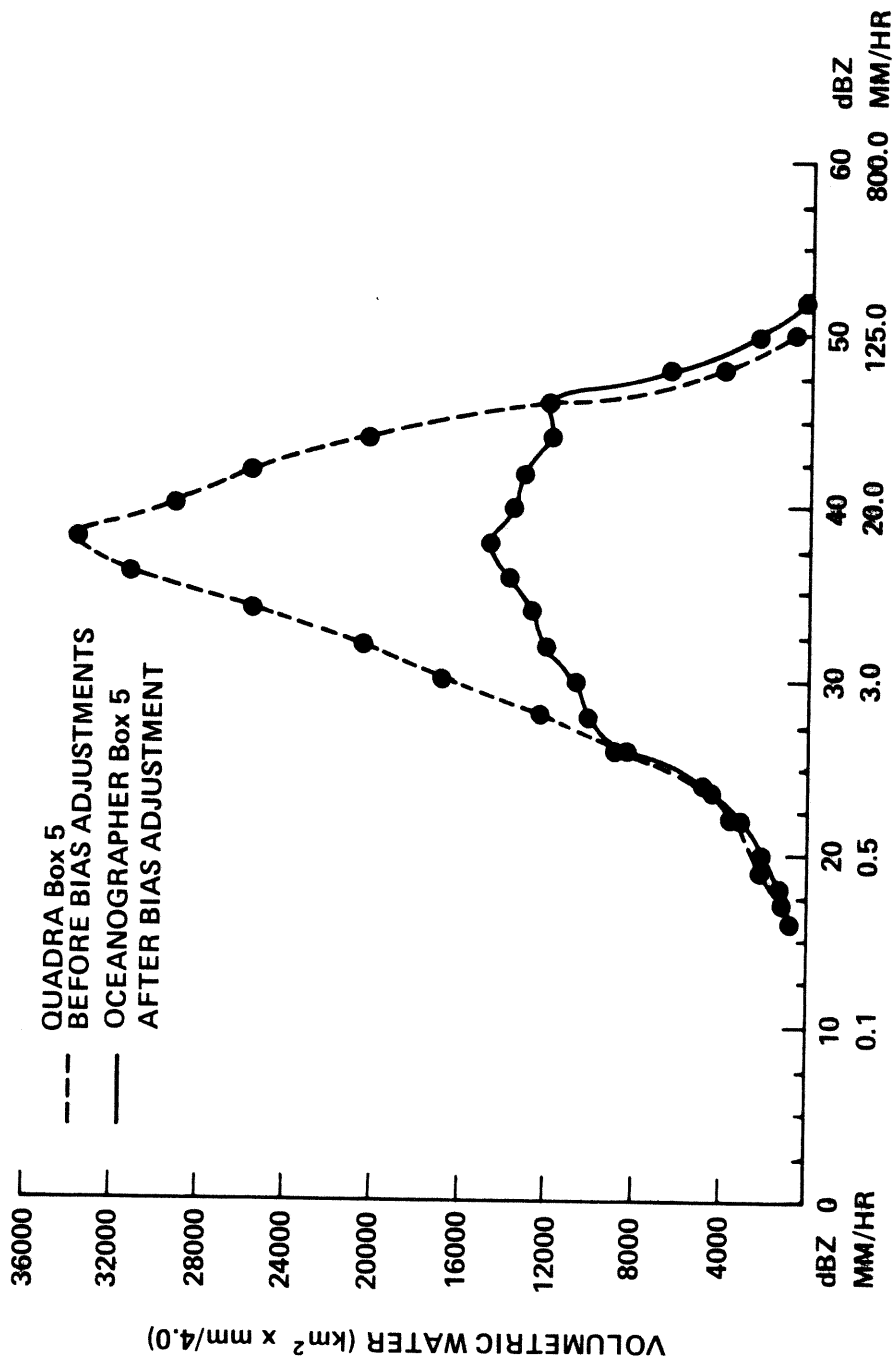


Figure 29. --Analogous to figure 28 except comparing the Quadra distribution curve before bias adjustment with the Oceanographer distribution curve after bias adjustment.

shows that they now agree well in both tails, but there remains a large discrepancy in the midrange. It was clear from the Quadra radar/rain-gage comparisons that the Quadra radar estimates were consistently too high (table 13). However, it was equally clear that a constant reduction (in decibels) over the dynamic range of the distribution was not appropriate, since this would result in the Quadra peak intensity estimates being significantly below those from the other three radars. If anything, we would expect the peak intensity estimates from the Quadra radar to be the highest, since it had the narrowest beam width (table 2) and thus, theoretically, the best capability to resolve the intense convective cores. The reason this did not prove true in practice was postulated to result from a problem with the receiver/digital-processor transfer function, the polar to Cartesian rectification, or both. While the source of the discrepancy could not be isolated, it was verified that the Quadra calibrations were essentially invariant for all of Phase III. Therefore, Geoffrey Austin, McGill University, concurred with us that the Quadra reflectivity values should be shifted to bring the Quadra volumetric water distribution into approximate agreement with the Oceanographer volumetric water distribution. It was essential that the calibrations of all four C-band radars be consistent during Phase III, enabling coherent merging of the data sets required for the derivation of the final rainfall estimates.

The procedure adopted for "mapping" the Quadra reflectivities into approximate agreement with the Oceanographer's consisted of first determining the ratios of the ordinate values given in figure 29, at the constant reflectivity levels indicated by the plotted points. Next, these ratios were converted to dBRs and then to dBZs. Finally, the differences in dBZs were rounded off in the direction of the Quadra data, normally to the nearest 1 dBZ but occasionally to 0.5 dBZ when this produced a smoother final curve. In other words, since it was conceivable that the "truth" fell somewhere between the Quadra and Oceanographer (but probably closer to the Oceanographer), we rounded in the direction that would minimize the amount that the Quadra values had to be shifted.

Table 14 gives the original reflectivity levels for the Quadra radar and those subsequent to the adjustments using the Oceanographer-Quadra dBZ differences, determined as described in the preceding paragraph. The difference between the original and the adjusted levels is zero below 25 dBZ and above 42 dBZ but reaches a maximum of 3.5 dBZ at 34 dBZ.

Using the adjusted reflectivity levels for the various radars, the volumetric water distribution curves and the total volumetric water for boxes 5, 12, and 13 were rederived. The total water volumes, adjusted for biases, are included in the last column of table 12. The revised water distribution curves are shown in figure 30. Once again, the Gilliss curve was scaled by the 0.45 multiplicative factor to approximately compensate for the longer analysis period. The total water values appearing in table 12 for the Gilliss, however, have not been scaled by this factor and represent estimates of the water totals for the full 20-day period in Phase III.

As discussed above for the Gilliss, Oceanographer, and Researcher, the radar estimates for the selected boxes used for comparison with the shipboard rain gages were rederived after the reflectivity levels were adjusted for the

Table 14.--Original and adjusted Quadra radar reflectivity levels (dBZ)

Original*	Adjusted
≤ 15**	0
16	16
17	17
19	19
22	22
24	24
26	25
28	26
30	27.5
32	29
34	30.5
36	33
38	35.5
40	38
42	41
44	44
46	46
48	48
50	50
52	52
54	54

*Because of a transcription error, the original translation table provided by McGill University gave 2 dBZ higher original values than those shown here. This difference is not included because it resulted from an inadvertent error and not a system calibration bias. The adjusted reflectivity levels are the same as those included with the documentation for the archived data (G. Austin, 1977).

**Many of the reflectivity values at 15 dBZ or less are contaminated by radio frequency (RF) interference and were therefore set to 0 dBZ.

estimated biases. Similarly, this was done for the Quadra radar and the revised estimates for all four radars are contained in table 13.

Examination of figure 30 reveals that the water distribution curves for the Oceanographer and Researcher for box 13 and the Gilliss for box 12 are now in close agreement. The fact that the total water volume estimate from the Oceanographer radar is about 1.0 dBR higher than the estimate from the Researcher (table 12) can be attributed to degradation with range of the Researcher radar estimates, as explained previously. Comparisons for these three radars with the shipboard rain gages (table 13) also confirmed that they were in reasonably good agreement with the selected "ground truth"

AFTER BIAS ADJUSTMENTS

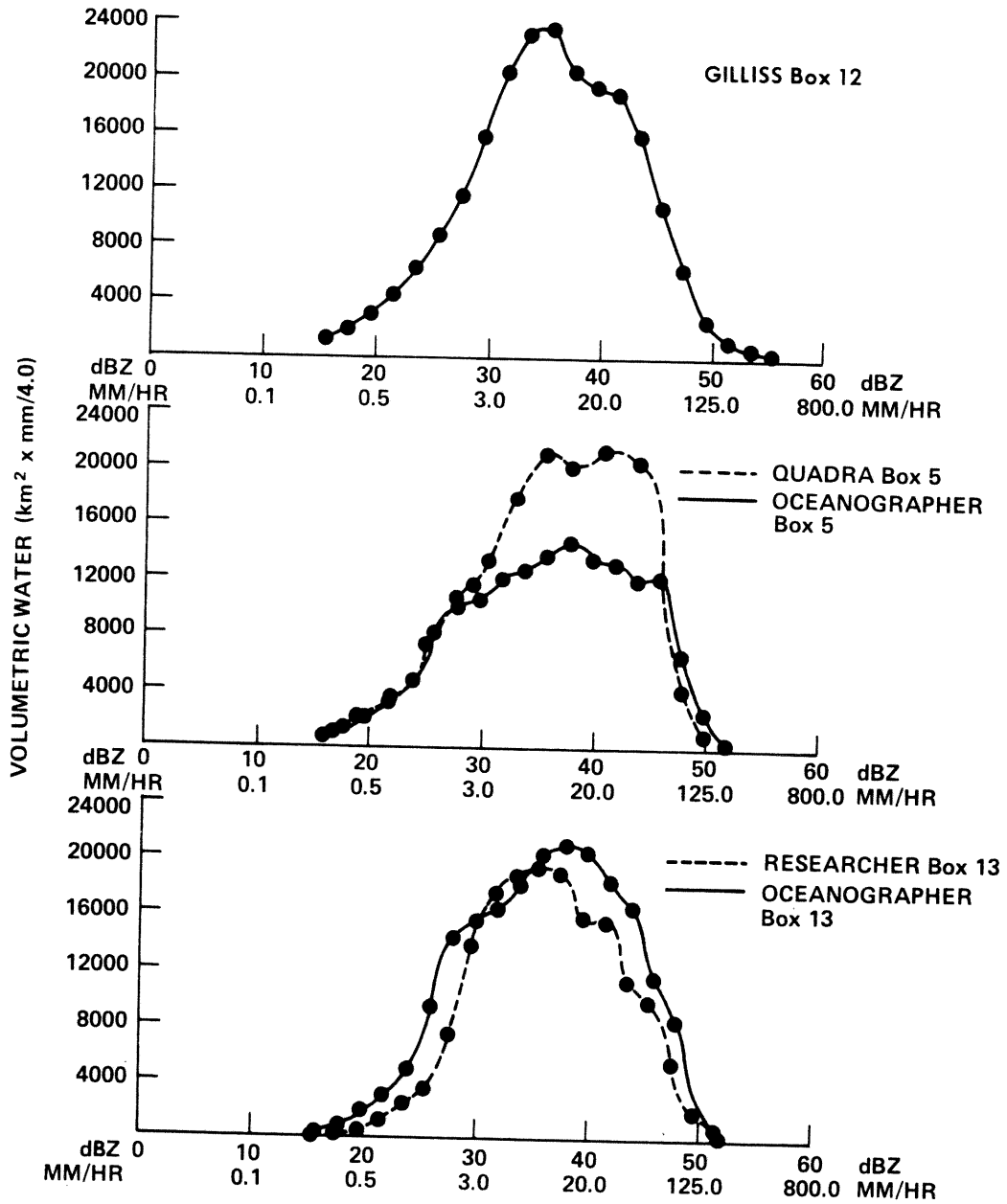


Figure 30.--Same as figure 28 for the water distribution curves from the various radars after bias adjustments.

catchments. However, the comparisons with the rain gages (table 13), consistent with the volumetric water distribution comparison in box 5 (fig. 30), show that the Quadra radar estimates are still consistently high by approximately 1.0 dBR. Whether the Quadra estimates remain high because the midrange reflectivities were not scaled down sufficiently (as fig. 30 would indicate if you believe the Oceanographer curve), or whether some other explanation exists, was not clear at this point in our intercomparison analyses. Regardless, the discrepancy was not believed to be too serious, since all radars at this point agreed, in the mean, to within about 1 dBZ. The question of whether the Quadra data should have an additional adjustment is examined in section 10.1.

9.5 Conclusions From Volumetric Water Comparisons and Mean GATE Distributions

As became apparent in sections 9.2, 9.3, and 9.4, the software described in section 9.1 proved to be a powerful means for deriving reflectivity distributions over specified space and time domains for the purpose of intercomparing radars, as well as for comparing radar estimates to selected "ground-truth" gage catchments. In fact, this comparison method ultimately provided the essential ingredients in the determination of the tentative bias corrections enumerated in section 9.4. These bias corrections will be summarized and verified in chapters 10 and 11.

To provide a standard of reference for ourselves and other investigators, a best estimate of the "true" rain-rate distribution produced by the Phase III convection in the B-scale was obtained by pooling the reflectivity data (adjusted for biases) from the Oceanographer and Gilliss radars. Figure 31 shows the resultant relative-frequency distribution of the nonzero reflectivities in dBZ classes and the percent of the total rain water produced by each reflectivity class. As illustrated in figure 31, 50 percent of the rain was produced by instantaneous rain rates between about 3 and 30 mm hr⁻¹. The distributions show that rarely did the reflectivities exceed 50 dBZ, or 130 mm hr⁻¹, a critical level above which rainfall attenuation in the C-band can become quite serious (sec. 7.1).

10. MEAN BIAS CORRECTIONS USED IN DERIVATION OF FINAL RAINFALL ESTIMATES

10.1 Verification of Quadra-Oceanographer Relative Bias Through Comparison of Instantaneous Reflectivity Fields

As discussed in section 9.4, a question still remained whether the Quadra instantaneous radar reflectivities should be further adjusted in the midrange of intensity levels to bring them into closer alignment with the Oceanographer volumetric-water distribution curve (fig. 30) and with the "ground truth" measurements for selected gage catchments (table 13); or whether the apparent small bias which remained after inclusion of the larger bias adjustments described in section 9.4 should be ignored during the merging process to obtain the final rainfall estimates. To help resolve this question, selected instantaneous reflectivity contours from the Oceanographer and Quadra radars were compared. Examples of two of these comparisons are shown in figures 32 and 33.

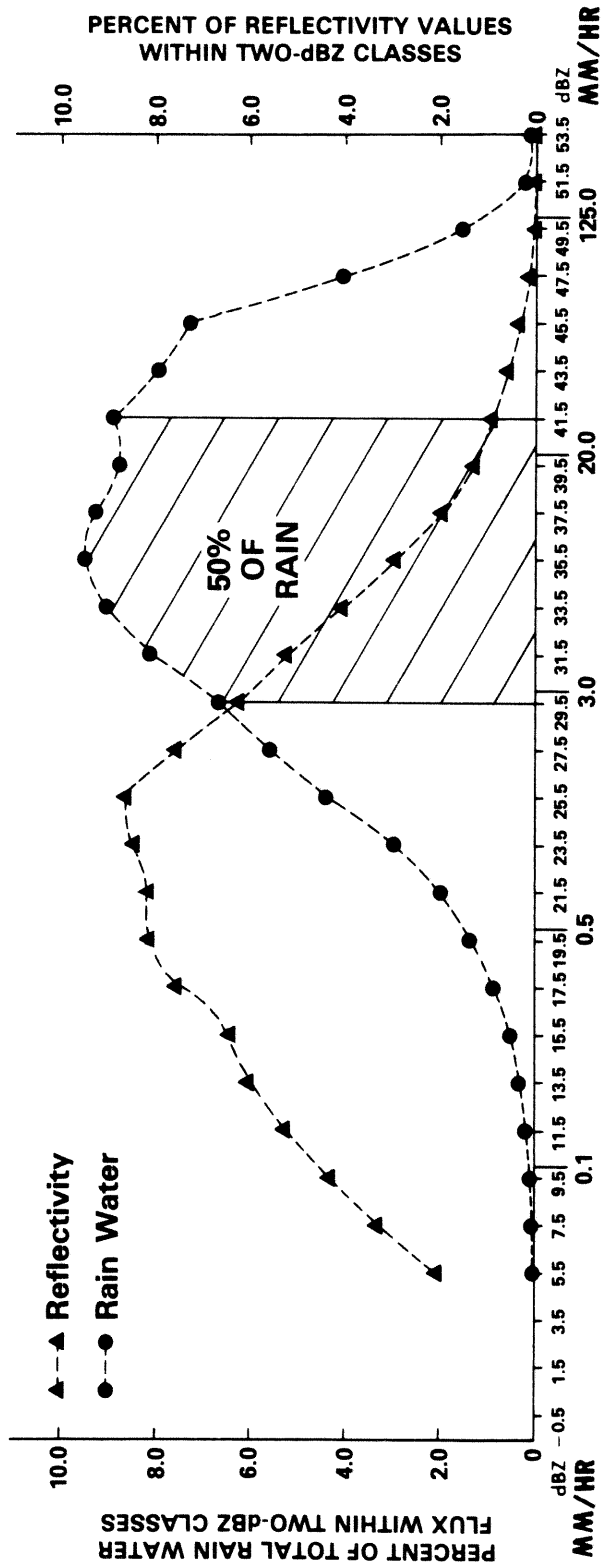


Figure 31.--Relative frequency of the nonzero reflectivities in 2-dBZ classes and percent of the total rain water produced by each reflectivity class, based on all the Phase III (4-km x 4-km) data bins falling inside boxes (8000 km² each) located at optimum ranges from the radars. These distributions were determined by combining data, which had been corrected for atmospheric attenuation and system biases, from the Oceanographer and Gilliss C-band radars.

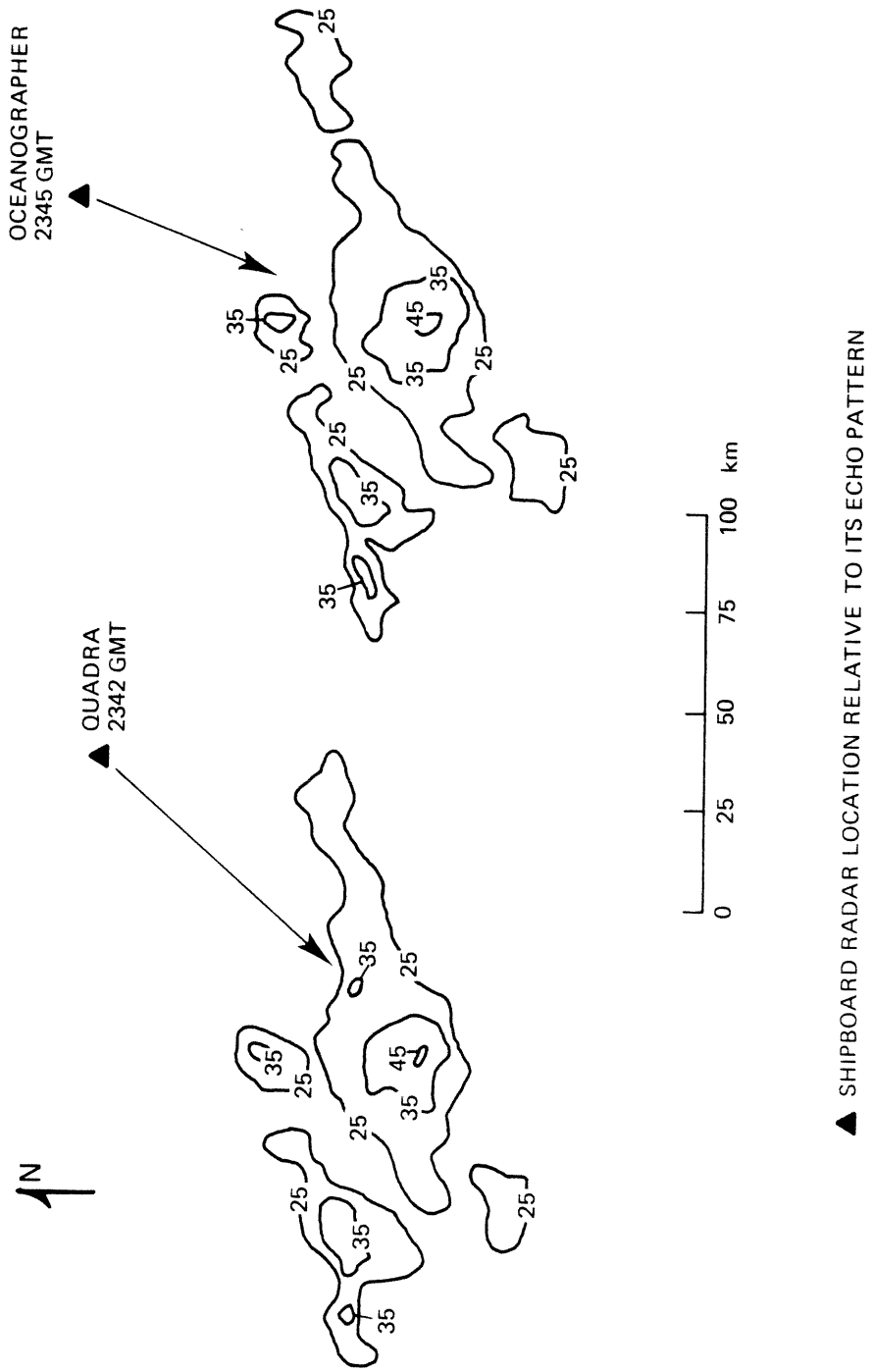
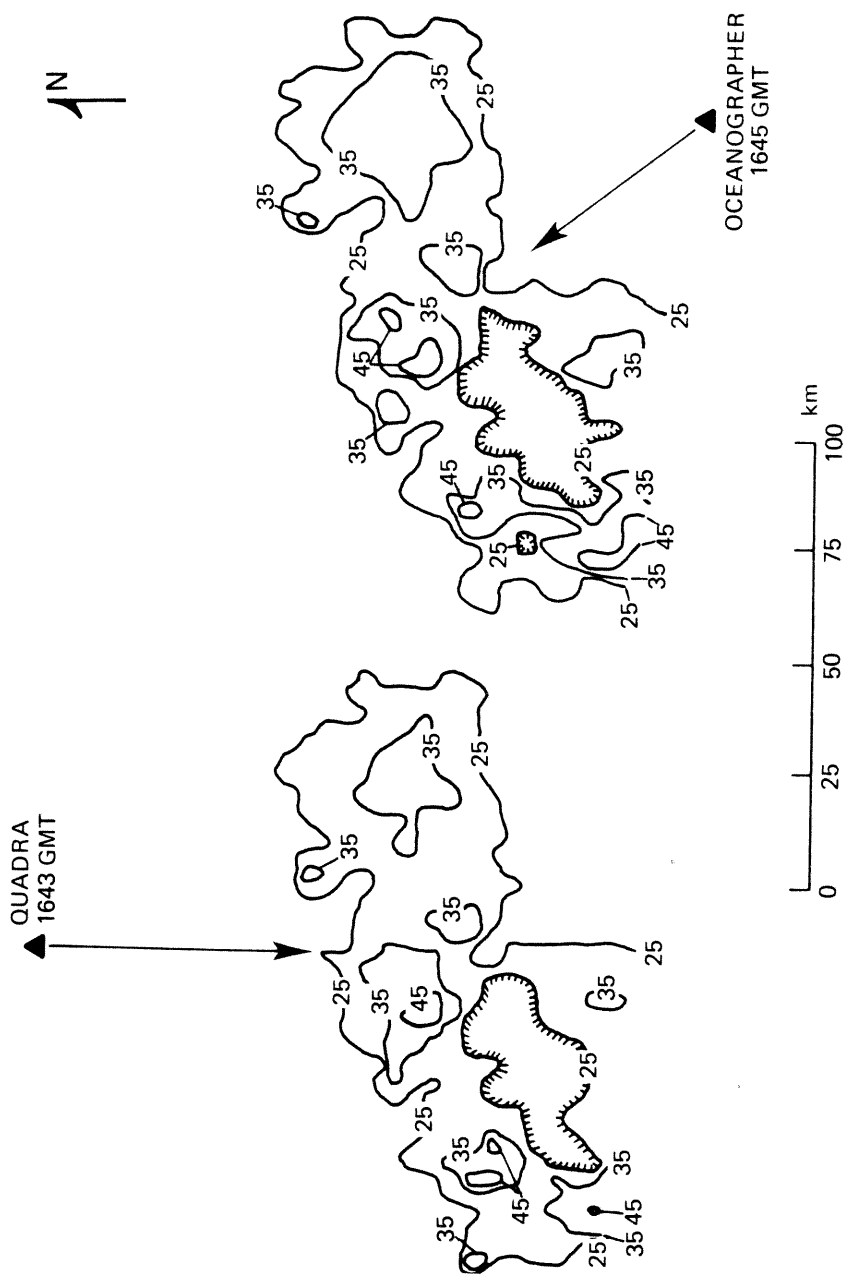


Figure 32. Comparison of the reflectivity contours (dBZ) for common echoes detected by the Quadra and Oceanographer radars on July 30 when the Oceanographer passed close to the Quadra en route to Dakar for a medical evacuation.



▲ SHIPBOARD RADAR LOCATION RELATIVE TO ITS ECHO PATTERN

Figure 33. --Comparison of the reflectivity contours (dBZ) for common echoes detected between the Quadra and Oceanographer radars on September 2, while the ships were on their respective stations in the B-scale array.

From comparison of the reflectivity contours (figs. 32 and 33), it does not appear that the Quadra instantaneous reflectivities should be lowered further in the midrange. In fact, the structure of the fields agree very well for all of the displayed reflectivity levels. The reflectivity contours from the two radars on July 30 are almost identical (fig. 32). The data on July 30 were collected when the Oceanographer was located only 40-km due west of the Quadra; thus, both radars were viewing the echoes within optimum ranges and in approximately equal directions. Based on these comparisons, we concluded that the adjusted Quadra reflectivity levels given in table 14 are quite valid for use with the Quadra instantaneous Cartesian data, at least for Phase III, which was the only Phase for which Quadra data were considered in the rainfall analysis at CEDDA.

10.2 Synopsis of Bias Corrections for All Four Radars

The bias corrections that were tentatively selected for our final rainfall analysis are summarized in table 15. These bias corrections reflect all of those enumerated in section 9.4, and an additional 1-dBZ reduction that was applied to the Quadra hourly rainfall estimates before they were merged with those from the other C-band radars to obtain the final rainfall estimates during Phase III (Patterson et al., 1979). As was concluded in section 10.1, the adjusted Quadra reflectivity levels given in table 14 appear to be the best estimates for use with the instantaneous Cartesian data from the Quadra radar. However, the volumetric water estimates obtained from the Quadra data using table 14 are about 1 dB too high relative to the Oceanographer radar (table 12) and relative to the shipboard rain gages (table 13).

The merging procedure for Phase III required that the instantaneous rainfall estimates from the individual radars first be integrated to obtain hourly estimates, which were subsequently merged (Patterson et al., 1979). Therefore, a convenient and reasonable method for removing the remaining 1-dBZ

Table 15.--Synopsis of systematic bias corrections used to adjust the data from the C-band radars as part of the derivation of the final rainfall estimates

<u>Oceanographer</u>	<u>Researcher</u>	<u>Gilliss</u>	<u>Quadra</u>
+2.2 dBR (+2.75 dBZ)	+1.8 dBR (+2.25 dBZ)	Ranges < 25 km -0.8 dBR (-1.0 dBZ)	*
		Ranges > 25 km +0.8 dBR (+1.0 dBZ)	

*The Quadra instantaneous reflectivities were adjusted as shown in table 14, and the hourly rainfall estimates were lowered by an additional 0.8 dBR before the merging process.

bias in the Quadra rainfall estimates consisted of lowering the hourly estimates 0.8 dBR (1 dBZ) before they were merged with the data from the other radars.

Why the additional 0.8-dBR correction was needed for the integrated rainfall estimates from the Quadra radar is not clear. Possibly it stems from the fact that the Quadra radar echoes sometimes covered slightly more area than, for example, did the Oceanographer radar echoes, although this is not obvious for the echoes shown in figures 32 and 33 that were bounded by a threshold of 25 dBZ. The polar to Cartesian rectification procedure used for the Quadra did tend to smear the echoes somewhat more than did the procedures used for the other three radars. Regardless of the origin of the residual bias, the adjustment was needed to coherently merge the rainfall estimates during Phase III. All biases as summarized in table 15 are verified through comparisons with "ground truth" in the next chapter.

11. VERIFICATION OF BIAS CORRECTIONS

To verify the validity of the biases summarized in section 10.2, the only source of "ground-truth" measurements was once again considered; i.e., the shipboard rain gages. In section 11.1, the refined rainfall estimates from the individual radars are compared with rain-gage measurements from all ships within the field of view of the various radars. These comparisons differ in two respects from those made in section 9.3: (1) they include more gages, and (2) the data were navigated more accurately based on the high resolution "re-navigated" ship positions (Seguin and Crayton, 1975). The rain-gage data were taken from those published by Seguin and Sabol (1976) and Seguin and Crayton (1977). Data were available from two or more gages for some ships. For these cases, the maximum of the gage values was usually selected for comparison with the radar estimates, since most potential sources of gage error produce deficit gage catches (sec. 12.2).

Another question to be answered is whether new biases were introduced when the data from the various radars were merged to quantitatively cover the B-scale array (Patterson et al., 1979) or if residual biases remained after the merging process. Sections 11.2 and 11.3 deal with gage-to-radar comparisons of the Phase-mean and daily rainfall rates, respectively, using the merged radar estimates.

Finally, gage-to-radar comparisons are made between hourly rainfall rates from the refined NOAA radar estimates and from the collocated gage catches (sec. 11.4). Although it was realized that the scatter would be large for the hourly comparisons, our objective was to determine if any residual biases remained throughout the dynamic range of the hourly rates.

Even for averaging periods as long as a Phase, it is difficult to relate rain estimates from radar to point estimates from isolated gages. However, some information can be gained about the accuracy of the radar estimates from such comparisons if the large spatial variabilities and the impreciseness with which the radar precipitation fields can be positioned are considered. Some of the factors that potentially limited the precision with which the shipboard rain gages could be absolutely positioned in the radar fields follow:

1. Uncertainties in the ships' estimated positions were sometimes 1-2 km.
2. Time-variant antennae azimuth errors, usually small, may have occasionally become significant.
3. Data resolution prevented navigation of individual radar fields to better accuracy than 2 km.
4. The merging of fields from two or more radars could further deteriorate the navigation accuracy for parts of the B-scale array.
5. Areas that were obstructed by the ships' superstructures in the individual NOAA radar scans sometimes were filled by data from the same radar, 15-min removed (Richards and Hudlow, 1977), or from another radar as part of the merging process.
6. Wind shear between beam level and the surface could cause the precipitation to drift laterally and reach the surface a significant distance from the point of radar observation.

None of the above six factors would have a significant impact on the accuracy of the rainfall estimates, except on those applications requiring extremely accurate absolute location of the radar data and/or gage data; for example, "point"⁵ estimates are needed in order to make comparisons between radar observations and the individual gage catches.

Considering the large spatial variability inherent in convective precipitation and the six factors enumerated above that affect the precision with which the rain gages can be positioned relative to the radar fields, it seems likely that the positional error can be as large as 4 km. To minimize the errors resulting from positional uncertainties (Hudlow and Patterson, 1979), each "point" radar estimate, for the gage-to-radar comparisons of the Phase-mean rates or accumulations (secs. 11.1, 11.2, and 12.2), was determined as follows: (1) a set of four, 4-km x 4-km data bins, consisting of the one containing the Phase-mean ship (gage) position plus the three nearest neighboring bins, was determined, and (2) from this set, the radar rainfall value in closest agreement with the rain-gage catch was selected as the appropriate estimate.

Because of the even larger spatial gradients existing in the daily isohyetal maps, compared to the Phase maps, it seems likely that the errors resulting from positioning uncertainties of the rain gages relative to the radar fields would be somewhat greater for the daily scale. Consequently, an analogous procedure to the one used for the Phase comparisons was adopted for the daily radar-to-gage comparisons (secs. 11.3 and 12.2), except the optimizing was done by selecting the best-matched radar data bin from a set of nine bins, as opposed to the set of four used for the Phase comparisons (Hudlow and Patter-

⁵"Point" radar estimates in the context of this report refer to the values for the elemental 4-km x 4-km data bins.

son, 1979). The 9-bin set consisted of a central bin containing the daily-mean ship (gage) position plus the eight surrounding bins.

11.1 Comparison of Phase III Mean Rainfall Rates From Individual Radars with Gage Catches

Radar-to-gage comparisons were made between the Phase III mean rain-rates from the four C-band radars and those from rain gages for all ship stations underneath the umbrellas of the various radars. (See Hudlow, 1977b, for approximate ship locations.) Table 16 summarizes these comparisons. The radar ranges to the remote gage locations are also given in table 16, so that comparisons can be made between these results and the range performance curves (sec. 7.2).

The average difference (dBR) between the gage and radar estimates for all gages within 175-km range, excluding the Vanguard gage, are given at the bottom of table 16. The Vanguard gage measurement is believed to be erroneously high (Hudlow, 1977b).

Based on the results shown in table 16, it appears that the systematic biases, as previously assessed for the individual radars (sec. 10.2), are quite valid. The average difference between the gages and the Gilliss radar (+1.14 dBR) is the only one of the four radar-to-gage differences being sufficiently large to indicate a potential residual bias. However, even for this radar, closer examination of table 16 reveals that: (1) the average difference is significantly weighted by the Meteor and Bidassoa gages, which are located at quite far ranges, and (2) the collocated Gilliss-radar/Gilliss-gage comparison is within approximately 0.5 dBR and with opposite sign. These results, therefore, do not suggest a residual bias when one takes into account the range performance characteristics of the radar (sec. 7.2).

11.2 Comparison of Phase-Mean Rainfall Rates From Merged Radar Data with Gage Catches

Figure 34 is a scatter diagram that summarizes the results of the comparison between the Phase-mean rain rates from the final merged radar data, and the B-scale shipboard rain gages, for all three Phases of GATE. The plotted numbers give the frequency of radar-gage pairs falling within the 2-dBR classes delineated by the vertical and horizontal lines. The rainfall rates are averages over the Phases expressed in mm hr^{-1} and in dBR, where $\text{dBR} = 10 \log (R)$.

Examination of figure 34 shows that for 18 out of the 24 comparisons the radar and gage values fall within the same class and that the other 6 are within one class. More importantly, there is no evidence of residual systematic biases as a result of the merging process, at least not for the Phase time scale.

Table 16.--Comparison of Phase III mean rainfall rates from individual radars with gage catches

Ship	Gages				Oceanographer radar				Quadra radar					
	Rain rate mm/h	(dBR)	Rain rate mm/h	(dBR)	Gage minus radar (dBR)	Distance to gage (km)	Rain rate mm/h	(dBR)	Gage minus radar (dBR)	Distance to gage (km)	Rain rate mm/h	(dBR)	Gage minus radar (dBR)	Distance to gage (km)
Meteor	0.39	-4.09	0.52	-2.81	-1.28	157	0.39	-4.09	0	110	0.39	-4.09	0	110
Vanguard	0.45	-3.47					0.20	-6.99	+3.52	145				
Quadra	0.51	-2.92	0.46	-3.38	+0.46	148								
Oceanographer	0.34	-4.69	0.35	-4.53	-0.16	0	0.32	-4.95	+0.26	148				
Researcher	0.48	-3.19	0.52	-2.81	-0.38	159								
Bidassoa	0.51	-2.92												
Gilliss	0.59	-2.29												
Planet	0.39	-4.09	0.40	-3.95	-0.14	175	0.46	-3.37	-0.72	41				
Dallas	0.48	-3.19	0.46	-3.38	+0.19	93	0.46	-3.37	+0.18	56				
Hecla	0.35	-4.56	0.60	-2.24	-2.32	152	0.39	-4.09	-0.47	62				
Average difference (dBR) between gage and radar estimates within 175-km ranges, excluding Vanguard estimates														
-0.52														
-0.15														
Ship	Gages				Researcher radar				Gilliss radar					
	Rain rate mm/h	(dBR)	Rain rate mm/h	(dBR)	Gage minus radar (dBR)	Distance to gage (km)	Rain rate mm/h	(dBR)	Gage minus radar (dBR)	Distance to gage (km)	Rain rate mm/h	(dBR)	Gage minus radar (dBR)	Distance to gage (km)
Meteor	0.39	-4.09	0.44	-3.54	-0.55	156	0.19	-7.14	+3.05	175				
Vanguard	0.45	-3.47					0.06	-12.51	+9.04	170				
Quadra	0.51	-2.92	0.09	-10.29	+7.37	238	0.04	-13.85	+10.93	245				
Oceanographer	0.34	-4.69	0.32	-4.89	+0.20	159								
Researcher	0.48	-3.19	0.44	-3.54	+0.35	0								
Bidassoa	0.51	-2.92	0.44	-3.54	+0.62	150	0.42	-3.79	+0.87	173				
Gilliss	0.59	-2.29					0.66	-1.78	-0.51	0				
Planet	0.39	-4.09	0.05	-12.99	+8.90	240	0.12	-9.16	+5.07	206				
Dallas	0.48	-3.19	0.24	-6.24	+3.05	194								
Hecla	0.35	-4.56	0.32	-4.89	+0.33	195	0.19	-7.14	+2.58	195				
Average difference (dBR) between gage and radar estimates within 175-km ranges, excluding Vanguard estimates														
+0.16														
+1.14														

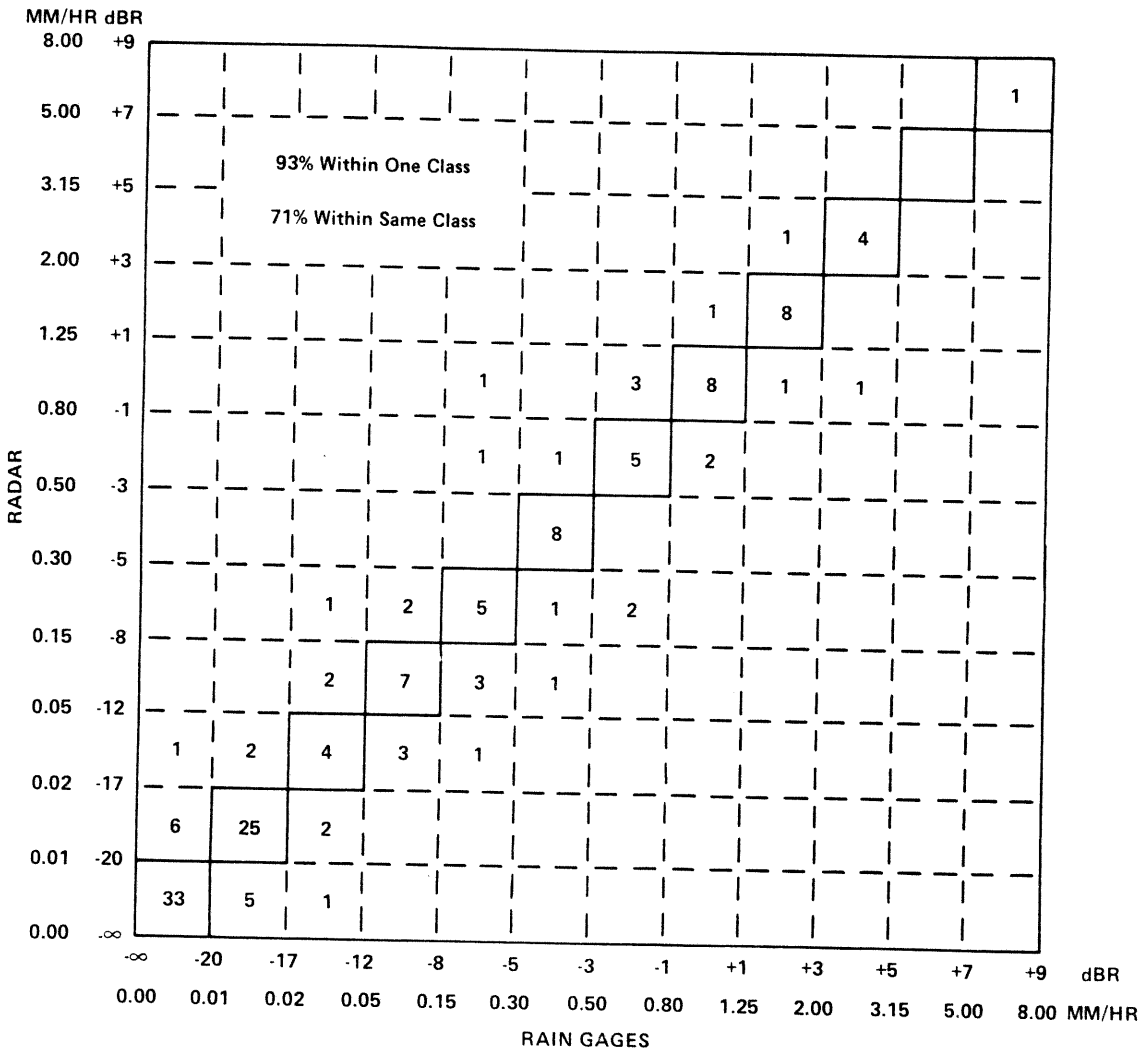


Figure 35.--Scatter diagram of daily mean radar-rainfall rate estimates versus those from rain-gage measurements for all days in GATE using rain gage data from stations maintained by the Gilliss, Oceanographer, and the Meteor. The numbers give the frequencies with which the estimates fall within the indicated classes.

The class intervals are 2 dBR, except 3 to 5 dBR classes are used below -5 dBR because of poor resolution in the rain-gage data at light rain rates. The percentage of the gage and radar values that are within the same class, and within one class, are 71 percent and 93 percent, respectively. While, as expected, the scatter for the daily scale increased over that for the Phase time scale (fig. 34), no residual systematic biases are apparent for either scale.

11.4 Comparison of Hourly Rainfall Rates From NOAA Radars with "Collocated" Gage Catches

Only collocated gage and radar data were used for the hourly comparisons. This was accomplished by using the objective analysis model described by Patterson et al. (1979), which is a modified version of the one developed by Hudlow et al. (1976), to obtain interpolated radar estimates at the radar origin. These interpolated values could then be used for the "collocated" comparisons with rain-gage data aboard the same ship.

The hourly collocated comparisons were made using the refined rainfall estimates from the Oceanographer and Researcher radars, individually, before the fields were navigated and merged. This approach virtually eliminated the positional errors, which may be significant for the daily and Phase comparisons of the remote radar and gage observations. However, the interpolation errors accompanying the hourly radar estimates can be large, since the closest observed data used in the objective analysis were 4 km from the radar origin. Hudlow et al. (1978) show that the mean correlation radius (distance at which the autocorrelation coefficient first diminished to e^{-1}) is only approximately 4 km for GATE instantaneous rain-rate fields.

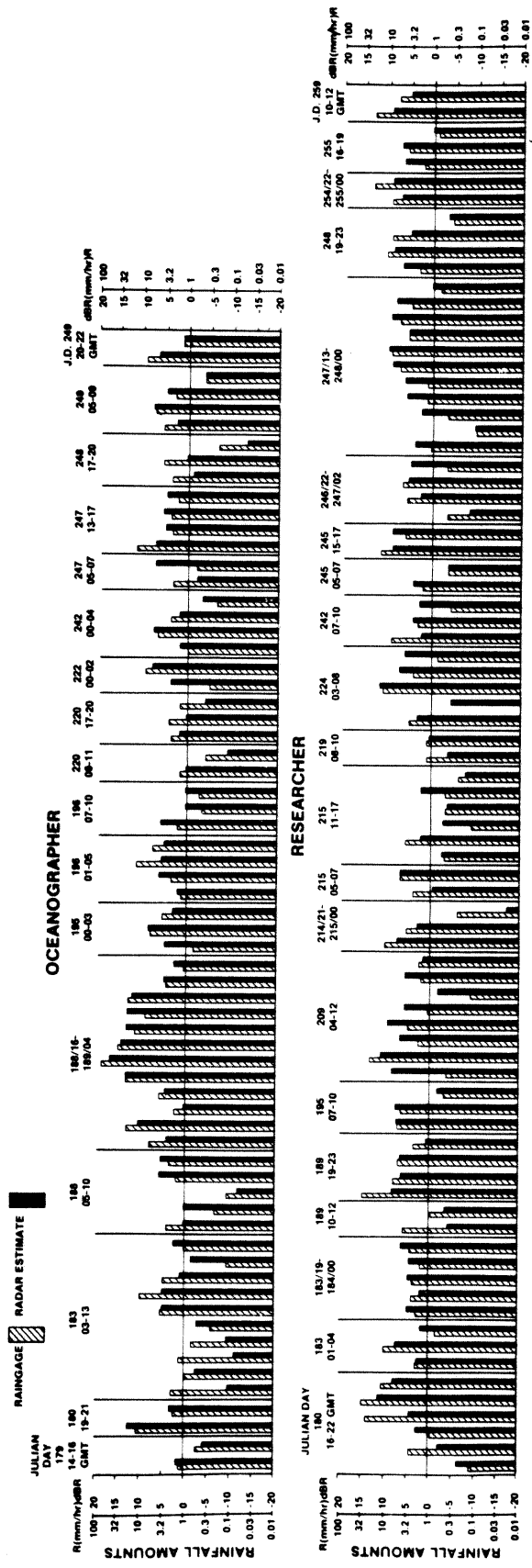
Figure 36 compares the hourly time series of interpolated rainfall estimates, from the Oceanographer and Researcher radars during rain periods, with those from the shipboard rain-gage measurements. To isolate possible biases for periods of significant precipitation, a scatter diagram of the hourly radar-versus-gage estimates, determined by taking all hourly values from figure 36 that exceed 2.5 mm hr^{-1} at the Oceanographer and Researcher, is presented in figure 37.

Examination of figures 36 and 37 verify two important facts: (1) there is no tendency for the radars to give unrealistic overestimates during heavy rain events, which could occur if, for example, the wet-radome attenuation correction procedure for the Oceanographer radar had introduced large errors, and (2) no significant residual biases are apparent throughout the dynamic range of the hourly rates.

11.5 Overall Validity of Bias Corrections

In summary, none of the analyses presented in section 11.1 through 11.4 suggests that any systematic biases remain between the radar estimates and the shipboard rain gages taken as a whole. Therefore, in this sense, the assessed biases, summarized in section 10.2, have been verified as being completely valid. However, this does not preclude the possibility of there being small biases within localized areas of the B-array, since the limited number of gages allowed "ground-truth" checks at only a few points within the array. Furthermore, the accuracy of some of the gage measurements could certainly be questioned.

Potential errors in the shipboard rain-gage data also should be considered when using them to assess the absolute accuracy of the radar estimates. Significant variability often is observed between measurements from differ-



ent gages aboard the same ship. For example, the mean absolute percent difference, in daily collections, between the stern 1 gage and the bow gage on the Gilliss was 18 percent (Seguin and Crayton, 1977). Furthermore, the difference between the stern 1 and the stern 2 gages was 12 percent. As mentioned earlier, the maximum gage catch was normally used for comparison with the radar estimates, since most potential sources of gage error produce deficient gage catches (sec. 12.2). The observed variability among the various gage records further supports the appropriateness of matching the radar and gage pairs as described above for the radar-gage comparisons.

The question of biases in the rain-gage data are explored further in section 12.2. Also, using the results from sections 11.2 and 11.3 and assuming that the gage values are "truth," numerical expressions are presented in section 12.2 to summarize any absolute biases and to estimate the average expected errors in the Phase and daily radar "point" estimate. Then from these results, and certain assumptions regarding potential errors that could become significant at shorter time scales, a range of space and time scales, expected to give equivalent accuracies to the daily "point" estimates, are determined.

12. CONCLUDING REMARKS

12.1 Calibration and Intercomparison Procedures

The multifaceted procedures that were adopted to ensure that the GATE C-band radars were accurately calibrated, relative to each other and to "ground-truth," have been described in foregoing chapters of this report. Some of the specific calibration procedures used for GATE might not be appropriate, or necessary, for other experiments. The procedures may vary as a function of application, available intercomparison data, and with type and age of radar installation. In general, all radar systems will require some type of careful hardware calibration, and the radar rainfall estimates should be compared with available ground-truth measurements to ensure that accurate rainfall estimates are derived.

In most respects, the calibration procedures adopted for GATE were adequate and comprehensive. It is difficult to see how any of the calibration and intercomparison procedures described herein could have been eliminated from the GATE radar program, without having incurred a risk of an overall loss in quantitative accuracy. It was critical that the calibrations be checked, even before the field Phases of the experiment, and that they be monitored and validated throughout the key stages of the data collection and processing.

Indispensable calibration and analysis techniques were: (1) the pre-field test (sec. 4.4), (2) the near real-time quality control through spot checks of data via the shipboard minicomputer (fig. 2), (3) the analysis of variance of transmitter outputs and receiver/digitizer input-output transfer equations (sec. 3.2), (4) the system gain measurements with the standard horn method (sec. 5.1), (5) the comparison of volumetric-water versus echo-area relationships (sec. 6.3), (6) the evaluation of range effects (ch. 7), and (7) the comparison of volumetric water estimates between radars and between radars and gages (ch. 9).

Another calibration procedure that should have been used during GATE would have made use of the sun as a radio calibration source (Whiton et al., 1976). This approach potentially would have been very useful for checking the antenna orientation (azimuth and elevation). The antennas for the GATE radars were slaved to the ships' gyrocompasses, and special vertical gyros were used for the elevation references (fig. 2). Using the sun as an absolute reference has obvious advantages for shipboard radar operations because of the lack of a fixed land reference. Such a technique would be extremely valuable if it could be used to detect biases in the azimuthal alignment and/or antenna stabilization at an early stage.

The magnitude of the systematic biases for the U.S. radars ranged from the +1.0 dBZ (Gilliss > 25-km range) to +2.75 dBZ (Oceanographer). The reasons for these mean underestimates are not certain, but they probably reflect biases that existed in the original estimates of average intensity for the polar data bins, which in turn may have at least partially originated from one or both of the following sources: (1) low reflectivity estimates due to occasional strong reflectivity gradients within the polar bins (Sirmans, 1972) and (2) power losses related to the receiver bandwidths (Nathanson and Smith, 1972; Doviak and Zrinc', 1978). It is difficult to incorporate corrections for these effects directly into the radar equation, since the first effect is dependent on the magnitude of the reflectivity gradients (i.e. the meteorology) and the second effect is dependent on the type of receiver and is difficult to evaluate for a logarithmic receiver. The average magnitude of these two combined biases for the GATE radars and rain-rate regime may have been 1 or 2 dB, however, which would essentially explain the observed biases.

It is also possible that the biases for the NOAA radars partly resulted from slight overestimates for the system gains (table 2). This possibility seems somewhat more likely for the Oceanographer radar, since the Oceanographer reflectivity estimates were, in the mean, 0.5 dBZ lower than those from the Researcher radar (before the bias corrections were applied). Furthermore, while the antenna and radome for the Gilliss and Oceanographer radars were identical, the gain estimated for the Gilliss from the standard horn measurements (sec. 5.1) was 0.9 dB less than the gain estimate for the Oceanographer (table 2). This difference cannot be explained entirely by differences resulting from "microwave plumbing" losses. Based on reexamination of the gain measurements presented in chapter 5, it certainly seems possible that the gain estimates for both NOAA radars could be in error by as much as 0.5 dB. A 0.5-dB error in gain would explain 1.0 dB of the total bias, since gain appears as a squared quantity in eq. (1).

In arriving at the magnitudes of the systematic biases, considerable weight was given to the comparisons between the Phase rainfall totals from the individual radars and those from selected gages. Comparisons between radar estimates and gage catches also were made for shorter time periods (secs. 11.3 and 11.4); however, because the inherent noise in relating the point measurements from the single in situ sensors to the much larger volume measurements from the remote sensors increases with decreasing integration time, no attempt was made to dynamically adjust the radar fields for limited areas or times using gage calibrations. In fact, only time and space

invariant bias adjustments, defined here as systematic bias adjustments, were applied to the data sets from the individual radars. In addition, attenuation corrections were applied as described in section 7.1.

Because of the large spatial and temporal gradients, it is always difficult to establish the absolute accuracy of convective rainfall measurements, even over land areas. At sea it becomes more difficult, since adequate independent "ground truth" measurements are usually not available; especially for the smaller space and shorter time scales. Most radar hydrologists accept that comparisons made against a dense rain-gage network, within optimum range of a land-based radar, often provide the best information for assessing the accuracy of, and for calibrating, radar rainfall estimates. However, it would not have been logistically feasible, if possible at all, to erect and maintain a dense network of buoys instrumented with rain gages in the GATE B-scale area.

Although there were insufficient rain-gage data to use them for dynamic calibrations, it was possible, with the analysis techniques described in chapters 9 and 11, to use them as "ground truth" for identifying and verifying systematic biases. In fact, the rain-gage data were indispensable for this purpose, and even greater emphasis should be placed on improving the shipboard rain-gage measurements for future experiments. Since the number of gages will be few, every effort should be made to ensure that they are optimally sited. Also, the gages should be automatic and record at a nearly continuous frequency.

In addition to using the rain-gage data for assessing systematic biases, they can be used to estimate mean errors in the radar rainfall estimates. The assumptions that were made to do this, and a summary of the probable accuracies of the GATE radar rainfall estimates, are presented in section 12.2.

12.2 Probable Accuracies of the GATE Radar Rainfall Estimates

Because the rain-gage observations can be in error, and since significant variability (error) is encountered in relating the point measurements from the gages to the much larger volume measurements from the radar (ch. 11), it is difficult to assess the absolute errors in the final radar estimates from comparisons with the individual shipboard rain-gage catches. It is useful to summarize the observed differences between the radar and gage estimates, however. If one assumes to a first approximation that the gage measurements represent "ground truth" at the point of observation and that the effective data positional uncertainties are largely eliminated by using the radar value in closest agreement with the gage from the data bin sets as described in sections 11.2 and 11.3, then these observed differences can be interpreted as estimates of the expected error for the radar "point" measurements.

An evaluation of any overall residual biases in the final radar rainfall estimates can be obtained by computing the following statistic for each Phase:

$$\frac{[\Sigma(\text{Gage})_i - \Sigma(\text{Radar})_i] \times 100}{\Sigma(\text{Gage})_i} \quad (35)$$

Table 17.--Residual systematic bias evaluation between shipboard gage measurements and final radar "point" estimates

Observation period	percent differences	
	plus: radar < gage	minus: radar > gage
Phase I	+5	
Phase II	+6	
Phase III	-4	
All GATE	+2	

where the sum is over all B-scale ship stations (i). The results from this computation are given in table 17. The estimated biases for the three Phases are probably not significantly different from zero when one considers the uncertainties that may accompany the estimates from both sensors.

It should be emphasized that the rain-gage records could contain systematic biases, which are not reflected in the percentage differences given in table 17. In fact, most potential errors in shipboard rain-gage measurements tend to result in deficit catches (WMO, 1962). Laevastu et al. (1969) and Reed and Elliot (1977) suggest that the approximate magnitude of these deficits would be less than 10 percent for suitable shipboard installations. For those GATE ships that were equipped with two or more gages, the maximum gage value was normally selected for comparison with the radar estimate. This tended to minimize the effect of gage underestimates, resulting from bad gage exposure, in the assessment of systematic biases in the radar estimates. The difference between minimum and maximum gage values was frequently considerable. For example, the maximum deviation between gages was observed on the Gilliss, where there was consistently about a 20 percent greater Phase catch in one of the stern gages than in the bow gage. The stern gages on the GATE ships generally collected more rain than the mast or bow gages. This was probably due to the sheltering effect provided by the stern exposure. The standard operating procedure for the GATE ships was a drift and slow recovery mode, with the bow maintained into the wind when possible.

Assuming no systematic biases exist in the gage records, an estimate of the expected errors in the radar "point" rainfall estimates, for daily and Phase periods, is given by the mean absolute percent difference between the gage and radar values, i.e.

$$\sum \sum \left| \frac{(\text{Gage}_{ij} - \text{Radar}_{ij})}{\text{Gage}_{ij}} \right| \times 100/N, \quad (36)$$

where the sums are for all B-scale stations (i) used in the analysis and for all Phases or days (j) during GATE; N is the total number of gage-radar pairs. Table 18 gives this error statistic for the Phase and daily periods.

Because of the very large variability (scatter) observed in relating the hourly gage and radar values (fig. 37), it is not feasible to use these comparisons directly to assess the expected error for hourly "point" radar estimates. However, as mentioned in section 11.4, the scatter plot does show that no significant systematic biases exist between the radar and gage values throughout the dynamic range of the hourly rain rates.

The error estimate for the 1- to 3-hr time scale was subjectively determined by assuming that, although the errors from such sources as variability in the Z-R relationship (sec. 3.3) are locally correlated, for large enough space and time scales the errors would behave as random. Therefore, by averaging over more area, an equivalent accuracy to that for the "point" daily estimates can be achieved for the shorter (1- to 3-hr) time scale. Hudlow and Arkell (1978) experimentally show that potential error resulting from variability in the exponent of the Z-R relationship would monotonically decrease, for a given time scale, with increasing averaging area (their fig. 6). They also arrive at similar results for another source of error: inadequate temporal sampling (their fig. 5). Their results show that averaging over areas as large as, say, 1000 km² (≈ 1/4° x 1/4°) for the 3 h scale and 5000 km² for the 1 h scale should reduce the combined potential errors from these two sources to levels significantly below that given for the "point" daily scale in table 18. It is reasonable to assume that other sources of error would behave similarly, and therefore it is logical to expect that accuracies equivalent to those for the daily "point" scale should be achieved for the 1-3 h time scales by averaging over 1000-5000 km² areas (table 18).

Analogous arguments can be made with regard to error estimates for other time and space scales. For example, if the correlation of errors in the Phase "point" estimates weakens with relatively short spatial separations, then averaging in space would reduce the 14 percent expected "point" error. In fact, if the gage Phase totals, used as standards, contain no systematic biases, then the error in the Phase-mean radar estimates certainly should approach zero as the estimates are averaged over areas approaching the size of the total B-scale array. It is possible, however, that small residual biases could remain in localized areas of the B-scale array, since the limited number of gages provided "ground-truth" checks at only a few points within the array. Also, described above there could be systematic deficits in the gage collections, averaging as much as 10 percent.

In conclusion, it is encouraging to note that both Lord (1978) and Thompson et al. (1979) have found excellent agreement between the radar rainfall estimates and those based on B-scale moisture budget analyses. Lord has further demonstrated that the rainfall rates estimated from the Arakawa-

Table 18.--Summary of mean absolute percent differences between final radar rainfall estimates and shipboard rain-gage measurements

Time scale	Space scale	Mean absolute percent difference (error)	Comments
Phase	16 km ²	14%	Each radar estimate was taken as the value in closest agreement with the rain gage, from the set of four 4-km x 4-km data bins, consisting of the one containing the Phase mean ship position plus the three nearest neighboring bins.
Daily	16 km ²	23%	Each radar estimate was taken as the value in closest agreement with the rain gage, from the set of nine 4-km x 4-km data bins, consisting of the one containing the daily mean ship position plus the eight surrounding bins.
1-3 hours	1-5 x 10 ³ km ²	23%	Based on expected range of space scales over which the 4-km radar estimates must be averaged to obtain an accuracy equivalent to the daily estimates for time scales of 1-3 hours.

Schubert convective parameterization model are also in excellent agreement with the radar estimates. These findings are extremely significant, since they reveal that the quality of the principal GATE data sets should be adequate to achieve the central objectives of the experiment.

ACKNOWLEDGMENTS

The authors would like to acknowledge the many scientists, engineers, and technicians from several organizations and countries whose collective contributions to the GATE radar program are too numerous to mention here. More specifically, we are grateful to Arthur Hansen and David Braswell for their superb job as system engineers; to Robert Houze, Raul Lopez, and Wolfgang Scherer, who served as the radar meteorologists aboard the Researcher and participated in several pre-GATE planning workshops; to Pauline Austin and Geoffrey Austin for their many helpful suggestions throughout the GATE radar project; to Victor Wiggert for providing the "ground-truth" data for the Florida pre-GATE test; to Karl Pechmann, Melvin Schroeder, Frank Marks, and John Hoff for their assistance with the computer programming, analyses, and graphics; to Carolyn Mackie, who typed the draft manuscript; and to Marcia Collie, who typed the final copy.

Finally the authors thank the CEDDA, GATE Project Office, and NSF GATE management staff, especially Joshua Holland, Eugene Rasmusson, Douglas Sargeant, James Rasmussen, William Murray, and Richard Greenfield, for their consistent and enthusiastic support of the GATE radar projects.

REFERENCES

- Arkell, Richard and Michael Hudlow, GATE International Meteorological Radar Atlas, Center for Experiment Design and Data Analysis, NOAA, Washington, D.C., U.S. Gov. Printing Office, Stock No. 003-091-00038-1, 1977, 222 pp. (available from NTIS as PB-277 233/3ST)
- Austin, Geoffrey L., "Documentation for GATE Quadra Radar Digital PPI Data," GATE Processed and Validated Data, GATE World Data Center A, National Climatic Center, NOAA, Federal Bldg., Asheville, N.C., 1977, 27 pp.
- Austin, P. M., "GATE - A Summary of Objectives, the Experiment and the Role of Radar," Proc. 16th Radar Meteor. Conf., Amer. Meteor. Soc., Boston, Mass., 1975, pp. 182-185.
- Austin, Pauline, "Documentation for Gilliss Radar Cartesian Hybrid Data Set," GATE Processed and Validated Data, GATE World Data Center A, National Climatic Center, NOAA, Federal Bldg., Asheville, N.C., 1976, 79 pp.
- Austin, P. M. and S. Geotis, "The Radar Equation Parameters," Proc. 8th Weather Radar Conf., Amer. Meteor. Soc., Boston, Mass., 1960, 8 pp.
- Austin, Pauline M. and Spiros G. Geotis, "Raindrop Sizes and Related Parameters for GATE," J. Appl. Meteor., Vol. 18, No. 4, 1979, pp. 569-575.
- Austin, P. M., S. G. Geotis, J. B. Cunning, J. L. Thomas, R. I. Sax, and J. R. Gillespie, "Raindrop Size Distributions and Z-R Relationships for GATE," Presented at the 10th Tech. Conf. on Hurricanes and Tropical Meteor., Abstract published in the Bull. Amer. Meteor. Soc., Vol. 57, No. 4, 1976, p. 518.
- Bean, B. R., E. J. Dutton, and B. D. Warner, "Weather Effects on Radar," Ch. 24 in Radar Handbook, McGraw-Hill, N.Y., 1970, pp. 24-16 to 24-40.
- Betts, Alan K., "The Scientific Basis and Objectives of the U.S. Convection Subprogram for the GATE," Bull. Amer. Meteor. Soc., Vol. 55, No. 4, 1974, pp. 304-313.
- Betts, A. K. and D. R. Rodenhuis (assisted by J. L. Rasmussen and W. Murray), "Field Phase Report of the GARP Atlantic Tropical Experiment (GATE): Convection Subprogramme," GATE Report, No. 16, ICSU & WMO, Geneva, Switzerland, 1975, pp. 6-1 to 6-48. (available from UNIPUB, 345 Park Ave. South, New York, NY 10010)
- Catalfamo, R., "The Calibration of the Weather Radar on the C. C. G. S. Quadra during the GATE Experiment," M.S. Thesis, McGill Univ., Montreal, 1978, 81 pp.
- Cunning, J. B. and R. I. Sax, "A Z-R Relationship for the GATE B-Scale Array," Monthly Weather Review, Vol. 105, No. 10, 1977, pp. 1330-1336.

- Doviak, R. J. and D. Zrinc', "The Weather Radar Equation - Receiver Bandwidth Considerations," Preprints of the 18th Conf. on Radar Meteor., Amer. Meteor. Soc., Boston, Mass., 1978, pp. 484-489.
- Geotis, S. G., "Radar as a Quantitative Weather Instrument," IEE Eastern Conf., Washington, D.C., 1975, pp. 146A-146C.
- Geotis, Spiros G., Cited in the Report of the U.S. GATE Central Program Workshop, Sponsored by NOAA and NSF, Published by National Center for Atmospheric Research, Boulder, Colo., 1977, p. 182.
- Gibble, D., "Effects of Rain on Transmission Performance of a Satellite Communication System," presented at IEEE International Convention, New York, N.Y., 1964, (Abstract only, available in Conference Proceedings).
- Greene, D. R., R. A. Clark, J. J. Stephens, and V. E. Moyer, "An Investigation of Precipitation Attenuation and Its Application in Dual-Frequency Radar Morphology of Subtropical Precipitation," Tex. A&M Univ. Sc. Rept. 63-30T, College Station, Texas, 1963, 109 pp.
- Hildebrand, Peter H., "Iterative Correction for Attenuation of 5 cm Radar in Rain," J. Appl. Meteor., Vol. 17, No. 4, 1978, pp. 508-514.
- Hudlow, Michael D., "Collection and Handling of GATE Shipboard Radar Data," Preprints 16th Radar Meteor. Conf., Amer. Meteor. Soc., Boston, Mass., 1975, pp. 186-193.
- Hudlow, Michael D., "Documentation for GATE NOAA Radar Hybrid Data," GATE Processed and Validated Data, GATE World Data Center A, National Climatic Center, NOAA, Federal Bldg., Asheville, N.C., 1976, 31 pp.
- Hudlow, Michael D., Peter J. Pytlowany, and Frank D. Marks, "Objective Analysis of GATE Collocated Radar and Rain Gage Data," Preprints 17th Radar Meteor. Conf., Amer. Meteor. Soc., Boston, Mass., 1976, pp. 414-421.
- Hudlow, M. D., "Documentation for Hourly Radar Precipitation Data," GATE Processed and Validated Data, GATE World Data Center A, National Climatic Center, NOAA, Federal Bldg., Asheville, N.C., 1977a, 15 pp.
- Hudlow, Michael D., "Precipitation Climatology for the Three Phases of GATE," Preprints Second Conf. on Hydrometeor., Amer. Meteor. Soc., Boston, Mass., 1977b, pp. 290-297.
- Hudlow, Michael D. and Richard E. Arkell, "Effect of Temporal and Spatial Sampling Errors and Z-R Variability on Accuracy of GATE Radar Rainfall Estimates," Preprints 18th Radar Meteor. Conf., Amer. Meteor. Soc., Boston, Mass., 1978, pp. 342-349.
- Hudlow, M. D., V. Patterson, and F. Richards, "Spatial and Temporal Structure of Rainfall in the ITCZ over the Eastern Atlantic as Revealed by Radar During GATE," Presented at the Conf. of Meteor. Over the Tropical Oceans, Royal Meteor. Soc., London, England, 1978.

- Hudlow, Michael D. and Vernon L. Patterson, "GATE Radar Rainfall Atlas," NOAA Special Report, Center for Environmental Assessment Services, NOAA, U.S. Dept. of Commerce, Washington, D.C., 1979, 155 pp.
- Jones, R. F. and S. G. Bigler (Chairmen), "Use of Ground-Based Radar in Meteorology," WMO Tech. Note No. 78, WMO-No. 193.TP.99, WMO, Geneva, Switzerland, 1966, 104 pp.
- Kuettner, J. P., D. E. Parker, D. R. Rodenhuis, H. Hoefer, H. Kraus, and G. Philander, "GATE Final International Scientific Plans," Bull. Amer. Meteor. Soc., Vol. 55, No. 7, 1974, pp. 711-744.
- Laevastu, T., L. Clarke, and P. M. Wolff, "Oceanic Part of the Hydrologic Cycle," Report No. 11 on WMO/IHD Projects, WMO, Geneva, Switzerland, 1969, p. 33.
- Lord, Stephen J., "Development and Observational Verification of a Cumulus Cloud Parameterization," Ph.D. Dissertation, Univ. of California, Los Angeles, 1978, 359 pp.
- Marks, F. D., Jr. and M. D. Hudlow, "A Study of the Precipitating Cloud Population During GATE," Preprints of the 17th Conf. on Radar Meteor., Amer. Meteor. Soc., Boston, Mass., 1976, pp. 498-504.
- Marshall, J. S. and W. Hitschfeld, "Interpretation of the Fluctuating Echo from Randomly Distributed Scatterers, Part I," Canadian Journ. Phys., Vol. 31, 1953, pp. 962-1009.
- Nathanson, F. E. and P. L. Smith, Jr., "A Modified Coefficient for the Weather Radar Equation," Proc. 15th Radar Meteor. Conf., Amer. Meteor. Soc., Boston, Mass., 1972, pp. 228-230.
- Patterson, Vernon L., Michael D. Hudlow, Peter J. Pytlowany, Frank P. Richards, and John D. Hoff, "GATE Radar Rainfall Processing System," NOAA Tech. Memo. EDIS 26, Center for Environmental Assessment Services, NOAA, U.S. Dept. of Commerce, Washington, D.C., 1979, 34 pp. (available from NTIS as PB-297 530/8ST).
- Probert-Jones, J. R., "The Radar Equation in Meteorology," Quart. J. Roy. Meteor. Soc., Vol. 88, No. 378, 1962, pp. 485-495.
- Reed, R. K. and W. P. Elliot, "A Comparison of Oceanic Precipitation as Measured by Gage and Assessed from Weather Reports," J. Appl. Meteor., Vol. 16, No. 9, 1977, pp. 983-986.
- Richards, Frank and Michael D. Hudlow, "Use and Abuse of the GATE Digital Radar Data," 11th Tech. Conf. on Hurricanes and Tropical Meteor., Amer. Meteor. Soc., Boston, Mass., 1977, pp. 216-223.
- Seguin, Ward R. and Raymond Crayton, "Documentation for the U.S. GATE B-Scale Navigation Data," GATE Processed and Validated Data, GATE World Data Center A, National Climatic Center, NOAA, Federal Bldg., Asheville, N.C., 1975, 25 pp.

- Seguin, Ward R. and Paul Sabol, "GATE Convective Subprogram Data Center: Shipboard Precipitation Data," NOAA Tech. Rept. EDS 18, 1976, 73 pp. (available from NTIS as PB-263 820/3ST).
- Seguin, Ward R. and Raymond B. Crayton, "U.S. National Processing Center for GATE: B-Scale Ship Precipitation Data," NOAA Tech. Rept. EDS 23, 1977, 402 pp. (available from NTIS as PB-270 222/3ST).
- Shreeve, K. H., "Design and Operation of a Digital Video Integrator Processor (DVIP)," NOAA Tech. Memo. NWS EDL 13, 1974, 177 pp. (available from NTIS as COM-74-11430-7).
- Silver, William M. and Spiros G. Geotis, "On the Handling of Digital Data," Proc. 17th Radar Meteor. Conf., Amer. Meteor. Soc., Boston, Mass., 1976, pp. 462-467.
- Simpson, Joanne and William L. Woodley, "Florida Area Cumulus Experiments 1970-1973 Rainfall Results," J. Appl. Meteor., Vol. 14, No. 5, 1975, pp. 734-744.
- Sirmans, D., "Digital Processing of Meteorological Radar Signals," Meteor. Study No. 25, Australian Bureau of Meteor., Canberra, 1972, 35 pp. and 5 Append.
- Sirmans, Dale and R. J. Doviak, "Meteorological Radar Signal Intensity Estimation," NOAA Tech. Memo. ERL NSSL-64, 1973, 62 pp. (available from NTIS as COM-73-11923/2).
- Smith, P. L., Jr., "Measurement of Antenna Gain in Radar Systems," Micro-wave J., Vol. 17, No. 4, 1974, pp. 37-40.
- Thompson, R. M., Jr., S. W. Payne, E. E. Recker, and R. J. Reed, "Structure and Properties of Synoptic-Scale Wave Disturbances in the Intertropical Convergence Zone in the Eastern Atlantic," J. Atmos. Sci., Vol. 36, No. 1, 1979, pp. 53-72.
- Van Vleck, J. H., "The Absorption of Microwaves by Oxygen," Phys. Rev., Vol. 71, No. 7, 1947a, pp. 413-424.
- Van Vleck, J. H., "The Absorption of Microwaves by Uncondensed Water Vapor," Phys. Rev., Vol. 71, No. 7, 1947b, pp. 425-433.
- Weigand, R. M., "O'Hare ASDE-2 Radome Performance in Rain; Analysis and Improvement," Final Report FAA-RD-73-22, Transportation Systems Center, DOT, Cambridge, Mass., 1973, 71 pp. (available from NTIS AD-757 744).
- Whiton, R. C., P. L. Smith, Jr., and A. C. Harbuck, "Calibration of Weather Radar Systems Using the Sun as a Radio Source," Preprints of the 17th Conf. on Radar Meteor., Amer. Meteor. Soc., Boston, Mass., 1976, pp. 60-65.
- Wiggert, V. and S. Ostlund, "Computerized Rain Assessment and Tracking of South Florida Weather Radar Echoes," Bull. Amer. Meteor. Soc., Vol. 56, No. 1, 1975, pp. 17-26.

Wilson, J. W. and D. M. Pollock, "Rainfall Measurements During Hurricane Agnes by Three Overlapping Radars," J. Appl. Meteor., Vol. 13, No. 8, 1974, pp. 835-844.

Woodley, W. L., A. R. Olsen, A. Herndon, and V. Wiggert, "Comparison of Gage and Radar Methods of Convective Rain Measurement," J. Appl. Meteor., Vol. 14, No. 5, 1975, pp. 909-928.

World Meteorological Organization, Commission for Marine Meteorology (H. U. Roll, Chairman), "Precipitation Measurements at Sea," Tech. Note No. 47, WMO-No. 124. T.P.55, WMO, Geneva, Switzerland, 1962, 18 pp. (available from UNIPUB, 345 Park Ave. South, New York, NY 10010).

★ U.S. GOVERNMENT PRINTING OFFICE: 1979-311-046/346

(Continued from inside front cover)

- EDS 16 NGSDC 1 - Data Description and Quality Assessment of Ionospheric Electron Density Profiles for ARPA Modeling Project. Raymond O. Conkright, March, 1977, 80 pp. (PB-269-620)
- EDS 17 GATE Convection Subprogram Data Center: Analysis of Ship Surface Meteorological Data Obtained During GATE Intercomparison Periods. Fredric A. Godshall, Ward R. Seguin, and Paul Sabol, October 1976, 73 pp. (PB-263-000)
- EDS 18 GATE Convection Subprogram Data Center: Shipboard Precipitation Data. Ward R. Seguin and Paul Sabol, November 1976, 73 pp. (PB-263-820)
- EDS 19 Separation of Mixed Data Sets into Homogenous Sets. Harold Crutcher and Raymond L. Joiner, January 1977, 167 pp. (PB-264-813)
- EDS 20 GATE Convection Subprogram Data Center--Analysis of Rawinsonde Intercomparison Data. Robert Reeves, Scott Williams, Eugene Rasmussen, Donald Acheson, Thomas Carpenter, and James Rasmussen, November 1976, 75 pp. (PB-264-815)
- EDS 21 GATE Convection Subprogram Data Center: Comparison of Ship-Surface, Rawinsonde and Tethered Sonde Wind Measurements. Chester F. Ropelewski and Robert W. Reeves, April 1977, 22 pp. (PB-268-848)
- EDS 22 U.S. National Processing Center for GATE: B-Scale Surface Meteorological and Radiation System, Including Instrumentation, Processing, and Archived Data. Ward R. Seguin, Paul Sabol, Raymond Crayton, Richard S. Cram, Kenneth L. Ecatemacht, and Monte Poindexter, April 1977, 94 pp. (PB-268-816)
- EDS 23 U.S. National Processing Center for GATE: B-Scale Ship Precipitation Data. Ward R. Seguin and Raymond B. Crayton, April 1977, 401 pp. (PB-270-222)
- EDS 24 A Note on a Gamma Distribution Computer Program and Computer Produced Graphs. Harold L. Crutcher, Grady F. McKay, and Danny C. Fulbright, May 1977, 55 pp. (PB-269-697)
- EDS 25 GATE Convection Subprogram Data Center: Final Report on Ship Surface Data Validation. Ward R. Seguin, Raymond B. Crayton, Paul Sabol, and John W. Carlile, January 1978, 77 pp. (PB-279-560)
- EDS 26 Temperature and Precipitation Correlations Within the United States. Harold L. Crutcher. February 1978, 39 pp. (PB-278-831)
- EDS 27 U.S. IFYGL Ship System: Description of Archived Data. Robert E. Dennis. February 1978. 65 pp. (PB-278-830)
- EDS 28 Comparison of Mast and Boom Wind Speed and Direction Measurements on U.S. GATE B-Scale Ships. Katherine B. Kidwell and Ward R. Seguin, March, 1978, 41 pp. (PB-281-887)
- EDS 29 GATE Convection Subprogram Data Center: Final Report on Rawinsonde Data Validation. Robert W. Reeves, March 1978, 31 pp. (PB-281-861)
- EDS 30 Gamma Distribution Bias and Confidence Limits. Harold L. Crutcher and Raymond L. Joiner, September 1978, 112 pp. (PB-289-721)

NOAA SCIENTIFIC AND TECHNICAL PUBLICATIONS

The National Oceanic and Atmospheric Administration was established as part of the Department of Commerce on October 3, 1970. The mission responsibilities of NOAA are to assess the socioeconomic impact of natural and technological changes in the environment and to monitor and predict the state of the solid Earth, the oceans and their living resources, the atmosphere, and the space environment of the Earth.

The major components of NOAA regularly produce various types of scientific and technical information in the following kinds of publications:

PROFESSIONAL PAPERS — Important definitive research results, major techniques, and special investigations.

CONTRACT AND GRANT REPORTS — Reports prepared by contractors or grantees under NOAA sponsorship.

ATLAS — Presentation of analyzed data generally in the form of maps showing distribution of rainfall, chemical and physical conditions of oceans and atmosphere, distribution of fishes and marine mammals, ionospheric conditions, etc.

TECHNICAL SERVICE PUBLICATIONS — Reports containing data, observations, instructions, etc. A partial listing includes data serials; prediction and outlook periodicals; technical manuals, training papers, planning reports, and information serials; and miscellaneous technical publications.

TECHNICAL REPORTS — Journal quality with extensive details, mathematical developments, or data listings.

TECHNICAL MEMORANDUMS — Reports of preliminary, partial, or negative research or technology results, interim instructions, and the like.



Information on availability of NOAA publications can be obtained from:

**ENVIRONMENTAL SCIENCE INFORMATION CENTER (D822)
ENVIRONMENTAL DATA AND INFORMATION SERVICE
NATIONAL OCEANIC AND ATMOSPHERIC ADMINISTRATION
U.S. DEPARTMENT OF COMMERCE**

**6009 Executive Boulevard
Rockville, MD 20852**

NOAA--S/T 78-274